Title

Longitudinal Control Development For Ivhs Fully Automated And Semi-automated Systems - Phase 1

Authors

Hedrick, J. K.
Mcmahnon, D.
Swaroop, D.
et al.

Publication Date

1995

CALIFORNIA PATH PROGRAM
INSTITUTE OF TRANSPORTATION STUDIES
UNIVERSITY OF CALIFORNIA, BERKELEY

Longitudinal Control Development for IVHS Fully Automated and Semi-Automated Systems - Phase 1

J.K. Hedrick, D. McMahon, D. Swaroop, V. Garg, J. Gerdes, D. Maciuca, T. Blackman, P. Yip

Department of Mechanical Engineering
University of California, Berkeley

California PATH Research Report
UCB-ITS-PRR-95-4

This work was performed as part of the California PATH Program of the University of California, in cooperation with the State of California Business, Transportation, and Housing Agency, Department of Transportation; and the United States Department of Transportation, Federal Highway Administration.

January 1995

ISSN 1055-1425

LONGITUDINAL CONTROL DEVELOPMENT FOR IVHS FULLY AUTOMATED AND SEMI-AUTOMATED SYSTEMS - PHASE I

FINAL REPORT - JANUARY 31, 1994

Submitted to : PATH (MOU 101)

J. K. Hedrick, P. I
D. H. McMahon
D. Swaroop
V. Garg
J. C. Gerdes
D. B. Maciuca
T. T. Blackman
P. P. Yip

Department of Mechanical Engineering,
University of California, Berkeley

Abstract

Automated Highway Systems (AHS) are being developed as a means of safe and efficient transportation. Central to successful implementation of AHS is the proper functioning of Advanced Vehicle Control Systems (AVCS). This report addresses some of the important longitudinal vehicle modeling and control issues of AVCS such as brake dynamic model development and validation, decentralized longitudinal control algorithms which guarantee the stability of the entire platoon and fault detection and isolation in the longitudinal vehicle dynamics of controlled vehicles.

A thorough understanding of vehicle's powertrain components is necessary to ensure the much needed precise longitudinal control for closely-spaced vehicle platoons. While detailed models of propulsion dynamics have been used in the development and analysis of longitudinal controllers, the brake system dynamics have not received comparable attention. In this report, we have developed a brake model that reflects the demands of IVHS. Specifically, the developed brake system model is an appropriate model for developing model-based controllers for portotype systems and secondly, it makes the control problems associated with each brake system components explicit, thereby allowing for evaluating the trade-offs between controller performance and hardware redesign.

One of the key control problems in closely-spaced vehicle platoons is that of designing decentralized control algorithms that guarantee stability of the entire platoon, even in the presence of parametric uncertainties such as the mass of the vehicle, aerodynamic drag and tire drag. In this report, we have not only developed controllers which ensure stability of the entire platoon, but we have also characterized their performance in terms of the guaranteed attenuation in the maximum spacing error from vehicle to vehicle that can be achieved along the platoon, in the absence of initial spacing errors. We have also developed a gradient parameter adaptation law to compensate for the initial parameter estimation errors.

Fault tolerant control is increasingly becoming important in systems, such as AHS, which demand high degree of performance. For example, faulty measurements

or faulty throttle/brake actuator performance could deteriorate the platoon's performance and may even cause accidents. In this report, we have investigated schemes to detect faults in sensors (such as engine speed sensor and radar) and in throttle and brake actuators.

We have summarized the experimental data obtained from vehicle tests performed during this year at the California Highway Patrol Academy in Sacramento and at the Richmond Field Station in Richmond, California.

We have also evaluated a commercial code called VDANL for combined lateral/longitudinal vehicle control.

Lastly, we have developed a simulation package that describes the longitudinal vehicle dynamics. It can be made available to other research groups via electronic mail/ftp.

Key words :

IVHS, AHS, AVCS, Longitudinal Control, Brake model and control, String/Platoon stability, Fault detection and isolation, Adaptive Longitudinal platoon control, Experimental Platoon Control Systems.

Executive Summary

We have developed a user-friendly and modular simulation package for a 20 vehicle platoon, which incorporates a realistic vehicle model and a simplified controller model. Any new control algorithms can easily be verified by changing the "controller" routine of the package. Anonymous ftp site and/or an account has been set up for other researchers to transfer this package to their respective computers.

Due to the highly nonlinear behavior of the brake system, a model is critical for the development of an automatic brake controller. The model emphasises the behavior of the vacuum booster which is an essential component of the brake system. The model is also ideally suited for control because all the states are measurable.

String Stability is an important concern for platooning. Various platooning strategies have been investigated for string stability. It has been established that lead vehicle information is required for string stability. Other performance tradeoffs, like complexity of implementation, have also been addressed.

Smaller intervehicular spacing requires high performance controllers, which satisfy platooning specifications in the presence of parametric uncertainities. A decentralised adaptive control algorithm has been developed to this end. Performance improvement has been demonstrated in simulation.

The problem of failure detection and signal reconstruction for various sensors used in the longitudinal control system of the vehicle has been addressed. Experimental verification for the vehicle speed sensor failure and information reconstruction was done. Throttle and brake actuator faults are being studied too with an aim to develop some backup plan for emergency situation. Experiments have been conducted at the California Highway Patrol Academy, Sacramento to test various control algorithms developed earlier.

Contents

List of Figures

Acknowledgements

The authors would like to thank Mr. Peter Develin for his help with the hardware development, Dr.Sei-bum Choi and Mr. Leon Chen for their help with the real-time vehicle control code. The authors acknowledge PATH engineers, Mr. Scott Baysinger and Mr. Erik Johnson, Cal Trans Engineers Mr. Randy Woolley and Mr. Bob Battersby, for their help in organizing and conducting the four vehicle experiments at the California Highway Patrol Academy in Sacramento.

For their insights into vacuum booster design and operation, the authors acknowledge Mr. Victor DeGrazia of the Ford Motor Company, Mr. Mike Vetter and Mr. Kevin Johnson at ITT Teves America and Mr. George Stangas at Bendix Automotive Systems. Sgt. Stephen Foulds of the California Highway Patrol deserves recognition for his role in coordinating the moving tests.

Chapter 1

Introduction

1.1 Background

This report describes the work during phase I of a proposed three phase research project on "Longitudinal Control Development for IVHS Fully Automated and Semi-Automated Systems". During the first year particular emphasis was placed on developing and evaluating vehicle simulation programs for longitudinal vehicle operation. We have used these models to develop throttle and brake control algorithms that can be used in an automated highway environment. The control algorithms have been evaluated by computer simulation and also by limited field testing at the California Highway Patrol Test Facility in Sacramento and at the Richmond Field Station in Richmond, California.

Chapter 2 describes our longitudinal vehicle model and makes it available for other research groups to access by electronic mail.

Chapter 3 describes computer modeling of the vehicle's brake system including the existing actuator on one of the test vehicles, the brake pedal, the vacuum assist and master cylinder system. This model is currently being used for control algorithm development.

Chapter 4 discusses the propagation of disturbances in a string of automated vehicles. It will be essential to ensure that these disturbances attenuate as they travel upstream. This chapter investigates vehicle to vehicle communication requirements

required to ensure string stability.

Chapter 5 introduces adaptive control techniques to estimate in real time several important vehicle parameters for the control algorithm such as the vehicles' mass and aerodynamic properties.

Chapter 6 discusses techniques to detect actuator and sensor failure and how to ensure that system safety is preserved in the presence of such failures.

Chapter 7 summarizes the data obtained from vehicle tests performed during the year at the California Highway Patrol Test Facility. These tests were conducted to verify conclusions made on the basis of computer simulations.

Appendix A describes a commercial code called VDANL that was evaluated for use in combined longitudinal/lateral studies.

Chapter 2

Simulation Package: Longitudinal Vehicle Model

2.1 Introduction

In order to facilitate the development of a longitudinal controller for platoon purposes, a model of a vehicle's longitudinal dynamics was necessary. The purpose of this model was twofold: Firstly, a simulation model was needed to accurately describe the highly nonlinear dynamics of an automobile. It was used to test the various control schemes before experimental implementation. Thus we can minimize the number of problems encountered during experimental field testing. Secondly, the control design technique chosen for the problem requires a knowledge of the vehicle plant dynamics.

The mathematical model described in section **2 . 1** is simplified version of the complex model described in McMahon et. al, [28], and is based on Cho and Hedrick, [5], Moskwa and Hedrick, [30]. It was constructed using tabulated data for a 1990 Ford Lincoln Town car. The model captures the essential features of the complex model with decreased computational effort. The simulation package, "**lon_sim_release_1.0**", contains the simplified longitudinal plant and its corresponding spacing control algorithm. Details on obtaining the software, specific operating instructions, and a description of the program structure are given in section 2.2.

2.1.1 Simplified Vehicle Model

In this section we describe the four state simplified vehicle model. In this development we make the following assumptions:

1. time delays associated with power generation in the engine are negligible

2. no torsion of the drive axle

3. no slip at the wheels.

The states are :

1. Mass of air in the manifold (,)

2. Engine speed (ω_e)

3. Turbine speed (ω_t)

4. Brake torque (T_{br}).

A free body diagram depicting this simplified model is shown figure 2.1. With these assumptions, the flow of air in the intake manifold is governed by the continuity equation:

$$m_a = m_{ai} - m_{ao} \tag{2.1}$$

where m_{ai} and m_{ao} are the mass flow rates into and out of the intake manifold, respectively. The form of the empirical relationships for these rates are:

$$\dot{m}_{ai} = MAX \; TC(\alpha) \; PRI \tag{2.2}$$

$$\dot{m}_{ao} = c_1 \eta_{vol} m_a \omega_e \tag{2.3}$$

where the parameter MAX is the maximum flow rate corresponding to a fully open throttle valve. The function TC is the normalized throttle characteristic, a nonlinear function of the throttle angle α. The function PRI is the normalized pressure influence function which is a nonlinear function of the pressure ratio $PR = \frac{P_m}{P_{atm}}$, where

P_{atm} is atmospheric pressure. Using the ideal gas law, the manifold pressure, P_m, is calculated by

$$P_m = \frac{RT_m}{M_{air}\, V_m} m_a \tag{2.4}$$

where M_{air} is the molecular weight of air. The rotational dynamics of the engine is given by:

$$J_e^* \dot{\omega}_e = T_{net}(\omega_e, P_m) - T_{pump}(\omega_e, \omega_t) \tag{2.5}$$

where J_e^* is the effective engine inertia and T_{net} is the net engine torque defined as the difference between the combustion torque and the torque due to friction and other losses. It is empirically known to be a nonlinear function of the engine speed and the manifold pressure. T_{pump}, a nonlinear function of the states ω_e and ω_t, is the effective load torque on the engine.

The single transmission state is associated with the rotation dynamics of the turbine. The state equation is given by:

$$J_t^* \dot{\omega}_t = T_{turb}(\omega_e, \omega_t) - T_{load} \tag{2.6}$$

where T_{turb} is the turbine torque and T_{load} is the effective load torque on the transmission. Under the assumptions stated above the vehicle velocity and the engine speed are related by the relation:

$$v = h \quad R_g^* \omega_t \tag{2.7}$$

where h the effective tire radius and R_g^* is a variable that depends on the vehicle transmission gear ratio. Consequently the term J_t^* is an effective turbine inertia which includes the turbine, driveshaft, tire and vehicle inertias. Its functional form is therefore:

$$J_t^* = J_{t,g} + R_g^{*2}(J_{wf} + J_{wr} + M\, h^2) \tag{2.8}$$

where $J_{t,g}$ is the transmission inertia in gear g, J_{wf} and J_{wr} are the combined inertias of both front and rear wheels, respectively, and M is the vehicle mass. Included in

the expression for the load torque are all the longitudinal dynamics terms (i.e. drag, rolling resist ance).

$$T_{load} = R_g(T_{bf} + T_{br} + C_a R_g^{*2} h^3 \omega_t^2 + h F_{r,total}) \tag{2.9}$$

where T_{bf} and T_{br} are the front and rear brake torques, respectively, C_a is a "drag coefficient" and $F_{r,total}$ is the total rolling resistance. The final state is the combined brake torque, T_b. Since the brake model is linear and the time constant for the front and rear brake torques is assumed to be same, the two states can be lumped together. The combined dynamics are given by:

$$\tau_{b,v} \dot{T}_b + T_b = T_{b,cmd} = K_b \, P_b \tag{2.10}$$

where and $\tau_{b,v}$ is the brake system time constant, and $K_b = K_{bf} + K_{br}$ is the total brake torque constant of proportionality. This a very simplified model of brake dynamics. For a more complete model description see chapter 3.

2.2 Longitudinal Simulation Package

2.2.1 Installing and Running the Program

The longitudinal simulation package, "long_sim_release_1_0", is a collection of C-programs/functions developed for running on a Unix platform. The software is available from the Vehicle Dynamics Laboratory at UC Berkeley via the **f t p** utility. From any machine on the network simply type:

ftp vehicle.berkeley.edu

At the prompt for a user name type, "path". The password to gain entry to the directory is "motorcar".

If you are running on a unix platform supporting the make utility, you can use the included makefile to compile the platooning longitudinal simulation program.

Using the make utility to install the platoon simulations with the sample controller and measurement modules included type:

"make long_sim"

for the closed-loop sim with the simple longitudinal dynamic model for the Lincoln Towncar. The executable will be named long_sim. To run the platoon simulation program with the simple longitudinal model type:

long_sim

This will automatically initialize the states of the model and output the simulation result in a file called "sim.out". For details of initialization, see init_long.c.

To run the program specifying initial conditions with a data file type:

long_sim i ic_file_name

Each row of the initial condition file should contain the states of each car starting from the first car after the lead car. See long_ic.dat for an example.

To run the program specifying name of output file type:

long_sim o output_file_name

The list of outputs printed out is specified in output.c. The user can modify output.c to output the appropriate variables of interest. test.dat is a sample program output by running the long_sim program as provided with initial conditions determined by init_long.

2.2.2 Description of the program structure

main function: long_sim.c

The main file for the simple longitudinal simulation is in long_sim.c. It sets up the overall structure of the simulation and the time integration loop to update the state variables. After performing some initialization tasks, it calls up "controller"

to update the controls. It then calls up "rk4" to perform a 4-th order Runge-Kutta time integration to update the state variables. (rk4 makes call to "simple_long" to obtain the state derivatives). This time integration loop keeps going until the specified simulation end time is exceeded.

long_sim defines the following run time simulation parameters:

NUM_CAR - number of cars in the platoon following the lead car
dt - integration time step in sec
tf - simulation end time in sec
ctrl_freq - how frequent the controls are updated

e.g. if ctrl_freq is set to 5, then the controls will be updated every 5*dt
wrt_freq - how frequent the simulation result is recorded to a text file

e.g. if wrt_freq is set to 5, then the simulation result will be recorded on a text file every 5*dt

long_sim also has 2 parameters defining the number of states and controls for each car. If you plan to modify the dynamics model, make sure you update the following parameters in long_sim appropriately:

NUM_STATE - number of states for each car NUM_CTRL - number of controls for each car

The state and control vectors for each car in the platoon are held in the 2d matrices x and u. The first index of the matrix specifies the car in the platoon and the second index specifies the appropriate state or control. Also, the indices start from 1, not 0. For example x[2] denotes the state vector for the second car after the lead car and x[2][3] denotes the the third state of that car.

Simple longitudinal dynamics model: simple_long.c

The simple longitudinal dynamics model is contained in simple_long.c. Given the current states and controls, it returns the time derivative of the states. The symbolic names for the states and controls are defined in the file simple_long.h. Note that the index for the state and control vectors start from 1, not 0. Modeling parameters like mass of vehicle, moment of inertia, drag coefficient, actuator time constants, etc.

are contained in the file simple_car.h.

The simple model has two engine states (manifold air mass and engine speed), and two car states (wheel speed and car speed). A linear model is used for the tire force model with tractive force proportional to the slip ratio. Two actuator states are included for the first order dynamics assumed for the throttle and brake actuator dynamics. A position state is also included to keep track of the longitudinal position of each car.

The user can develop a customized dynamics model by modifying the existing simple_long module. Remember to update the header files simple_long.h and simple_car.h if there are changes in the definition of the states or controls, or other modeling parameters. Alternatively, the user can replace the entire simple_long module by another brand new module that follows the same input/output argument list. In either way, the user also has to update the parameters NUM_STATE and NUM_CTRL defined in the long_sim module if the number of states or controls are modified.

Longitudinal controller: controller.c

A sample longitudinal controller with throttle and actuator control is included in the file controller.c. The supplied controller performs spacing control between adjacent cars in the platoon. The velocity and acceleration profile of the lead car is specified in the function profile.c as a function of time. The user can easily replace the module with another controller by following the calling convention demonstrated in the controller module. Remember to update the header files simple_long.h if the definition of the controls is changed. The user also needs to update the parameter NUM_CTRL defined in the long_sim module.

Technical Support

If there are problems/concerns regarding the longitudinal simulation package questions may be e-mailed to "path@vehicle.berkeley.edu".

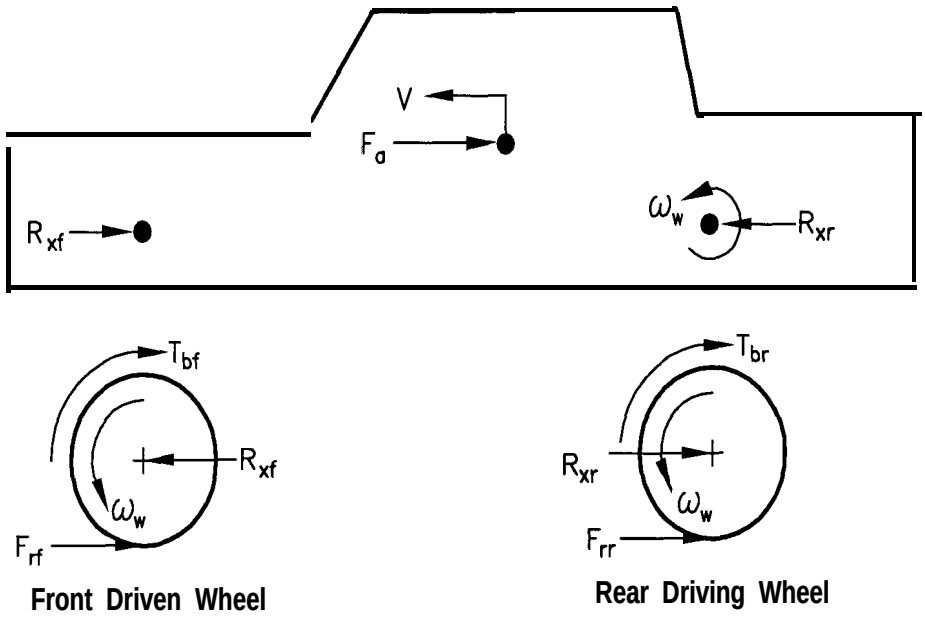

Figure 2.1: Simplified Freebody Diagram of Vehicle Motion

Chapter 3

Brake System Modeling

3.1 Modeling Demands of IVHS

With rising public concern about such transportation issues as roadway capacity, traffic congestion and highway safety, interest in Intelligent Vehicle Highway Systems (IVHS) has never been greater. Among the proposed systems, much attention has been focused on the use of Advanced Vehicle Control Systems (AVCS) to produce lanes of automated vehicles travelling in closely-spaced platoons. One of the key control problems in such a scheme is the longitudinal positioning of the vehicles such that spacing on the order of a meter is maintained during routine merge and following maneuvers. Obviously, controller design under such specifications requires a thorough understanding of all components of a vehicle's powertrain. Yet while detailed models of propulsion dynamics have been used in the development and analysis of longitudinal controllers, the brake system dynamics have not received comparable attention.

In order to maximize ride quality while simultaneously minimizing spacing error between vehicles, very tight tracking of the desired brake torque must be realized. Under such conditions, pure delays of the type often associated with brake application can force constraints on vehicle spacing that otherwise would not exist. The magnitude of this problem becomes clear when considering the fact that a 50 millisecond delay (comparable with those often used in simple brake models) trans-

lates to about 4 feet of vehicle motion at highway speeds. Before such constraints can be eliminated, the physical mechanisms behind the time delay must be identified. In addition, the required brake torques associated with normal following and merge maneuvers on automated highways are generally low. Since the dead zones and nonlinearities associated with brake dynamics are more pronounced at lower brake torques, these factors need to be quantified.

This is in sharp contrast to the types of modeling issues usually associated with braking systems. Since brakes are generally viewed as an open-loop system, with driver inputs taken as given, modeling for control is rarely an issue. Applications that do require a closed-loop model, such as radar braking or driver-vehicle interactions, focus more on collision avoidance, where the brake torques are much higher and the tracking demands are lower. Since the objective in collision avoidance is to apply as much braking force as possible as rapidly as possible, brake delays are small compared to recognition or response times and the subtleties of accurate profile following are not present (Faris et al., [10]) Conversely, when the objective is pure longitudinal motion with low brake torques, traditional issues such as wheel lock-up, tire slip angles and weight shift are less significant. Because of these differences, a brake model that reflects the specific demands of IVHS is desirable.

A satisfactory model of brake system dynamics must be able to meet two distinct objectives. First, it should be an appropriate tool for developing model-based controllers for prototype systems. As research into IVHS technology progresses, successful demonstration of concepts on the test track becomes essential. Initial experiments with closed-loop braking schemes at U.C. Berkeley have shown that linear models of brake dynamics produce controllers with poor tracking capability and often instabilities. In order to make meaningful experimental statements regarding higher level research goals such as merging and fault-tolerant control schemes, the brake controller itself must be fairly robust. An accurate model is the key to developing such a controller.

Secondly, as IVHS progresses from conception to implementation, hardware limitations must be distinguished from system limitations (Shladover, [34]). With regards to brake actuation, the most straightforward approach mechanically is to

develop a device that acts directly on the brake pedal. Such a solution saves the engineering time and liability issues (Faris et al., [10]) associated with brake system modifications and requires comparatively little power since the brake power booster is incorporated. From a controls perspective, however, the combination of actuator dynamics, linkage inertia and brake system response makes controller design anything but straightforward. A brake system model that makes the control problems associated with each component explicit is therefore necessary for evaluating the trade-offs between controller performance and hardware redesign.

This chapter presents a model of brake system dynamics to meet the above criteria. After a brief treatment of the braking process, a commonly used linear approximation of the system response is presented and its limitations as a model for the development of closed-loop controllers are discussed. Next, the individual components of the brake system are detailed with careful attention paid to the dynamics of the vacuum booster and its interactions with the engine manifold. From these components, a control model which captures the essential dynamics is isolated. In the process, several simplifying assumptions must be made regarding the behavior of the braking system. The validity of these assumptions is confirmed by a comparison of simulation results with data obtained from vehicle tests. The implications for longitudinal controller design that result from the model conclude the chapter.

3.2 Brake System Overview

3.2.1 Brake System Components

Before discussing the operating details of individual brake system components, an overview of the elements considered in this chapter and their interactions is necessary. Figure 3.1 shows the components of a typical power braking system in the absence of ABS hardware. In manual operation, the pedal linkage amplifies the force applied by the driver and provides a mechanism for tactile feedback. Careful design ensures that the amplification ratio (generally about 3:1 for power brakes) remains approximately constant over the entire length of pedal travel. Unfortunately,

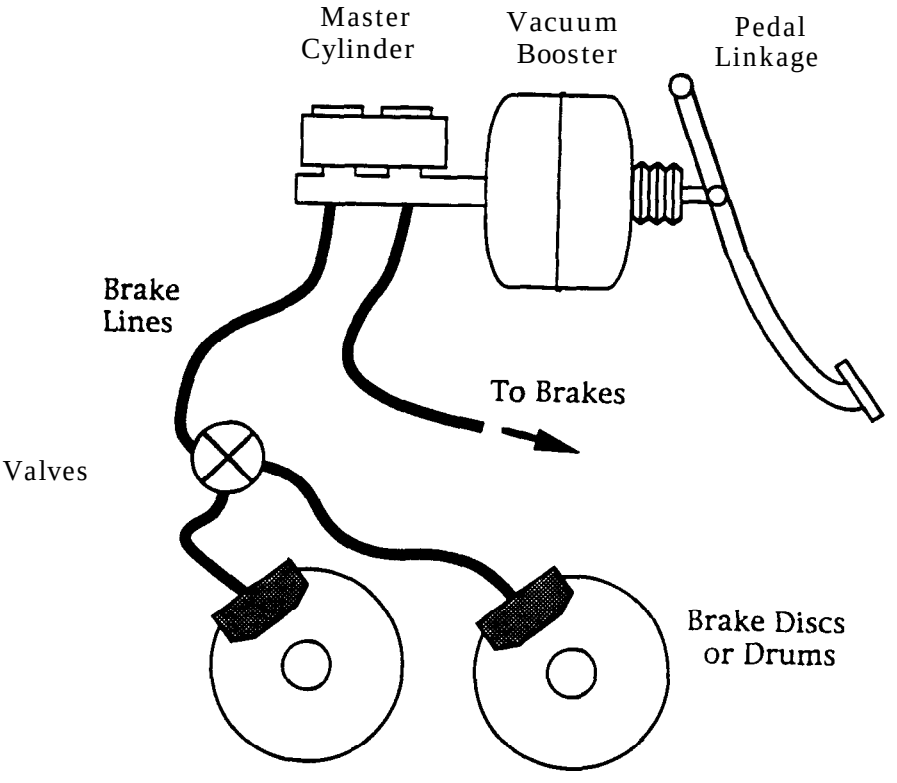

Figure 3.1: Principal Brake System Components

the mechanical advantage created by a pedal linkage of reasonable dimensions cannot achieve the forces required by disc brakes and heavier automobiles. The inclusion of a power assist overcomes this problem by providing the additional boost required for actuation. The power source for this boost is generally the vacuum created in the engine manifold, though in some cases the booster is hydraulic and connected to the power steering system. Since it is more common among passenger cars, only the vacuum booster is considered in the models that follow.

The force supplied by the pedal linkage and booster actuate the brake hydraulics, which consist of the master cylinder, proportioning valves and brake lines. The master cylinder acts as a reservoir for the hydraulic fluid and contains the main piston for the assembly. When force is applied to the master cylinder by the power booster, the piston forces the fluid under compression, resulting in flow to the brake lines. Modern cars possess tandem master cylinders with two separate pistons sharing a common bore. The two pistons may be split either between front and rear brakes or diagonally such that one piston controls the right front and left rear brakes. The

rationale behind such an arrangement follows from considerations of vehicle stability and safety in the event of a leak in one of the brake lines.

Each of the brake lines from the master cylinder lead either directly to the brakes or to a proportioning valve, which compensates for the weight shift of the vehicle at high decelerations by distributing more pressure to the front brakes. Since the characteristic forces and displacements needed to initiate braking with drums and discs are quite different, cars that combine front disc brakes with rear drum brakes occasionally include a metering valve as a compensating device (Puhn, [32]). This valve inhibits flow to the disc brakes at low brake pressures to account for the greater pressure required to initiate braking with drum brakes. After the valves, the fluid flows to the pistons that actuate the individual brakes, producing the vehicle deceleration up to the limits imposed by the tire-road interface.

3.2.2 Linear Approximations

Despite the complexity of the braking process, previous investigations into the longitudinal control problem have either concentrated exclusively on engine dynamics (Shladover, [36]) or incorporated an approximate model of the brake system dynamics (Frank et al., [12]; McMahon et al., [28]). In general, these approximate models consist of a pure time delay, first order linear dynamics and occasionally a saturation effect. Because these models appear in the literature of braking systems with great regularity, some motivation for the increased complexity proposed in this chapter should be provided.

Approximate models have been used successfully for well over twenty years to represent brake system lags in the study of vehicle stability and the development of ABS hardware. In fact, experimental responses of a brake system to approximate step inputs in pedal force show a high degree of qualitative similarity whether the input is applied by a human (Fisher, [11]) or by a mechanical actuator (Faris et al., [10]). While the exact duration of the pure time delay and the time constant of the first order dynamics vary according to the nature of actuation and the individual components of the brake system, the general shape is applicable almost without exception. As a

result, these dynamics have often been characterized as 'intrinsic' properties of the brake response.

By strict reliance on the response to a particular input, such a characterization obscures the relationship between the brake design parameters and the resultant dynamics. This can have a profound effect on closed-loop systems, since the underlying dynamics may be concealed in a step response. Because of return spring pre-loads in the vacuum booster, a certain input force must be achieved before any output (and, hence, any braking) is observed. As will be discussed in the subsequent section, the dynamics of the vacuum booster also involve a certain amount of pedal displacement before the assist is triggered. Since in reality forces and displacements cannot be achieved discontinuously, the booster thus exhibits a time delay when subjected to an approximate 'step' input. Time delays are not designed into a brake system, however, pedal travel and restoring spring pre-loads are. These characteristics are both design factors contributing to the 'feel' of a brake system and nonlinearities associated with closed-loop stability and should therefore be included explicitly in the model.

3.3 Dynamic Models

Only a few detailed dynamic models of such brake components as vacuum boosters and master cylinders have appeared in the literature, outside of restricted technical reports (Khan et al., [25]). Of these models, the two most relevant to this work are a detailed study of brake components by Fisher, [11] and a combined analytic/experimental study of the brake apply system by Khan et al., [25] . While both models have been validated in practice, they are intended for design purposes and are therefore too detailed for satisfactory use in controller development. Furthermore, the transients for which these models have been validated are slower than those associated with the tracking demands of longitudinal controllers. The objective of this section is to develop reduced-order models that nevertheless respond accurately to rapid transients.

3.3.1 Vacuum Booster

Booster Mechanics

The operation of a typical vacuum booster is detailed in figure 3.2, which is adapted from Puhn, [32]. In general, booster operation can be characterized by three stages, depending upon the interconnections between the chambers. In the initial release stage, figure 3.2a, the vacuum and apply chambers are connected, with the vacuum chamber linked to the engine manifold through a check valve and the pushrod and power piston resting on their respective limit stops. Once the force applied to the pushrod, F_{pr}, is sufficient to overcome the pre-load on the pushrod return spring, the pushrod begins to move to the left. After an initial displacement, this motion of the pushrod seals the vacuum chamber.

Further motion of the pushrod causes the control valve to open, as shown in figure 3.2b, releasing atmospheric air into the apply chamber. The resultant force on the diaphragm, after compensating for the piston return spring pre-load, causes the power piston to move to the left. The master cylinder responds to this displacement with a force on the rubber reaction washer. The washer, in turn, apportions the reaction force between the pushrod and the power piston according to their respective areas of contact. In this sense, the reaction washer is similar to an incompressible fluid (Khan et al., [25]), deforming to accommodate relative motion between the pushrod and power piston. Such a representation only approximates the true force distribution on the washer at low forces, but provides a reasonable analytical basis for the model.

The portion of the master cylinder force directed to the pushrod acts as a form of feedback, subsequently causing the control valve to close. At this point, the hold stage, the booster is at equilibrium with a specific pressure difference maintained between the two chambers, as in figure 3.2c. A decrease in the pushrod force results in the connection of the vacuum and apply chambers and a consequent return to the release stage. Should the apply chamber reach atmospheric pressure, the booster provides a 1:1 reflection of any further input force. Since this region of operation results in substantial brake pressures, it is not considered here.

Dynamic equations for the vacuum booster may be obtained from force

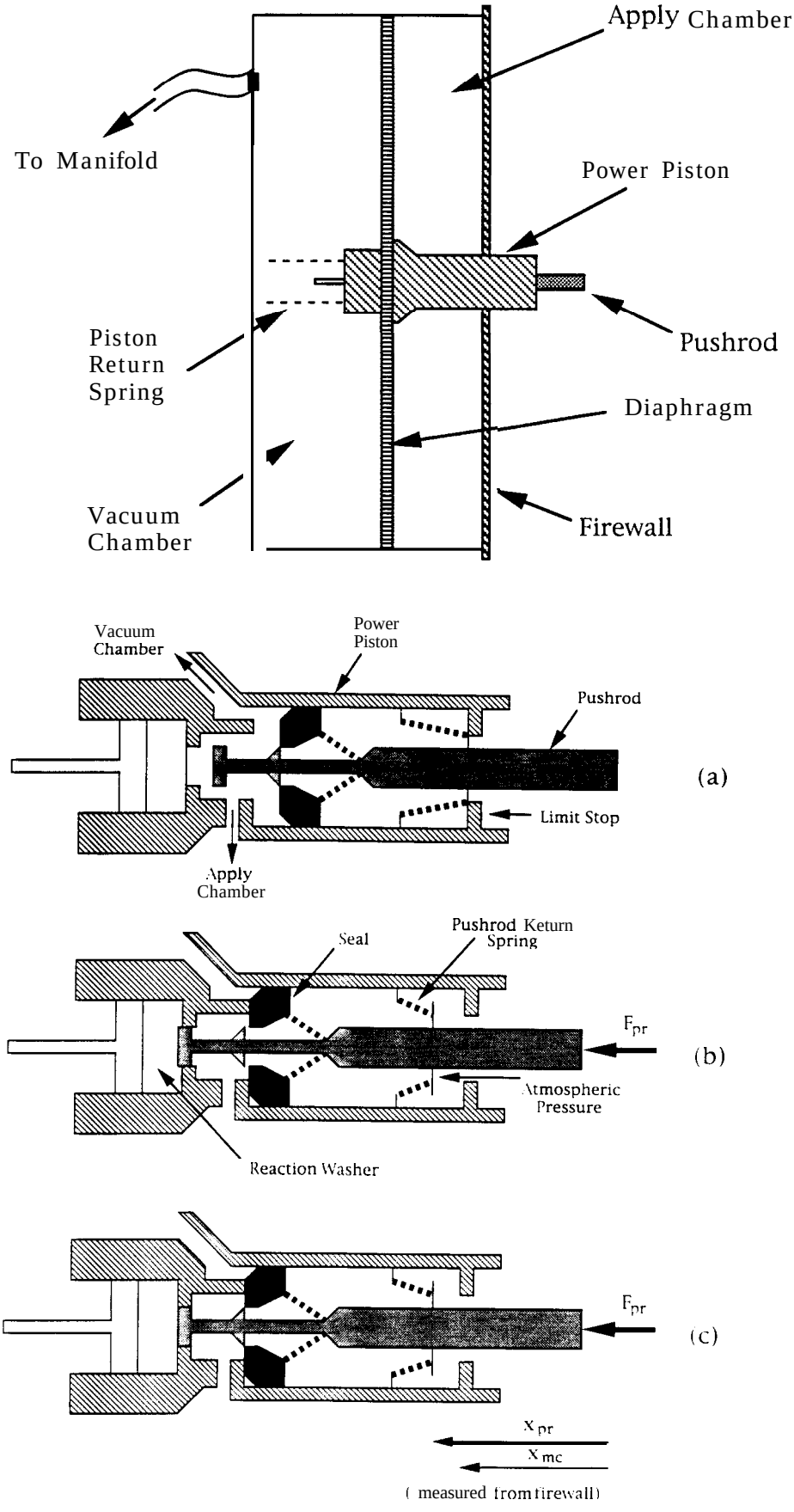

Figure 3.2: Vacuum Booster Operation

balances of the pushrod and power piston. After the pushrod leaves the limit stop, a force balance gives:

$$F_{pr} - F_{vs} - \left(\frac{A_{pr}}{A_{rw}} F_{mc}\right) = m_{pr}\ddot{x}_{pr} \tag{3.1}$$

where m_{pr} denotes the pushrod inertia and $A,$, and $A,$, represent the area of the reaction washer and the portion of that area in contact with the pushrod, respectively. F_{vs} is the combined force arising from the two springs attached to the pushrod, expressed as:

$$F_{vs} = F_{vs_o} + K_{vs}(x_{rel}) \cdot x_{rel} \tag{3.2}$$

where F_{vs_o} is the spring pre-load, K_{vs} is a nonlinear spring constant and $x_{rel} = x_{pr} - x_{mc}$.

Similarly for the power piston,

$$F_{vs} + F_d - F_{rs} - \left(\frac{A_{pp}}{A_{rw}}\right) F_{mc} = m_{pp}\ddot{x}_{mc} \tag{3.3}$$

where m_{pp} is the power piston inertia and $A,$ is the portion of the power piston area in contact with the power piston. The force on the power piston return spring, F_{rs}, is:

$$F_{rs} = F_{rs_o} + K_{rs}\Delta x_{mc} \tag{3.4}$$

where $\Delta x_{mc} = x_{mc} - x_{mc_o}$. The force on the diaphragm depends upon the pressure in each chamber and the diaphragm areas, $A,$ and $A,$, facing each chamber. Assuming these areas to be equal to a single value, A_d,

$$F_d = P_a A, - P_v A_v \approx (P_a - P_v) A_d \tag{3.5}$$

The stage of operation can be related to the relative motion of the power piston and pushrod as follows:

$$\begin{aligned} 0 \leq x_{rel} &\leq x_h \Longrightarrow \text{Release Stage} \\ x_h < x_{rel} &\leq x_a \Longrightarrow \text{Hold Stage} \\ x_a < x_{rel} &\leq x_s \Longrightarrow \text{Apply Stage} \end{aligned} \tag{3.6}$$

Here x_h and x_a represent the relative displacement between the pushrod and power piston required to initiate the hold and apply stages, In reality, the difference between x_h and x_a is quite small. However, both values must be included in simulation in order to generate the finite hold stage observed in practice. x_s is the limiting displacement reached when the pressure in the apply chamber equals atmospheric and is included only for completeness.

One difficulty with the above equations is the fact that the motion of the power piston is not readily observable. To eliminate the states associated with the power piston, the inertia is neglected, creating a static force balance in terms of the chamber pressures, master cylinder force and relative displacement:

$$F_{vs} + F_d - F_{rs} - \left(\frac{A_{pp}}{A_{rw}}\right) F_{mc} = 0 \tag{3.7}$$

The rationale behind such a simplification follows from the fact that the natural frequency of the effective mass-spring system created by the power piston and the combination of the master cylinder and piston return spring is higher than the frequencies associated with the air dynamics. Note that the pushrod inertia cannot be similarly ignored, since the pushrod is rigidly connected to the pedal and applied actuator forces must influence this combined inertia. The net effect of this approximation is to allow the air flow dynamics to dominate the vacuum booster dynamic response.

Air Chamber Thermodynamics

Figure 3.3 illustrates the changes in pressure that occur in the vacuum and apply chambers during the application of a braking force at time zero and its subsequent release 2.5 seconds later. When the force is applied, the vacuum chamber experiences an initial compression phase due to diaphragm motion, followed by the release of pressure as a result of air flow to the manifold. Similarly, the apply chamber pressure changes can be linked to both volumetric changes and the flow of air either from the atmosphere or to the vacuum chamber. For a complete description of the chamber thermodynamics, both the expansion or compression of the air and the various flows in and out of each chamber must be modeled.

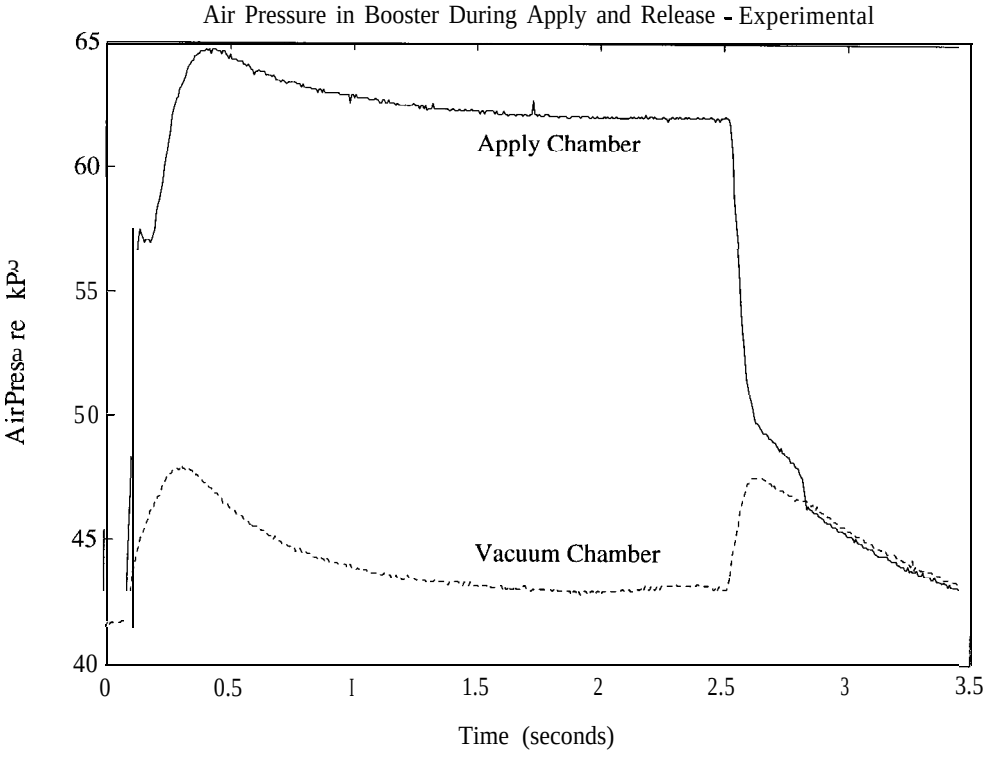

Figure 3.3: Pressure Changes in Booster Chambers During Braking

The air in the vacuum booster is considered to be an ideal gas undergoing isothermal expansion or compression. As a result, the pressure in each chamber is related to the mass of air in the chamber and the diaphragm motion by:

$$P_v = \frac{m_{av}RT}{(V_{vo} - A_d x_{mc})} \tag{3.8}$$

$$P_a = \frac{m_{aa}RT}{(V_{ao} + A_d x_{mc})} \tag{3.9}$$

Here V_{ao} and V_{vo} represent the volumes of the apply and vacuum chambers, respectively, when the booster is in the fully released position. m_{aa} and m_{av} denote the mass of air in each chamber.

The flow of air in or out of the apply chamber is determined by the stage of booster operation. In the apply stage, atmospheric air enters the chamber, while in the release stage, air flows from the apply chamber to the vacuum chamber. In the hold stage, the apply chamber is sealed. Regardless of the stage, the vacuum chamber connects to the intake manifold through a one-way check valve. This valve prohibits flow from the manifold to the booster and allows for flow from the vacuum chamber to the manifold only after a certain threshold pressure difference is achieved. Since the pressure differences driving flow in the vacuum booster remain within fairly tight bounds, linearized flow equations are incorporated into this model. Accordingly, the mass flow rate of air into the apply chamber may be determined from the stage of operation:

$$\dot{m}_{aa} = \begin{cases} C_{aa}(P_{atm} - P_a) & \text{apply} \\ C_{av}(P_v - Pa) & \text{release} \\ 0 & \text{hold} \end{cases} \tag{3.10}$$

with the corresponding flows into the vacuum chamber described by:

$$\dot{m}_{av} = \begin{cases} C_{vm}((P_m + P_o) - P_v) & \text{apply} \\ C_{vm}(\,(P_m + P_o) - P_v) + C_{av}(P_a - P_v) & \text{release} \\ C_{vm}((P_m + P_o) - P_v) & \text{hold} \end{cases} \tag{3.11}$$

In these equations, C_{aa}, C_{av} and C_{vm} are linearized flow resistances between the atmosphere and apply chamber, apply and vacuum chamber, and vacuum chamber and

intake manifold, respectively. The term P_o compensates for the pressure differential required to open the check valve. Assumed, but not explicit, in the above equations is the fact that the check valve prevents any flow from the manifold to the vacuum chamber.

Manifold Dynamics

Experiments conducted at Berkeley and elsewhere (Khan et al., [25]) have shown that the pressure in the vacuum chamber of the booster varies considerably over the course of brake application. In the previous section, these pressure transients were linked to air flow from the apply chamber to the vacuum chamber, compression of the vacuum chamber as a result of diaphragm motion, and air flow from the vacuum chamber to the engine intake manifold. The first two factors have been detailed above in the process of modeling the chamber thermodynamics. The third, however, merits special attention.

Despite the importance of the engine manifold pressure in determining the airflow from the vacuum chamber to the manifold (and, hence, the evolution of the pressure in the vacuum chamber), the authors are unaware of any brake model that includes manifold dynamics. Since the longitudinal controller developed at Berkeley utilizes the mass of air in the intake manifold as a state variable, the manifold pressure is directly available to the brake controller (McMahon et al., [28]). Furthermore, this pressure varies according to vehicle speed and acceleration, raising the spectre of coupling effects between throttle and brake controllers in automated vehicles. For these reasons, the manifold dynamics are included.

The intake manifold is considered to be a control volume and modeled according to the equations used by Cho and Hedrick, [5]. The accumulation or depletion of the mass of air in the manifold, $\dot{m}_a$, is governed by the continuity equation:

$$\dot{m}_a = \dot{m}_{ai} - \dot{m}_{ao} \tag{3.12}$$

The mass rate of airflow into the manifold, $\dot{m}_{ai}$, is given by:

$$\dot{m}_{ai} = \mathrm{MAX} \cdot \mathrm{TC}(\alpha) \cdot \mathrm{PRI} \tag{3.13}$$

where MAX represents the maximum flow rate achievable, TC(α) is a normalized characteristic of the throttle angle, α, and PRI is a pressure influence function used to model the compressible flow into the manifold.

$$\text{PRI} = 1 - \exp\left(9 \cdot \left(\frac{P_m}{P_{atm}} - 1\right)\right) \tag{3.14}$$

In practice, the throttle characteristic and volumetric efficiency must be obtained from empirical table look-ups or by best-fit approximations to experimental data. For simulation purposes, these quantities are determined from experimental data provided by the Ford Motor Company.

The mass rate of airflow from the manifold to the combustion chamber is described by:

$$\dot{m}_{ao} = \frac{V_e}{4\pi V_m} \cdot \eta_{vol}(\omega_e, m_a) \cdot m_a \cdot \omega_e \tag{3.15}$$

where V_e and V_m denote engine displacement and manifold volume, respectively, η_{vol} is the volumentric efficiency of the engine and ω_e is the engine speed. Since the manifold pressure depends upon the engine speed and the booster flow is, in turn, governed by the manifold pressure, the booster dynamics are not independent of the maneuvers performed by the vehicle.

In modeling the intake manifold dynamics, the mass rate of airflow from the vacuum chamber to the manifold is ignored. The manifold may therefore be taken as an ideal pressure source when calculating flow from the vacuum booster. Since the time constants associated with transient response of the intake manifold at highway speeds are approximately an order of magnitude faster than those associated with the flow out of the vacuum chamber, this approximation holds quite well.

3.3.2 Master Cylinder

Figure 3 . 4 illustrates the essential features of a tandem master cylinder. The power piston of the vacuum booster contacts the primary piston of the master cylinder, providing the link between the force input and brake hydraulics. Initially, brake fluid displaced by motion of the primary piston flows freely into the reservoir

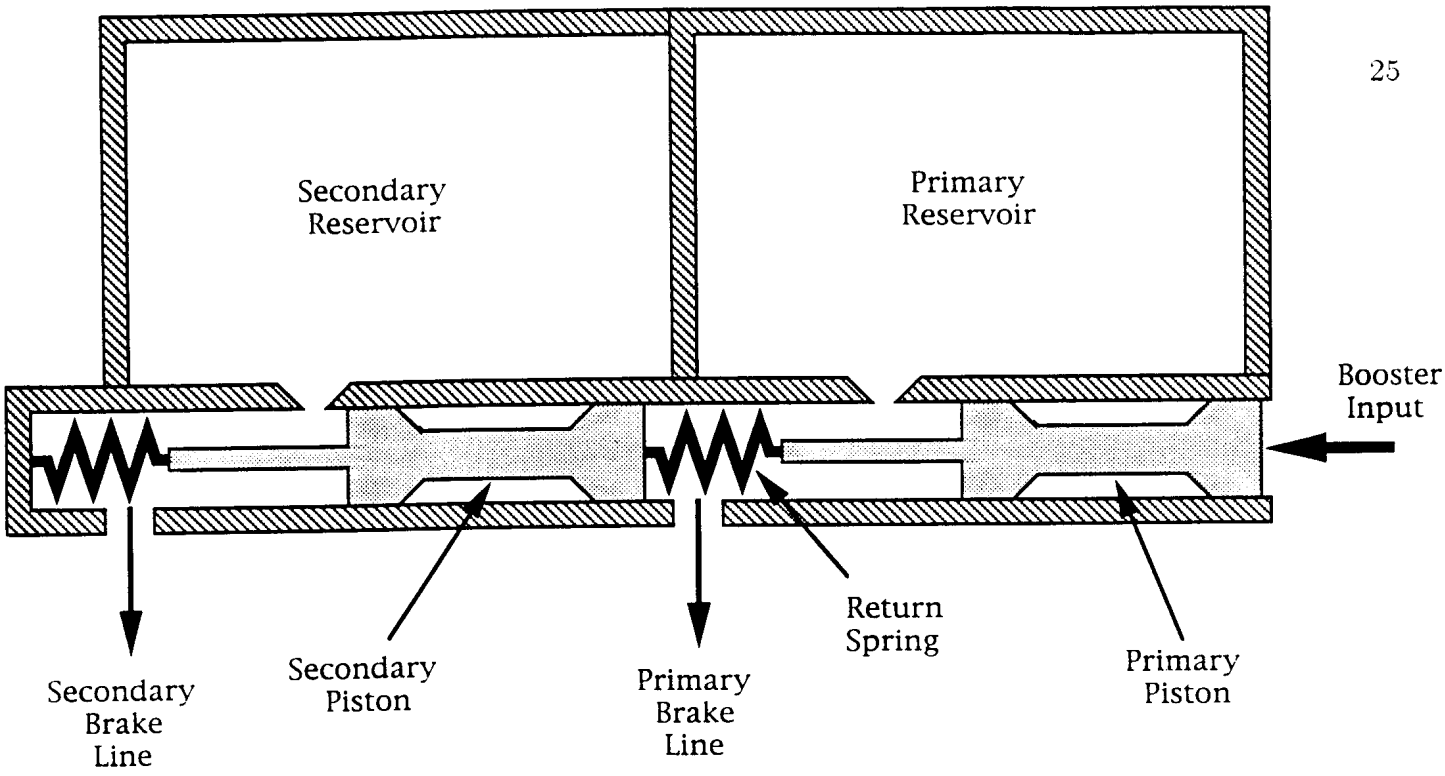

Figure 3.4: Master Cylinder Construction

through the compensating port. Once piston travel becomes sufficient to close this port, however, pressure begins to build and brake fluid is forced into the primary brake line(s). The pressure rise in the primary cylinder also results in a force on the secondary piston, thereby forcing fluid into the secondary brake line(s).

Fisher, [11] developed a detailed model of the master cylinder including such factors as the leakage flow required to prevent air from rushing past the seals during rapid release. Khan et al., [25], using the transformer notation of bond graphs to model the master cylinder, simplified these dynamics while retaining the distance required to close the compensating port. A slightly different approach is used here in that the master cylinder pressure comprises the output rather than the flow. Taking the masses of the pistons to be negligible, these considerations result in a direct transfer of booster force to master cylinder pressure, once the compensating port has been closed.

As will be shown in the following section, the direct transfer of booster force to master cylinder pressure correlates well with experimental evidence. Furthermore, hammer blows applied to the primary piston failed to induce any oscillations in the brake pressure. This evidence serves to rule out significant dynamics associated with

either motion of the primary piston or relative motion between the pistons. Since the only mechanical link between the primary and secondary pistons is the small return spring (Puhn, [32]), such relative motion can occur, but at frequencies well above those of interest.

The force applied by the master cylinder in response to piston motion may therefore be described by:

$$F_{mc} = K_{mc}(x_{mc}) \cdot (x_{mc} - x_{cp}) + F_{ps} \tag{3.16}$$

where K_{mc} is the compliance of the brake lines, fluid and brakes, determined from experimental data, x_{cp} represents the motion of the primary piston when the compensating port closes and F_{ps} is the pre-load on the primary piston return spring. The brake pressure measured at the master cylinder, P_b, is related to the force F_{mc} through the piston area, A_{mc}:

$$P_b = \frac{F_{mc}}{A_{mc}} \tag{3.17}$$

This static representation between force and displacement in the master cylinder correlates well with experimental data, though does remove the fluid flow from direct consideration.

3.3.3 Brake Lines, Valves and Brakes

The brake torque exerted in response to a pressure change in the master cylinder involves numerous variables. Fluid behavior, the fill characteristics of the brakes, brake line length, and frictional variations with regard to temperature and velocity (the so-called 'fade' effect) all contribute to the brake system response (Fisher, [11]). Furthermore, the modeling of such effects is subject to different interpretations, none of which provide a definitive solution (Gillespie, [15]). In order to produce a suitable control model, a compact manner of expressing the dynamics and uncertainties involved with the brakes and brake lines is sought.

For the purpose of longitudinal control, the apportioning of the brake force among the individual brakes is inconsequential; the overall magnitude of the braking

force is the important quantity. Therefore, the combination of the valves and the characteristics of the different brakes may be combined into a single nonlinear mapping between the pressure at the brakes and the brake torque exerted on the vehicle. In essence, the model becomes that of a single equivalent brake. This static gain between the brake pressure and brake torque is highly uncertain (due to frictional variations and fade) and potentially nonlinear (due to variations caused by proportioning valves and the threshold pressures needed to induce braking with drum and disc brakes).

To account for dynamics in the brake lines and the brakes themselves, the relationship between the pressure in the master cylinder and the pressure at the brakes is assumed to exhibit first-order lag characteristics. Therefore, the complete relationship between the brake pressure in the master cylinder, P_b, and the brake torque, T_b, may be written as:

$$\dot{T}_b = \frac{1}{\tau_b}\left(K_b(P_b) \cdot P_b - T_b\right) \tag{3.18}$$

where τ_b is the time constant of the brake line and brake subsystem and $K_b(P_b)$ is the equivalent 'single brake' static mapping discussed above. This representation serves to place the lag between the vacuum assist force and brake torque downstream from the master cylinder in accordance with experimental observation.

3.4 Experimental Validation

The development of the brake model presented above required that some key assumptions be met by the physical system. To verify these assumptions, experimental data was obtained from one of the Ford Lincoln Town Cars associated with the California PATH Program. This vehicle was equipped with a hydraulic actuator used to apply a brake force to the pedal and instrumented to record booster chamber pressures, brake pressure and pedal displacement, among other quantities. In order to isolate the dynamics of the power booster and apply system, tests were performed while the vehicle was stationary and the engine idling. Information on the effects

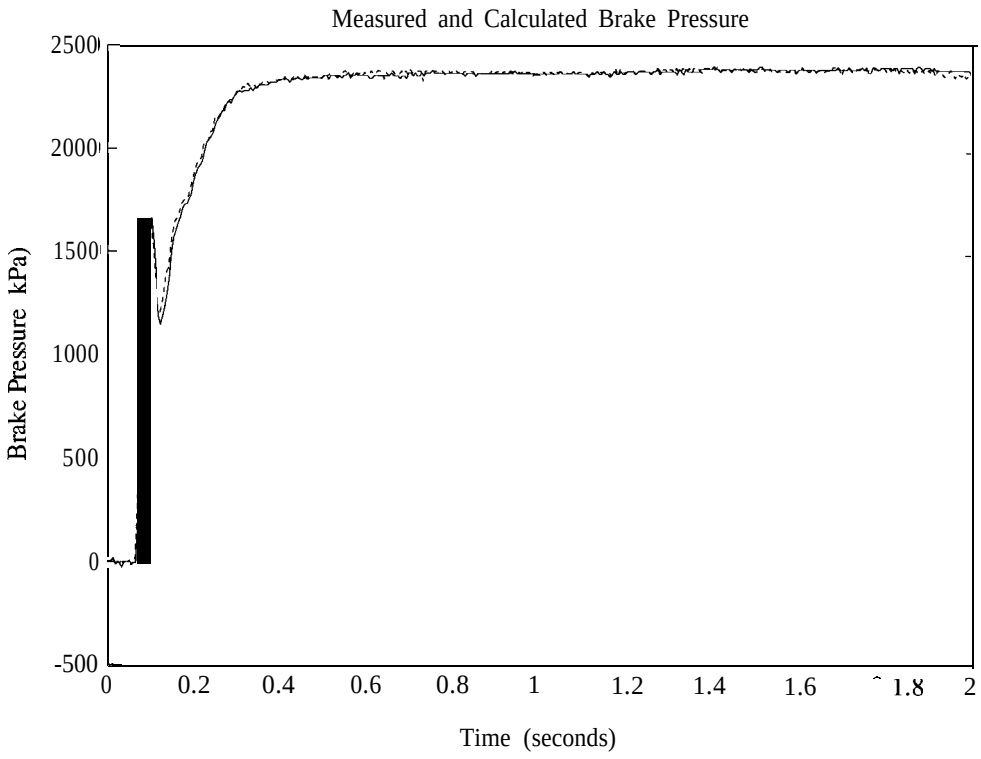

Figure 3.5: Actual and Calculated Brake Pressures

of vehicle motion on brake system dynamics was obtained from moving tests performed at the California Highway Patrol Academy in Sacramento. These tests serve to confirm the major assumptions made in modeling the brake system dynamics.

3.4.1 Inertia of Booster and Master Cylinder

To eliminate unobservable states and reduce the order of the model, the inertia of the booster power piston / diaphragm assembly and the master cylinder piston were neglected. This resulted in a static equation relating the force applied by the booster to the pressures in the air chambers and the displacements of the pushrod and power piston. To test this relationship, measurements of these air pressures and displacements were taken during braking tests and used to calculate the booster force. Figure 3.5 plots the brake pressure based upon this calculated booster force with the actual brake pressure as measured in the primary brake line immediately after the

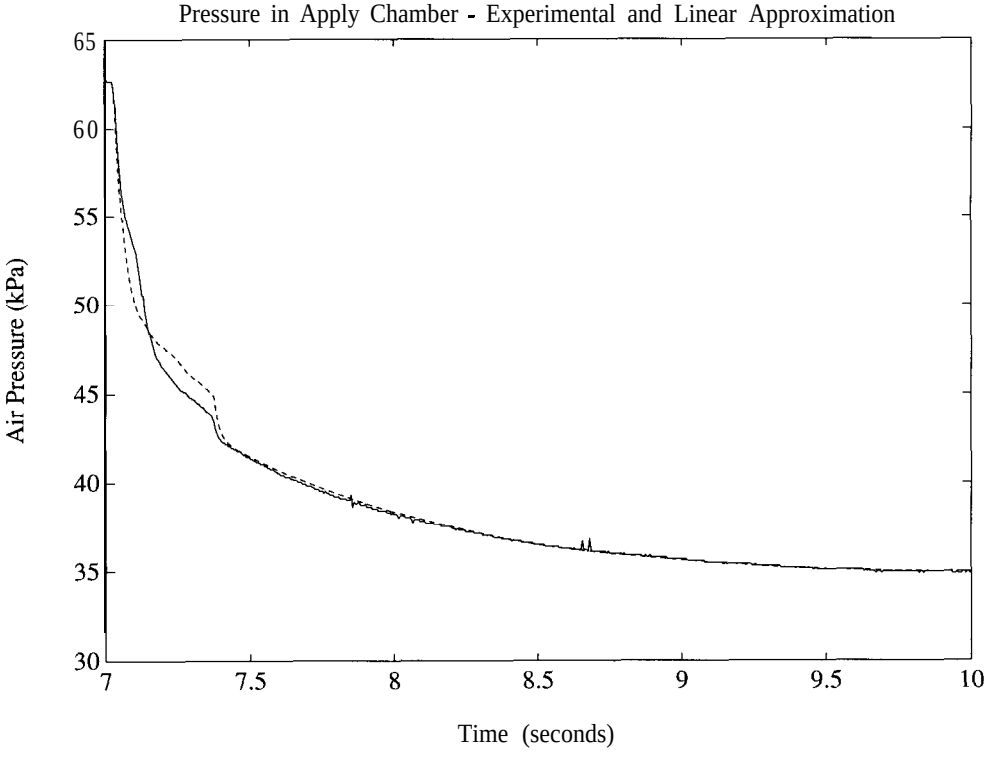

Figure 3.6: Apply Chamber Air Flow During Release Stage

master cylinder.

The close correlation between the calculated and actual pressures confirm that the unmodeled dynamics do not affect system response. The lack of any lags in brake pressure and the close qualitative reflection of the static characteristics in the brake pressure support the omission of this inertia and corroborate the immediate manifestation of brake pressure in the master cylinder. Furthermore, the time delay produced by the inclusion of the lost travel and spring pre-loads matches that exhibited by the system.

3.4.2 Linearized Flow Equations

Since the pressures in the apply and vacuum chambers are coupled during the release stage, errors in the flow model will propagate through both chambers. The release flow is therefore the true test of the linearization. Figure 3.6 shows the

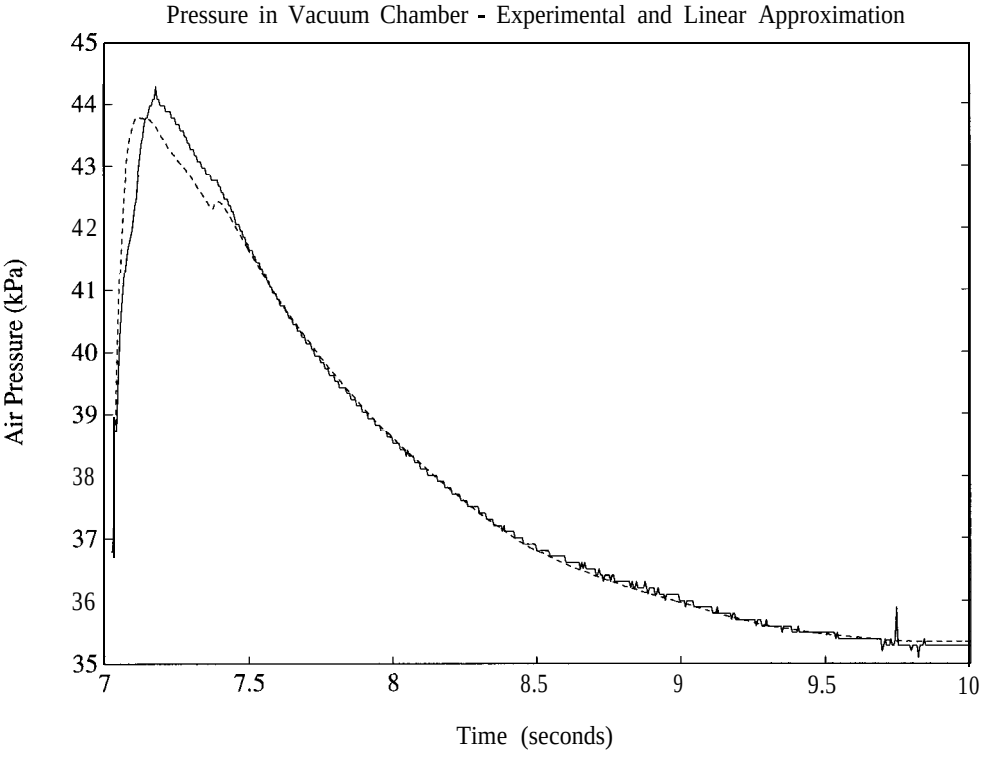

Figure 3.7: Vacuum Chamber Air Flow During Release Stage

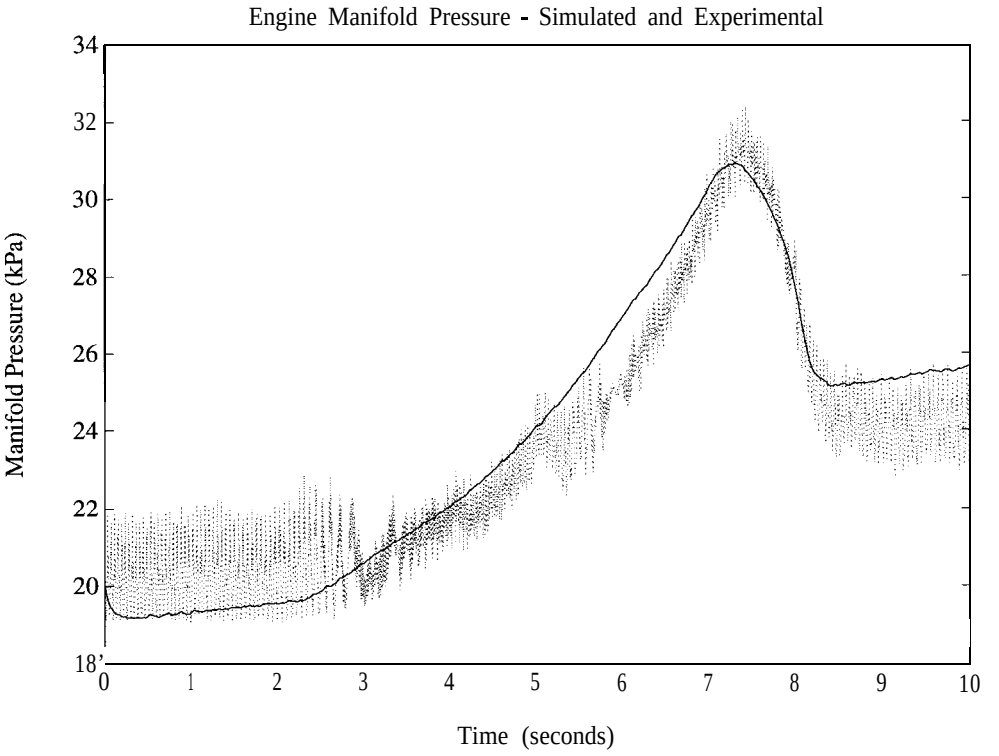

Figure 3.8: Engine Manifold Pressure Variation During Braking

actual pressure in the apply chamber during the typical release stage of a moving test and the pressure as calculated by the linearized flow equations. Although some error results from this approximation, a close qualitative fit remains for both the apply chamber and the vacuum chamber, as shown in figure 3.7. As the later portion of the vacuum chamber plot shows, the flow from this chamber to the manifold is very linear. One discrepancy that did arise in the moving tests was the tendency for the check valve to stick in the open position, allowing air to enter the booster from the manifold. This effect is currently under investigation.

3.4.3 Manifold Dynamics

Figure 3.8 shows the manifold pressure changes during a step braking maneuver initiated at 2 seconds (at a speed of approximately 60 mph) and completed at 7 seconds. While the manifold pressure seems to vary as a result of the braking, the

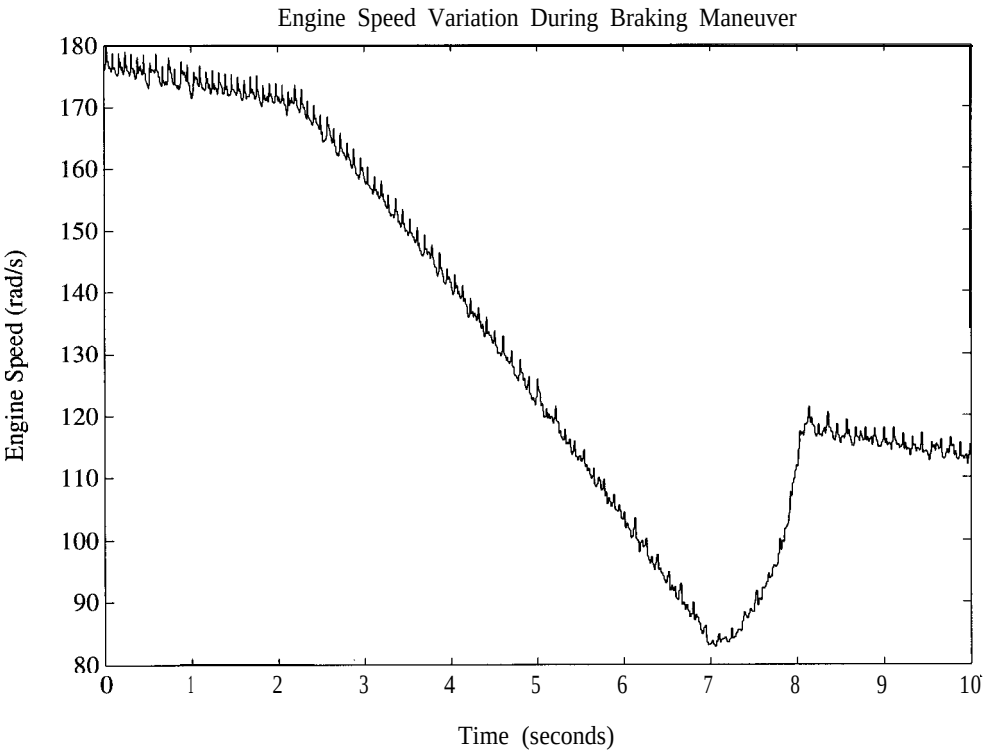

Figure 3.9: Engine Speed Variation During Braking

true source of this variation can be traced to the engine speed, illustrated in figure 3.9. Using the equations for manifold dynamics in Section 3, the pressure evolution was calculated and appears as the solid line in figure 3.8. Some variation between the actual and theoretical pressures are due to pressure variations across the manifold (which show up as 'noise' on the plot) and the fact that the nonlinear volumetric efficiency was calculated using a coarse table look-up. Nevertheless, the nature of the engine speed changes (including the gear shift at approximately 7 seconds) shows up very clearly in the theoretical calculation. Air flow from the booster fails to produce any transients in manifold pressure above those due to engine speed and hence may be safely neglected.

3.4.4 Steady-State Pressure vs. Torque

To experimentally verify the assertion that the steady-state brake torque can be mapped to the brake pressure as with a single equivalent brake, a battery of moving tests was performed. The methodology of these tests consisted of reaching a cruising speed of approximately 55 - 60 mph, shifting the car into neutral and applying a step pedal force. Once the transients due to the hydraulic actuator and the brake system lags decayed, the average brake pressure was measured. The brake torque was found from a force balance of the car (Gillespie, [15]):

$$Ma = -F_b - F_{rr} - C_a v^2 \tag{3.19}$$

The vehicle velocity, v, and acceleration, a, were measured and used to calculate the braking force, F_b, given such parameters as the vehicle mass, M, the rolling resistance, F_{rr}, and the aerodynamic drag coefficient, C_a. Assuming no slip at the wheels, the brake torque of the 'single brake', T_b, is related to brake force by:

$$F_b = \frac{T_b - J_w \frac{a}{r_w}}{r_w} \tag{3.20}$$

where J_w and r_w represent the wheel inertia and radius, respectively.

The results of these tests are shown in figure 3.10. The repeatability of the results was quite high and, furthermore, the torque-pressure curve approaches a fairly linear relationship with a nonzero intercept. Such a relationship compares favorably with results obtained by Fisher, [11] from dynamometer testing of a vehicle equipped with strain gages to measure brake torques. While only so much reliance can be placed on a single 'constant' measure of the gain from brake pressure to brake torque, the general trend is quite clear from the experimental data.

3.4.5 Dynamics of Brakes and Brake Lines

Figure 3.11 shows both the strengths and weaknesses of the simplified brake line model. As is evident from the plot, the brake torque lags the brake pressure (measured just after the master cylinder) and furthermore exhibits first-order filtering effects in the transient response. The time delay at the beginning of the the plot can

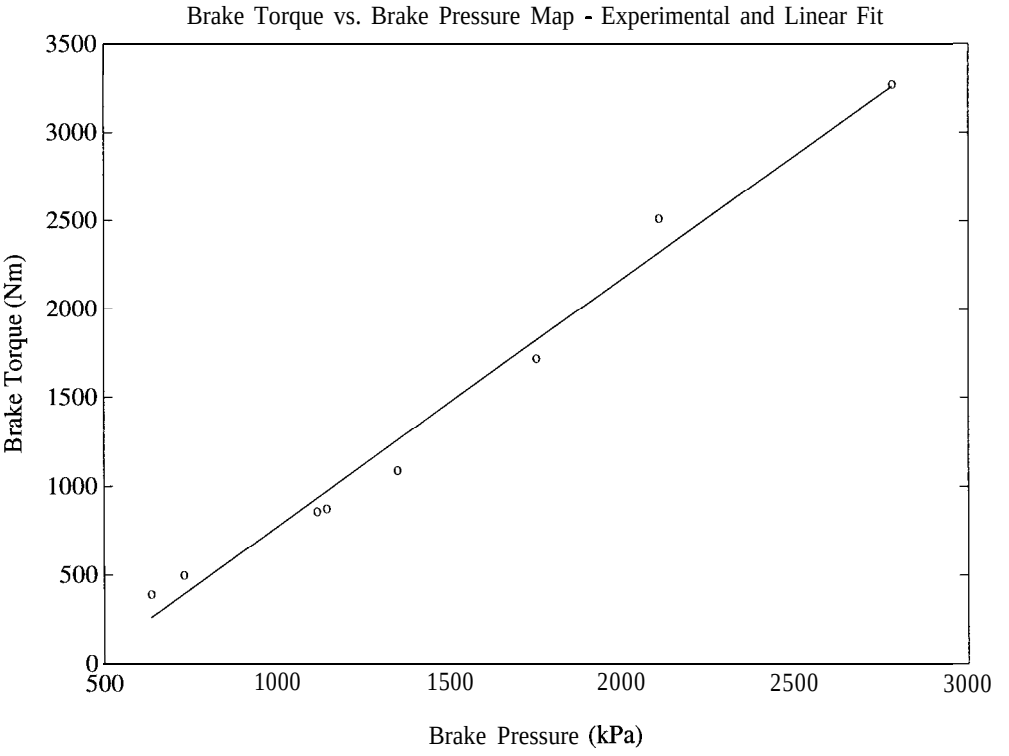

Figure 3.10: Static Brake Torque / Brake Pressure Mapping

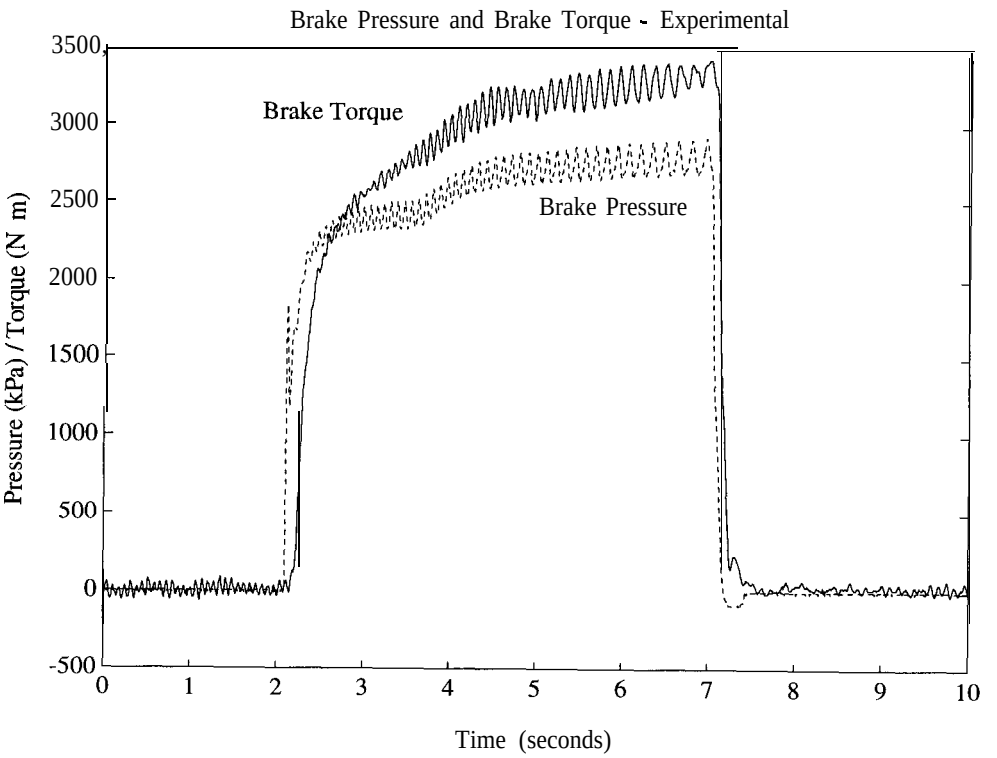

Figure 3.11: Dynamic Effects of Brakes and Brake Lines

be accommodated by an initial dead zone in the brake torque gain, $K_b(P_b)$, suggested by the nonzero intercept in figure 3.10.

The variations in brake torque and pressure visible after the initial transients have decayed result from serious deformation of one of the vehicle's brake drums, perhaps caused by repeated static testing. This deformation causes a 'loading' effect on the master cylinder, the frequency of which varies according to the wheel speed of the car. Since the fluid flow characteristics do not appear explicitly in the model, no mechanism exists for modeling such loading or the slight back flow of fluid in the master cylinder that occurs upon release of the brakes after 7 seconds. While extreme cases of deformation such as this are certainly the exception and not the rule, this example does indicate a limitation of the brake system model.

3.5 Implications for Controller Design

The dynamic model of the braking system presented above suggests several implications for the design of controllers. In phrasing these implications, the controller hardware is assumed to consist of an actuator attached to the brake pedal, though many of these results apply to other actuation schemes as well. The major contributions of this brake system model with respect to control may be summarized as follows.

- The dynamics of the vacuum assist unit have been simplified by the exclusion of the power piston inertia. This transforms the problem of controlling brake pressure to one of controlling the flow of air in the booster by careful positioning of the pedal/pushrod inertia.

- The pure time delay often associated with braking has been embodied in the spring pre-loads, lost travel in the booster and master cylinder and the nonlinear brake torque gain. The effects of these individual nonlinearities on the stability of a closed-loop control scheme may now be clearly observed.

- Since the dynamics of the air flow and compressibility dominate the vacuum assist, the coupling of the booster with the engine manifold has been presented.

Because the manifold dynamics depend upon the engine speed, vehicle maneuvers and brake dynamics are inter-related. A model-based brake controller must therefore either include the manifold dynamics described above or suitably bound out these variations as disturbances.

- A simplified model of brake lines and brakes, encapsulating several uncertainties and nonlinearities in the brake torque gain has been demonstrated. A robust controller must therefore compensate for the uncertainty in this term. Robustness with respect to major deformations in brake drums or discs, unfortunately, is not easily verified by this model, since the fluid flow does not appear explicitly.

Because of the number of nonlinearities involved with even a simplified model of brake dynamics, a robust nonlinear control scheme such as sliding control seems appropriate in this application. This approach also allows for easy incorporation of braking into the current multi-surface longitudinal sliding controller (McMahon et al., [28]). The construction of a such a controller, as well as further validation of the dynamic model presented here, are current research goals.

Chapter 4

String Stability

4.1 Introduction

Automatic Vehicle Following is a way to achieve high traffic capacities (see Shladover, [35]. There are three important aspects to automatic vehicle following:

1. Individual Stability of every controlled vehicle in the platoon: From the safety point of view, and hence, for a proper functioning of the platoon, it is necessary that every controlled vehicle follow its preceding vehicle with a bounded spacing error.

2. String Stability of the platoon : Individual stability of every controlled vehicle does not guarantee the attenuation of maximum spacing errors from vehicle to vehicle along the platoon. If string stability is not assured, it is possible that spacing errors amplify due to some lead vehicle maneuver and may result in a collision in the platoon. Hence, control algorithms should be designed to ensure string stability.

3. Zero Steady State Spacing Errors: Usually, the lead vehicle accelerates and/or decelerates from a steady speed to possibly attain a different steady speed. These maneuvers take only a finite time. It is necessary that, after such lead vehicle maneuvers, every controlled vehicle maintain the desired spacing from its predecessor. As a consequence of achieving this performance objective, safety

and reliable traffic capacities can be assured. However, performance objective (3) can be relaxed for simpler implementation at the expense of traffic capacity and yet satisfy the other two performance objectives. Safety, in such a scheme, is achieved if the steady state spacing error (in other words, the intervehicular spacing) increases with increasing lead vehicle speed.

These aspects of vehicle following have been touched upon by Levine and Athans, [27], Bender, [3], Sheikholeslam and Desoer, [33], Hedrick and Swaroop, [21] and [39]. In this chapter, we will present how communication of information like relative position of the controlled vehicle relative to the lead vehicle, lead vehicle acceleration and velocity, and preceding vehicle acceleration, etc., affect the performance of the platoon. Analysing control algorithms which use different information, serves two purposes:

1. We can, by some metric, determine the algorithms that perform better than others. A natural metric, is the factor with which the maximum spacing errors of vehicles attenuate with the vehicle index (ID) in the platoon. Naturally, the smaller the numerical value of the factor, the better.

2. If a sensor fault is detected, we could possibly reconfigure the platoon to a different control algorithm compatible with the available sensor information and yet have a satisfactory functioning of the platoon.

figure 4.1 illustrates the definitions of intervehicular spacing. Let γ be a

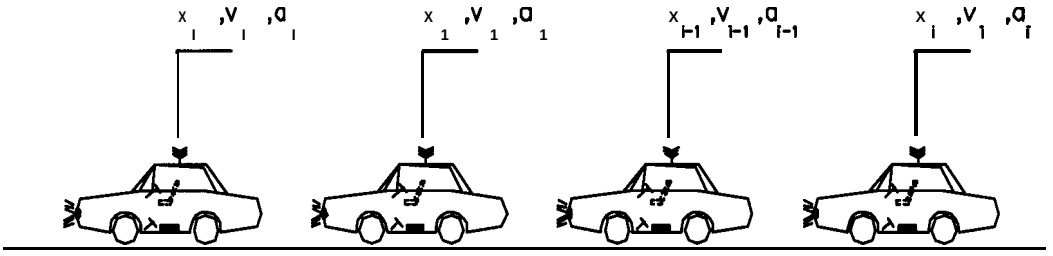

Figure 4.1: Distance between Vehicles in a String

metric for string stability (i.e. the maximum spacing error of the i-th vehicle is less

than or equal to γ times the maximum spacing error of the i-1st vehicle). For details on obtaining γ, see Swaroop et. al., [40]Mathematically,

$$||\epsilon_i||_\infty \leq \gamma||\epsilon_{i-1}||_\infty \tag{4.1}$$

where ϵ_i is the spacing error of the i-th following vehicle. If $\gamma > 1$, it is possible that maximum spacing errors may amplify. For string stability, $\gamma \leq 1$. If $\gamma > 1$, in order to avoid collisions, we can do the following:

1. Increase the intervehicular spacing from vehicle to vehicle by a factor of γ (i.e. the spacing that i-th vehicle maintains from its predecessor is γ times the spacing i-1st vehicle maintains from its predecessor). In other words,

$$L_i = \gamma L_{i-1} \tag{4.2}$$

2. Limit the size of the platoons.

Since we are not altering the control effort, spacing errors can amplify, leading to a high control effort in the vehicles at the tail of the platoon. Therefore, limiting the size fo the platoons, is a natural consequence to avoid saturation. However, this results in a reduction in traffic capacity.

For the sake of analysis for string stability, we will assume the following I/O linearized vehicle model:

$$\ddot{x}_i = u_i \tag{4.3}$$

where x_i is the position of the i-th vehicle relative to some fixed inertial frame, u_i is the control effort. For details on I/O Linearization, refer to Slotine and Li, [37] and Isidori, [23]. The measurements that are available for feedback for every controlled vehicle are as follows:

1. Relative velocity and position from its predecessor.

2. Acceleration of its predecessor.

3. Acceleration, velocity of the lead vehicle.

4. Acceleration of the second vehicle immediately preceding it and the relative velocity and position of predecessor from its preceding vehicle.

Of course, not all the information may be used, to simplify implementation.

4.2 Constant Spacing Control Strategies

4.2.1 Autonomous Control Strategy

In this section, we will consider strategies where the desired intervehicular distance does not change with the speed of the controlled vehicle. Consider the following autonomous control law:

$$u_i = -k_v\dot{\epsilon}_i - k_p\epsilon_i + k_1\dot{x}_i \tag{4.4}$$

where the control gains k_v, k_p, k_1 have to be chosen to satisfy the performance objectives. Then,

$$\hat{g}(s) = \frac{\hat{\epsilon}_1}{\hat{v}_l}(s) = \frac{-s - k_1}{s^2 + (k_v + k_1)s + k_p} \tag{4.5}$$

$$\hat{h}(s) = \frac{\hat{\epsilon}_i}{\hat{\epsilon}_{i-1}}(s) = \frac{k_v s + k_p}{s^2 + (k_v + k_1)s + k_p} \tag{4.6}$$

For individual vehicle stability, $k_v + k_1 > 0$, $k_p > 0$. For zero steady state error due to a finite time lead vehicle maneuver, $k_1 = 0$. For string stability, $k_1 \neq 0$. Therefore, an autonomous control law cannot guarantee string stability and zero steady state errors at the same time. If we let the desired spacing vary linearly with the controlled vehicle speed (thereby, relaxing the zero steady state error requirement), we can guarantee string stability. This is the basis for Autonomous Intelligent Cruise Control (AICC) developed by Ioannou et. al., [22].

4.2.2 Semi-Autonomous Control Strategy

Consider the following semi-autonomous (every controlled vehicle requires its predecessor's acceleration) control law :

$$u_i = k_a\ddot{x}_{i-1} - k_v\dot{\epsilon}_i - k_p\epsilon_i + k_1 v_i \tag{4.7}$$

$$\hat{g}(s) = \frac{(k, -1)s - k_1}{s^2 + (k_v + k_1)s + k_p} \tag{4.8}$$

$$\hat{h}(s) = \frac{k_a s^2 + k_v s + k_p}{s^2 + (k_v + k_1)s + k_p} \tag{4.9}$$

For zero steady state error, $k_1 = 0$. For individual vehicle stability, $k_v + k_1 > 0$, $k_p > 0$. For string stability, $k_a = 1$. It can be shown that this control algorithm does not possess the robustness in string stability due to signal processing/computation lags. figure 4.2 shows the simulation plot of a 5-vehicle platoon without lead vehicle information and with a signal processing lag of 50ms. The numbers in the plot denote the corresponding following vehicle. It can be seen that the maximum spacing errors increase with the vehicle index.

4.2.3 Semi-Autonomous Control with knowledge of vehicle ID

Suppose that, in addition to preceding vehicle acceleration, every controlled vehicle knows its ID in the platoon (no: of preceding vehicles in the platoon), then consider the following control law:

$$u_i = k_a \ddot{x}_{i-1} - k_{v_i} \dot{\epsilon}_i - k_{p_i} \epsilon_i \tag{4.10}$$

$$\hat{h}(s) = \frac{k_a s^2 + k_{v_{i-1}} s + k_{p_{i-1}}}{s^2 + k_{v_i} s + k_{p_i}} \tag{4.11}$$

Individual stability can be established by choosing k_{v_i}, $k_{p_i} > 0$. For string stability, these control gains increase with the vehicle ID. As a consequence, high control effort may be required at the tail of the platoon. Therefore, this scheme limits the size of the platoon and hence, the traffic capacity.

4.2.4 Control with lead vehicle information

Let us now consider a cooperative control architecture, where every controlled vehicle gets some lead vehicle information, in addition to its preceding vehicle acceleration information.

$$u_i = k_a \ddot{x}_{i-1} - k_v \dot{\epsilon}_i - k_p \epsilon_i + k_l a_l - c_v(\dot{x}_i - v_l) - c_p(x_i - x_l + \Sigma_{j=0}^{i} L_j) \tag{4.12}$$

$$\hat{h}(s) = \frac{k_a s^2 + k_v s + k_p}{s^2 + (k_v + c_v)s + k_p + c_p} \quad \textbf{(4.13)}$$

With all the control gains chosen as positive numbers, it can be shown that this algorithm satisfies control objectives (1) and (3). With proper choice of these control gains, γ can be made equal to $\frac{k_p}{k_p + c_p} < 1$ and hence, string stability can be assured. If, the only lead vehicle information available to every controlled vehicle is acceleration, then string stability cannot be ensured. However, the performance of the first controlled vehicle can be improved, thereby, improving the performance of the platoon. If lead vehicle velocity and acceleration information is available, then γ can be made less than unity, i.e. that the maximum spacing errors decrease geometrically with vehicle ID. Also, the robustness in string stability to small signal processing lags can be guaranteed. To implement the latter algorithm, every controlled vehicle needs its position relative to the lead vehicle. This can be obtained in two different ways:

1. by numerically integrating the difference in broadcast lead vehicle's velocity and the controlled vehicle's velocity.

2. by making every vehicle broadcast its position relative to the lead vehicle.

For implementation, 1) can be supplemented by 2). figure 4.3 is the simulation plot with every controlled vehicle having the knowledge of lead vehicle velocity and acceleration information. A 5-vehicle platoon is simulated again, with a signal processing lag of 50 ms. This control algorithm is currently employed for experimentation.

Consider the scenario when the lead vehicle communication system fails. In such a case, we can make the first controlled vehicle broadcast its velocity and acceleration information. If the platoon has a large number of vehicles , there is a significant (pure) transport delay in transmitting the information from the lead vehicle to the controlled vehicles at the tail of the platoon. Often, such delays can degrade the performance. In such a case, a platoon can be broken into miniplatoons of smaller sizes. The last controlled vehicle in the first miniplatoon becomes the lead vehicle for the second miniplatoon and the last controlled vehicle in the second miniplatoon becomes the lead vehicle for the third platoon and so on. This, however, leads to a more complex communication system.

4.2.5 Control with knowledge of two immediately preceding vehicle information

Decentralized controllers that require the information of nearby vehicles are easier to implement than the controllers that require lead vehicle information. The purpose of this section is to show that such schemes lack robustness to string stability and therefore, cannot be used for platooning.

Consider the following alternative control architecture, where every controlled vehicle has access to the information of its two immediately preceding vehicles, i.e

$$u_i = -k_v\dot{\epsilon}_i - k_p\epsilon_i + k_a\ddot{x}_{i-1} + k_l\ddot{x}_{i-2} - c_v(\dot{x}_i - \dot{x}_{i-2}) - c_p(x_i - x_{i-2} + L_i + L_{i-1}) \quad (4.14)$$

Then,

$$\hat{\epsilon}_i(s) = \frac{k_a s^2 + k_v s + k_p}{s^2 + (k_v + c_v)s + k_p + c_p}\hat{\epsilon}_{i-1}(s) + \frac{k_l s^2 + c_v s + c_p}{s^2 + (k_v + c_v)s + k_p + c_p}\hat{\epsilon}_{i-2}(s) \quad (4.15)$$

It can be shown that $||\epsilon_i||_\infty \leq ||\epsilon_1||_\infty$, i.e. that the maximum spacing error of the i-th following vehicle is less than or equal to that of the first following vehicle. This is a weaker version of the string stability. This scheme, however, lacks the robustness to signal processing/computation lags. These results hold even if every controlled vehicle has information of "r" vehicles ahead where "r" is a constant.

4.3 AICC

As mentioned earlier, string stability can be assured with the available onboard information if the desired spacing a controlled vehicle has to maintain from its predecessor, varies linearly with its speed. Define a new spacing error, δ_i, as

$$\delta_i = x_i - x_{i-1} + h_w\dot{x}_i + L_i \quad (4.16)$$

. where h_w is the time headway. Then, the control law is :

$$u_i = \frac{-\dot{\epsilon}_i - \lambda\delta_i}{h_w} \quad (4.17)$$

where $\lambda > 0$. It can be shown that

$$\hat{h}(s) = \frac{1}{h_w s + 1} \tag{4.18}$$

which means that $||\delta_i||_\infty \leq ||\delta_{i-1}||_\infty$ for all $h_w > 0$. If the time headway approaches zero, the spacing error reduces to the spacing error defined in the earlier section. From the previous section, we know that zero steady state error and string stability cannot be satisfied autonomously, at the same time. Hence, there is an inherent limitation on how small h_w can be and this limits the traffic capacity considerably. From the control law, it is clear that the control effort is inversely proportional to the headway.

We can, however, reduce the lower bound on h_w, if the preceding vehicle's acceleration information is available for feedback. With perfect estimation of such an information, the improvement in performance can be seen in figure 4.4 and figure 4.5

Future work will concentrate on the effect of spacing and velocity information of the two immediately preceding vehicles on the string stability of the platoon.

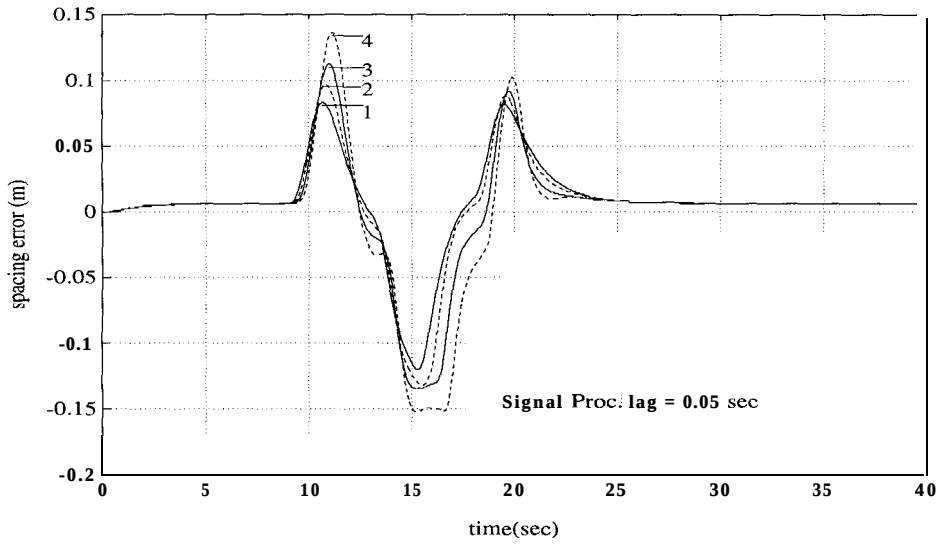

Figure 4.2: Control of a 5-vehicle platoon without lead vehicle information and with a signal processing lag of 50ms

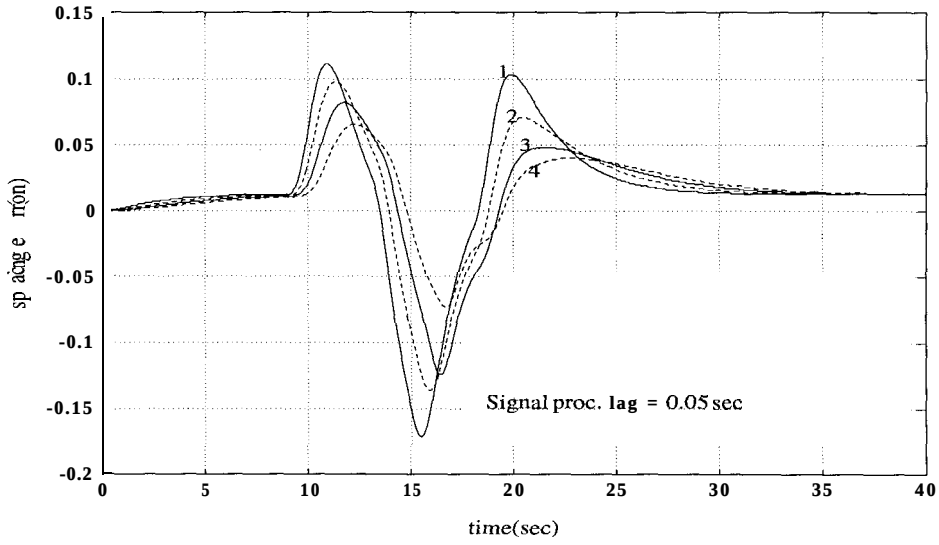

Figure 4.3: Control of a 5-vehicle platoon with lead vehicle velocity and acceleration information and with a signal processing lag of 50ms

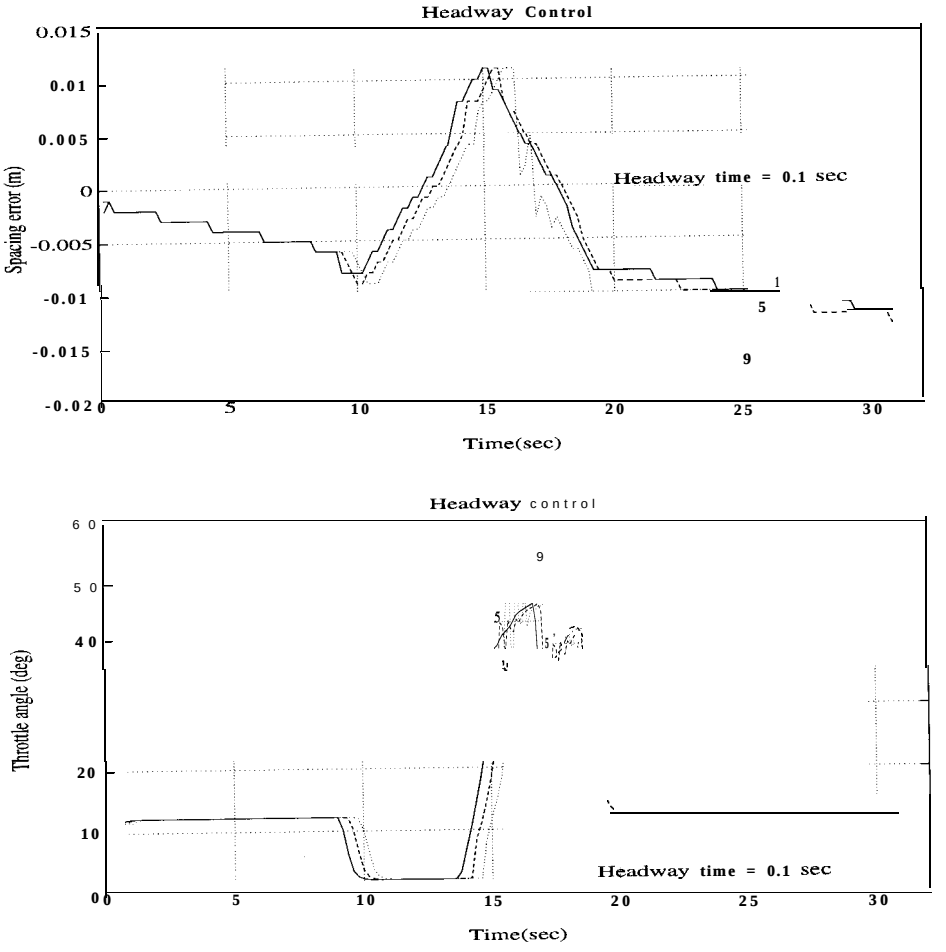

Figure 4.4: Headway Control without predecessor's acceleration information

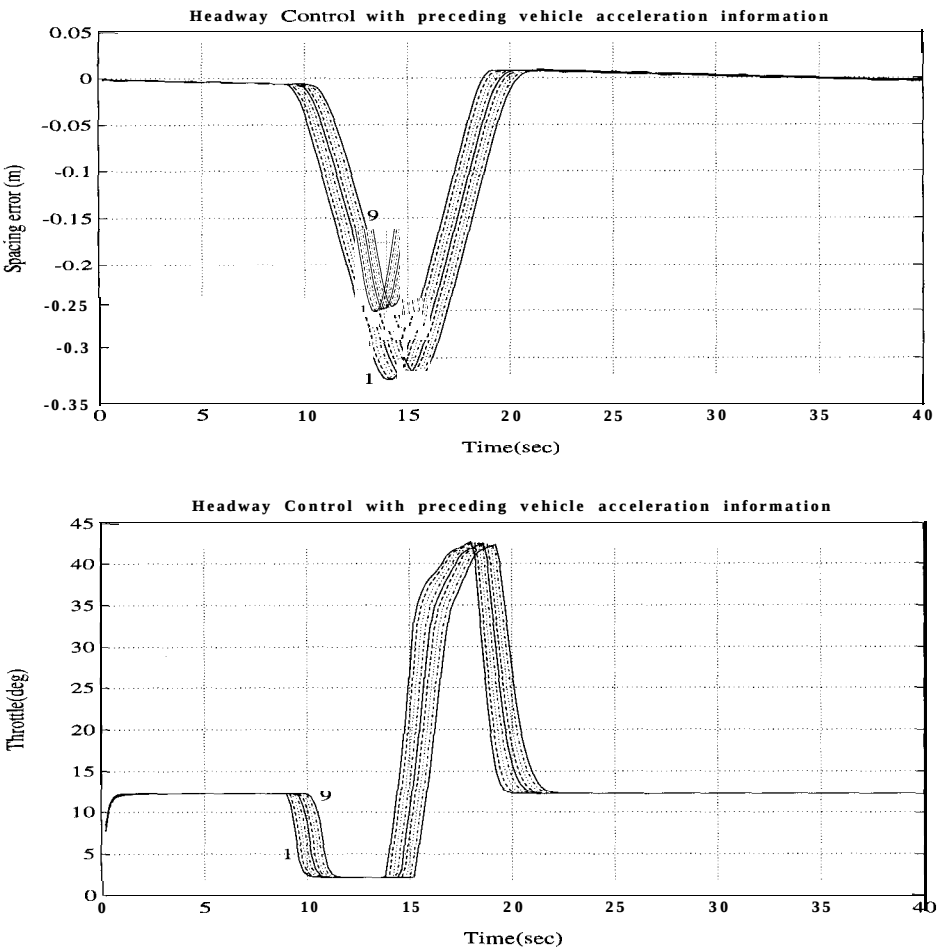

Figure 4.5: Headway Control with predecessor's acceleration information

Chapter 5

Adaptive Control Algorithms

5.1 Introduction

High traffic capacities demand smaller intervehicular spacing in a platoon and hence, there is a need for high performance controllers. Such controllers should ensure individual vehicle stability, string stability and zero steady state error, even in the presence of parametric uncertainty. In this section, we present a Lyapunov-based adaptive control algorithm to compensate for variations in aerodynamic drag coefficient, vehicle mass and rolling resistance friction. Before presenting the adaptive control algorithm, we estimate the maximum variation in mass from its nominal value, which would still ensure string stability. The analysis in the earlier section is based on the assumption that these parameters are known exactly.

5.2 Effect of Parametric Uncertainty on Platoon Performance

5.2.1 Effect of Uncertainty in the mass of the vehicle

For the sake of analysis, consider the following simplified vehicle model:

$$\ddot{x}_i = \frac{u_i - (c_i \dot{x}_i^2 + f_i) sgn \dot{x}_i}{M_i} \tag{5.1}$$

where c_i is the aerodynamic drag coefficient, f_i is the rolling resistance friction, M_i is the effective mass of the vehicle. Assuming that c_i, f_i are known exactly, but M_i is not known exactly, consider the following control law:

$$u_i = \hat{M}_i u_{isl} + (c_i \dot{x}_i^2 + f_i) sgn \dot{x}_i \tag{5.2}$$

where u_{isl} is the control associated with defining a sliding surface :

$$S_i = \dot{\epsilon}_i + q_1 \epsilon_i + q_3(\dot{x}_i - \dot{x}_l) + q_4(x_i - x_l + \Sigma_{j=0}^{j=i} L_j) \tag{5.3}$$

and u_{isl} is chosen to make $S_i = -\lambda S_i$. Hence, u_{isl} is given by:

$$u_{isl} = \frac{1}{1+q_3}[\ddot{x}_{i-1} + q_3 \ddot{x}_l - q_1 \dot{\epsilon}_i - q_4(\dot{x}_i - \dot{x}_l) - \lambda S_i] \tag{5.4}$$

Therefore, we obtain the following transfer function:

$$\hat{h}(s) = \frac{\alpha}{1+q_3} \frac{(s+q_1)(s+\lambda)}{s^2 + \alpha[(\frac{q_1+q_4}{1+q_3} + \lambda)s + \frac{\lambda(q_1+q_4)}{1+q_3}]} \tag{5.5}$$

where $\alpha = \frac{M_i}{M_{i-1}}$. It can be shown that if q_1, q_3, q_4, λ are chosen properly, it is possible to guarantee individual stability, zero steady state error and make $\gamma = \frac{q_1}{q_1+q_4}$ for all $\alpha \epsilon [\alpha_l, \alpha_h]$, where $\alpha_l < 1$, $\alpha_h > 1$. For $q_1 = 3, q_3 = 1, q_4 = 1$, $\lambda = 4$, we have $\alpha_l = .9, \alpha_h = 1.166$. The top plot of figure 5.1 depicts the simulation results for a 5-vehicle platoon. The nominal mass of the vehicle is 2200 kg, while the actual mass of the car is 3300 kg. The aerodynamic drag and the rolling resistance values used in the simulations are 40% less than their actual values.

5.2.2 Effect of Uncertainty in the rolling resistance and mass of the vehicle

With uncertainty in the rolling resistance friction and mass of the vehicle, control effort is given by

$$u_i = \hat{M}_i u_{isl} + (c_i \dot{x}_i^2 + \hat{f}_i) sgn(\dot{x}_i) \tag{5.6}$$

Hence,

$$\hat{\epsilon}_i(s) = \frac{\alpha}{1+q_3} \frac{(s+\lambda)(s+q_1)}{s^2 + \alpha((\frac{q_1+q_4}{1+q_3} + \lambda)s + \frac{\lambda(q_1+q_4)}{1+q_3})} \hat{\epsilon}_{i-1}(s) + \frac{\frac{\tilde{f}_{i-1}}{M_i} \frac{}{M_{i-1}}}{s^2 + \alpha((\frac{q_1+q_4}{1+q_3} + \lambda)s + \frac{\lambda(q_1+q_4)}{1+q_3})} \tag{5.7}$$

Therefore,

$$||\epsilon_i||_\infty \leq \frac{q_1}{q_1+q_4}||\epsilon_{i-1}||_\infty + \frac{(1+q_3)}{\lambda(q_1+q_4)}||\frac{f_i}{M_i} - \frac{f_{i-1}}{M_{i-1}}||_\infty \tag{5.8}$$

Hence, we can only guarantee bounded steady state errors and they depend on the magnitude of $||\frac{\tilde{f}_i}{M_i} - \frac{\tilde{f}_{i-1}}{M_{i-1}}||_\infty$ and $||\frac{\tilde{f}_1}{M_1}||_\infty$.

5.2.3 Effect of Uncertainty in aerodynamic drag

With uncertainty in all the parameters,

$$u_i = \hat{M}_i u_{isl} + (\hat{c}_i + \hat{f}_i)\dot{x}_i^2 sgn(\dot{x}_i) \tag{5.9}$$

The maximum velocity, L, of the vehicle is bounded due to the saturation of the throttle. Therefore,

$$\ddot{\epsilon}_i + \alpha((\frac{q_1+q_4}{1+q_3}) + \lambda)\dot{\epsilon}_i + \frac{\lambda(q_1+q_4)}{1+q_3}\epsilon_i) = \frac{\alpha}{1+q_3}(\ddot{\epsilon}_{i-1} + (q_1+\lambda)\dot{\epsilon}_{i-1} + q_1\lambda\epsilon_{i-1}) + \phi$$

$$|\phi| \leq 2|\frac{\tilde{c}_i}{M_i}|L|\dot{\epsilon}_i| + |\frac{\tilde{c}_i}{M_i} - \frac{\tilde{c}_{i-1}}{M_{i-1}}|L^2 + |\frac{\tilde{f}_i}{M_i} - \frac{\tilde{f}_{i-1}}{M_{i-1}}| \tag{5.10}$$

To guarantee the individual stability of every vehicle in the platoon, we require,

$$\alpha(\frac{q_1+q_4}{1+q_3} + \lambda) > 2\frac{|\tilde{c}_i|}{M_i}L \tag{5.11}$$

The last condition indicates that higher control gains (and hence, higher control efforts) are required to establish the individual stability of every vehicle in the platoon.

If f_i is not known exactly, it leads to non-zero steady state errors. Integral action in the sliding surface can eliminate the steady state errors resulting due to such a mismatch. However, in the presence of uncertainty in the aerodynamic drag coefficient, higher control is required to assure the individual stability of the vehicles in the platoon. Adaptation of these parameters guarantees zero steady state errors. With sufficient excitation (i.e. sufficiently frequency rich maneuver of the lead vehicle – this means that if the change and the frequency content in lead vehicle's speed is high), convergence of parameters to their true values can also be guaranteed.

5.3 Adaptation Laws:

The control law is :

$$u_i = \hat{M}_i u_{isl} + (\hat{c}_i \dot{x}_i^2 + \hat{f}_i) sgn \dot{x}_i \tag{5.12}$$

so that

$$\dot{S}_i + \lambda S_i = \frac{\tilde{M}_i u_{isl} + \tilde{c}_i \dot{x}_i^2 + \tilde{f}_i}{M_i} \tag{5.13}$$

A gradient adaptive algorithm, (see Sastry and Bodson, [38]) can be obtained from the following Lyapunov function:

$$V = M_i \frac{S_i^2}{2} + \frac{\gamma_1 \tilde{M}_i^2 + \gamma_2 \tilde{c}_i^2 + \gamma_3 \tilde{f}_i^2}{2} \tag{5.14}$$

The adaptation laws are:

$$\dot{\hat{M}}_i = -\frac{1}{\gamma_1} S_i u_{isl} \tag{5.15}$$

$$\dot{\hat{c}}_i = -\frac{1}{\gamma_2} S_i \dot{x}_i^2 \tag{5.16}$$

$$\dot{\hat{f}}_i = -\frac{1}{\gamma_3} S_i \tag{5.17}$$

$$\tag{5.18}$$

With parameter adaptation, we can guarantee that the spacing errors go to zero asymptotically. We can also guarantee that the spacing errors are uniformly bounded whenever the initial spacing errors and initial parameter errors are uniformly bounded. Uniform boundedness of spacing errors means that all the spacing errors are less than some constant number. For collision avoidance, the spacing errors should be uniformly bounded by $.5L$, where L is the fixed intervehicular distance to be maintained. Without parameter adaptation (specifically for aerodynamic drag coefficient), we cannot guarantee the uniform boundedness of spacing errors. figure 5.1 shows the simulation results for a 5-vehicle platoon with and without parameter adaptation. With parameter adaptation, it can be seen that the spacing errors go to zero asymptotically. Without parameter adaptation, we can see that there are non-zero steady state errors. For the simulations, we have assumed that all the

vehicles are identical and also that all the values of the parameters, true and initial estimates, are the same. If this were not true, the steady state spacing errors would not have decreased with vehicle index, when there was no adaptation. figure 5.2 shows how the parametric estimates behave during adaptation. We can see that the inertia parameter converges quickly to within 10% of its true value. Since the velocity of the lead vehicle changes from 15-16 m/s, it is too small a variation in velocity to distinguish between the contribution of aerodynamic drag and rolling resistance friction.

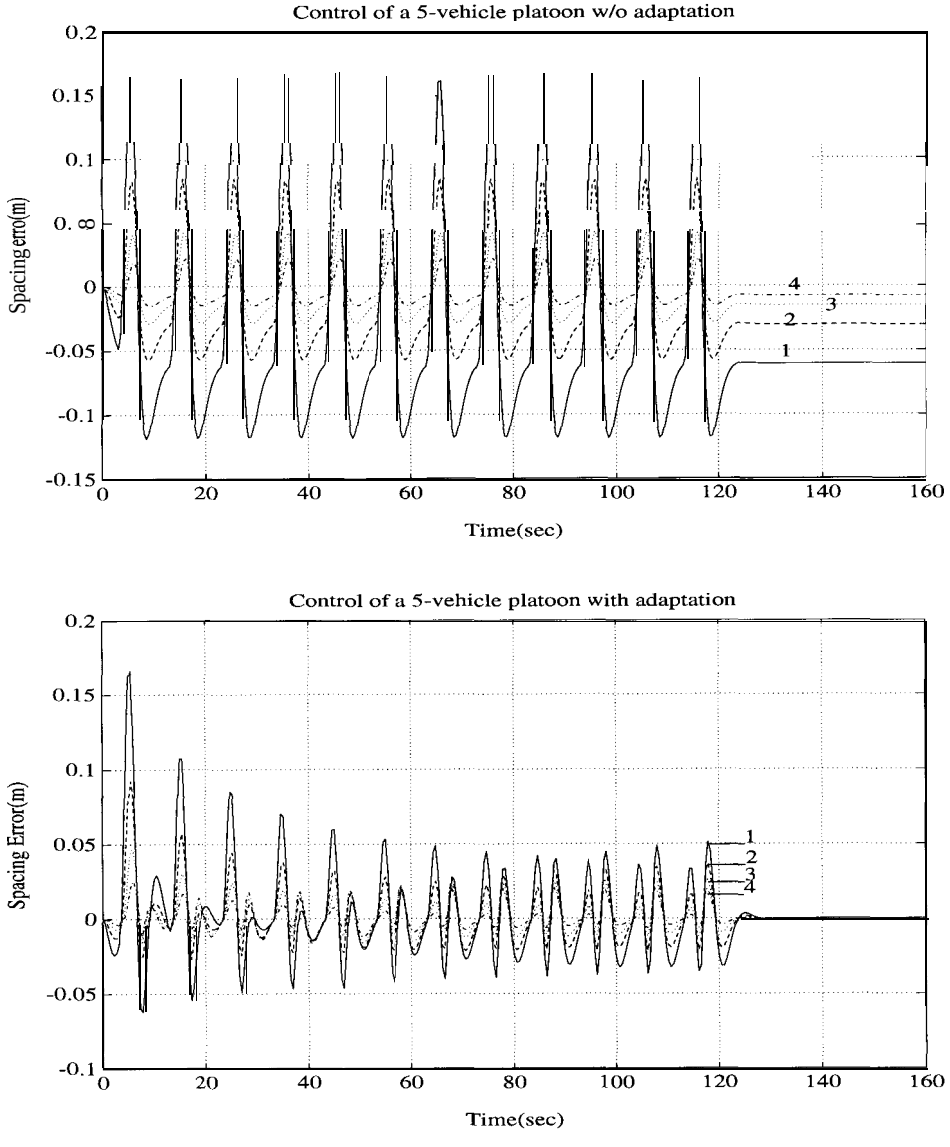

Figure 5.1: Comparision of spacing errors with and w/o parameter adaptation

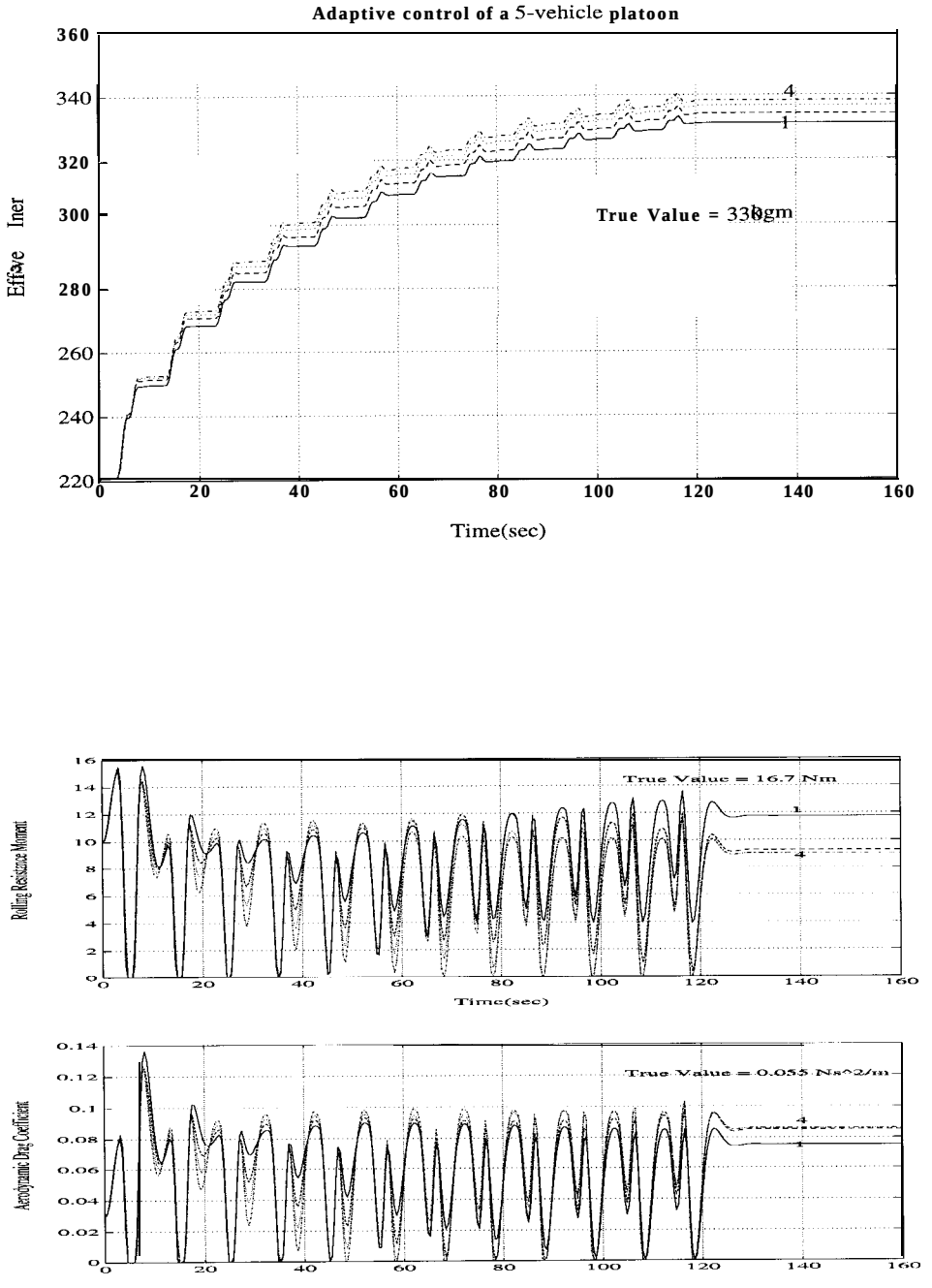

Figure 5.2: Parameter estimates during adaptation

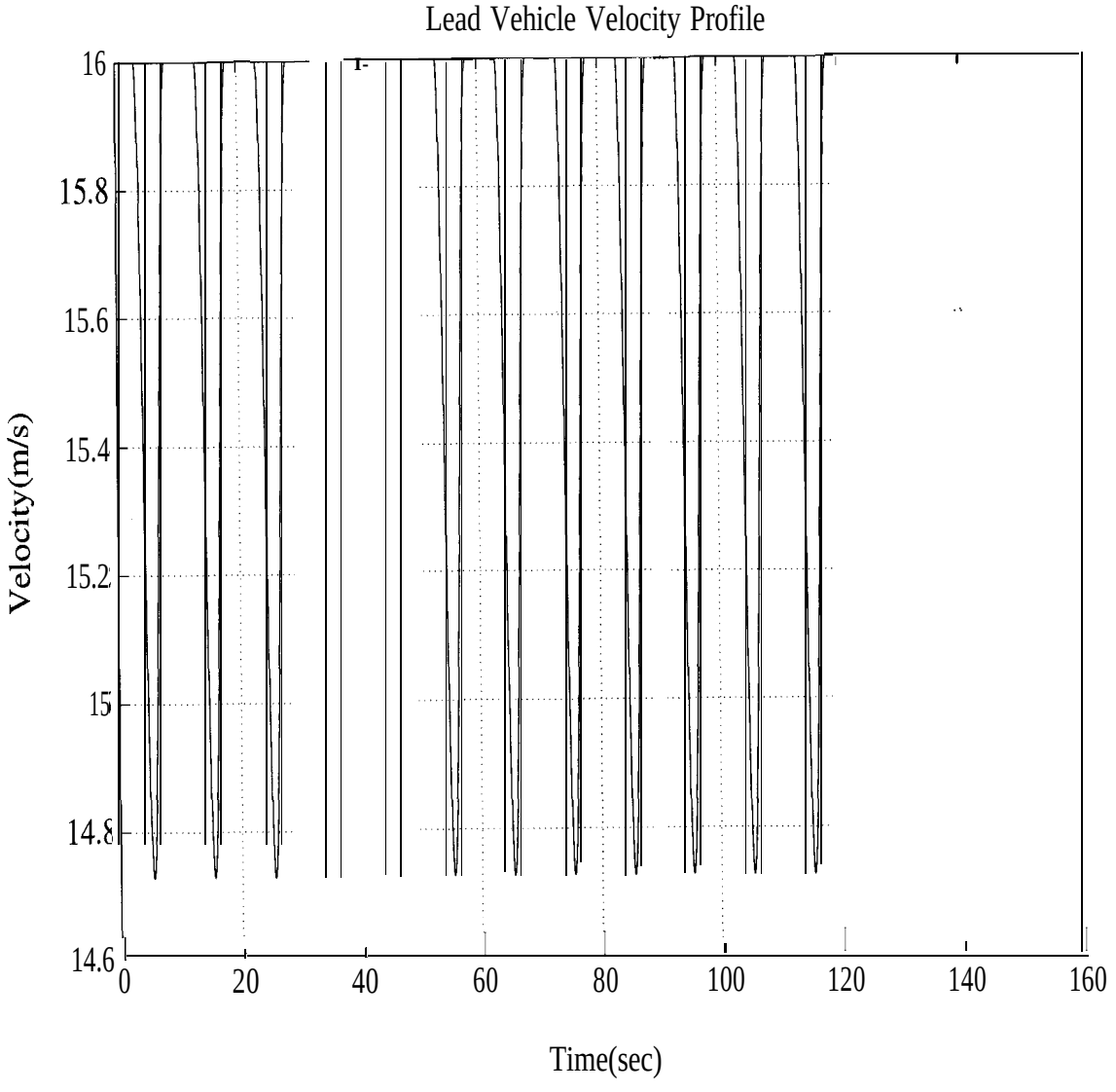

Figure 5.3: Lead Vehicle Velocity Profile

Chapter 6

Fault Tolerant Longitudinal Control of Vehicle Platoons

Fault tolerant control refers to control of systems with emphasis on minimizing performance degradation in event of faulty behavior of sensors, actuators or other system components. It involves ascertaining safe behavior of the system in emergency situations. Fault tolerant control is increasingly becoming a priority in systems that demand high degree of performance, reliability like aircraft flight control. Automated vehicle systems are heavily dependent on sensor measurements like radar spacing measurements, vehicle speed measurements, vehicle-vehicle communication etc. Hedrick and Garg [17]showed that faulty measurements or faulty throttle/brake actuator performance could deteriorate the platooning performance and may even cause accidents. Therefore, it is imperative to study issues regarding the ability of the system to detect faults early enough and if detected whether there could be a backup strategy, even if suboptimal, that would ensure satisfactory performance.

Our research focus has been in general to develop fault detection schemes that can be applied to general nonlinear systems. The dynamics of automated highway systems (both lateral and longitudinal) is nonlinear in nature, for example, aerodynamic force is proportional to square of velocity, table lookups are used for nonlinear engine maps between engine speed, indicated torque,throttle angle.

6.1 Fault Detection

One of the facets of an efficient Fault Tolerant control system is diagnosing faults promptly and identifying the faulty element. The subject of Fault Detection and Identification has been studied extensively especially in linear time invariant dynamical systems. Some of the often used methods are : 1. Detection filters 2. Parity Space methods 3. Parameter Identification methods 4. Kalman Filter banks.

Parity space methods are open loop schemes which look for changes in analytical relations between state variables called parity equations to detect faults. The main disadvantage of this method is the fault residuals (fault carrying information) can be lost after a finite amount of time. This could result in a missed fault detecton.

Parameter identification methods are difficult to extend to nonlinear systems as nonlinear systems identification is a difficult task in itself.

Kalman Filter banks are often used in linear systems for fault diagnostics and their obvious advantage is that the sensor noise characteristics can be taken into account too. But, the extended Kalman filter version which is used for nonlinear systems is computationally very intensive for large systems as the filter gains are computed online.

Detection filters are essentially observers designed such that the output residuals, i.e. the difference between the actual output and the observer output vector, exhibit directional properties corresponding to the fault that has occured. Needless to say, that the directionality property exploited in detection filters in linear systems is not easily translated to nonlinear systems. The problem of nonlinear systems fault detection is coupled to the nonlinear observer problem which is still in the rudimentary stage in controls research. We show that in the case when all state information is available and the nonlinearity is Lipschitz fault detection filter can be designed. We have also shown that this can be directly applied to the longitudinal control problem, see Garg and Hedrick [13].

6.2 Detection Filter Design

The detection filter designed for the longitudinal control problem is essentially a Luenberger observer with the following simplification.

- Torque converter dynamics is neglected.

The most important property of the filter is to estimate states accurately in absence of faults and to indicate faults by exhibiting directional growth of output residuals in presence of faults. The filter gain is chosen high enough to counteract the nonlinearity and thereby force the error dynamics (error between actaul states and estimator states) to behave linearly, in order to extend the theory of detection filters developed for linear systems. It turns out that even with high estimator gain, for general Lipschitz nonlinear systems, all states need to be measurable, which is often too much to ask for. High gain estimators result in lower steady state values of the residuals. Therefore, the choice of the filter gain has to be a compromise. High estimator gain has another disadvantage namely noise in sensor measurement would get amplified, therefore, sensor measurements should be filtered of its high frequency components before being used.

When all states are not measurable, banks of system observers can be used such that each observer is independent of one measurement and therefore if that measurement is faulty, the corresponding observer will not be faulty whereas all other observers would be faulty. Though this seems to be a reliable method of fault detection, the underlying assumption is that the system be observable from all combinations of measurements after leaving one out. Moreover, this methodology is computationally intensive because the number of observers required is equal to the number of measurements and in any system with many states, this would be problem. Detection filters on the other hand, are capable of detecting many faults with one filter. Therefore, fault detection would be possible and in addition, an estimate of the faulty measurement would be available for control purposes. In this paper the fault detection is capable of detecting only one fault at a time. To detect simultaneous faults more redundancy would be necessary.

6.3 Sensor Fault Detection

List of sensors used in longitudinal control :

- Engine speed sensor
- Vehicle wheel speed sensor
- Radar/Sonar
- Intake Manifold pressure sensor
- Throttle angle sensor
- Brake pressure sensor
- Accelerometer

Since engine speed, vehicle speed, inter-vehicle spacing, brake torque (directly related to brake pressure), mass air flow rate (related to manifold pressure) are states in the system we can formulate our problem such that these sensor measurements are directly under surveillance through the detection filter. In addition, the redundancy in the vehicle dynamic system can be exploited. Examples of the redundancy present are :

- Direct relation between engine speed and wheel speed at high gear positions.
- Inter-vehicle spacing is available from the radar/sensor and can be estimated by inter-vehicle communication too.

6.4 Actuator Faults

Throttle actuator and brake actuator faults are considered in this study. Actuator faults are modeled similar to sensor faults in detection filter design, see Garg and Hedrick [13].

6.4.1 Throttle Actuator Fault

An issue that arises immediately is how to differentiate between faults in sensors and actuators, since the number of residuals available is equal to the number of the sensors. From the longitudinal dynamics context, if the residual corresponding to the engine speed starts growing, the cause could be either the engine speed sensor or the throttle actuator malfunctioning (aasuming the intake manifold dynamics are fast compared to the rest of vehicle dynamics). This problem can be obviated by checking the throttle angle measurement from the throttle angle sensor. If the desired throttle angle is significantly different from the throttle angle sensor measurement and the engine speed residual is growing then it can be concluded that the throttle actuator is malfunctioning and if the throttle angle sensor shows a value tracking the desired throttle angle then the engine speed sensor is faulty. If the discrepancy between the throttle angle sensor measurement and the desired value is significant but the engine speed residual is not, then the conclusion would be the throttle angle sensor is playing tricks.

6.4.2 Brake Actuator Fault

Brake actuator faults can be detected similar to throttle actuator detection. The corresponding residual is the brake torque state in the longitudinal dynamic model. Brake actuator fault can be concluded if the brake torque residual is high and the difference between the brake pressure measurement and the desired brake pressure is significant.

6.5 Signal Reconstruction

Since faulty information can destabilize the closed loop system tracking it is necessary to regenerate lost information by some means. In this section, we show how in event of sensor faults, the state information can be reconstructed.

6.5.1 Engine Speed Sensor Failure

Alternative ways to estimate engine speed in event of the engine speed sensor failure are:

- Use intake manifold dynamics and engine maps available as table lookup. Manifold pressure sensor, and throttle angle sensor measurements can be used to estimate the engine speed.
- Assuming locked torque converter, the engine speed is related to the wheel speed by a known constant factor, which depends on the transmission ratio.
- An observer can be constructed using other measurements like wheel speed, mass air flow rate, radar/sonar. This method relies on the observability of engine speed from other measurements.

6.5.2 Wheel Speed Sensor Failure

- Wheel speeds of the front and rear wheels are available, either could be used, thereby giving some redundancy.
- Engine speed multiplied by a factor.

6.5.3 Radar/Sonar Failure

Alternative measurements are:

- Inter-vehicle communication can be utilized to reconstruct spacing information between vehicles when radar/sonar measurements are not available. Since speed of the previous vehicle is communicated back and the estimate of own vehicle's speed is available using the observer, the relative speed can be calculated. Therefore, the closing rate is known and can be integrated in intervals to find the range.

6.5.4 Manifold Pressure Sensor Failure

- Engine speed sensor and throttle angle sensor can be used to estimate the manifold pressure, when the manifold pressure sensor has failed.
- It has been shown that considering manifold dynamics is not critical for longitudinal control as manifold dynamics is much faster than the rest of the vehicle longitudinal system. Therefore, loss of the manifold pressure may not be an emergency issue.

6.6 Safety Measures for Actuator Faults

6.6.1 Throttle Actuator Fault

The following are some of the options available in the event of a throttle actuator failure to prevent a disaster.

- Equip each vehicle with a redundant throttle actuator which can be used when the regular one has failed. Startup for the replacement actuator will not be a problem because the throttle actuator speed of 400 degrees/sec. is fast enough to catch up to any reasonable desired speed requirement. The mechanism of the switch needs to be worked out.

- A possibility could be to use the brake actuator to slow the vehicle down and essentially designate the vehicle in question as the lead vehicle temporarily, for the rest of the platoon. After ascertaining a safe speed, the cruise control in the vehicle could be activated to cruise at that speed, and the platoon tracks a lower speed until the 'sick' vehicle is able to exit the automated lane with manual control. It is assumed that the cruise control is independent of the throttle actuator function. Obviously, an alarm should be sounded to all vehicles in the platoon about the state of the vehicle in question, promptly.

6.6.2 Brake Actuator Fault

- A redundant brake actuator is recommended to avoid emergency situations under a brake actuator failure. An issue to be looked into, with a redundant brake actuator, is the time lag associated with the brake dynamics, which will result in delay in the new brake being effective promptly.

6.7 Experimental Results

6.7.1 Single Vehicle Speed Tracking

Single vehicle speed tracking tests were done in Sacramento and various sensor faults were simulated at freeway speeds. The faults simulated were fault in vehicle speed sensor, engine speed fault and throttle actuator fault.

Experimental results for the case of the vehicle speed sensor failure are shown in Figures 1 and 2. To simulate the vehicle speed sensor fault the control algorithm was given a faulty vehicle speed measurement which was one and a half times the actual measurement after 10 seconds of steady operation. The vehicle started slowing down since the vehicle controller thought that the vehicle is going too fast and so tried to slow it down. The fault was detected in the vehicle speed residual immediately. After detecting the fault, the vehicle speed was reconstructed using the engine speed measurement. The tracking error is satisfactory after reconstruction as seen in Figure 2 . The vehicle speed sensor had to be filtered since it was noisy.

6.8 Conclusions

The problem of fault detection and signal reconstruction for various sensors used in the longitudinal control system of the vehicle has been addressed. Experimental verification for the vehicle speed sensor failure and information reconstruction was done. Throttle and brake actuator faults are being studied too with an aim to develop some backup plan for emergency situations.

6.9 Future Work

- Experimental verification of throttle and brake actuator fault detection.
- Quantitative evaluation of the fault detection system developed in terms of false alarms/sensitivity issues.
- Improvement in fault detection methodology for general nonlinear systems. Formalization of fault tolerance in systems will be attempted because fault tolerant control strategies used in research so far have been largely adhoc.

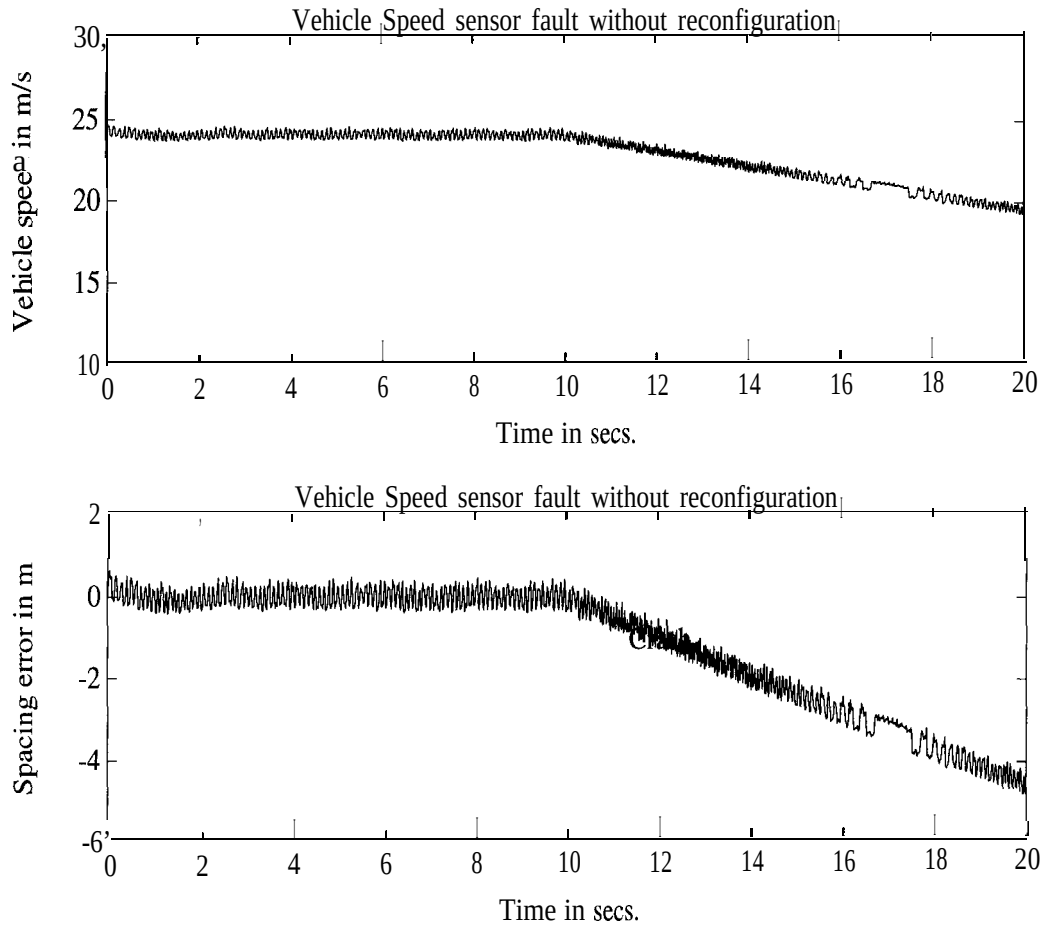

Figure 6.1: Speed Profile and Spacing Error w/o reconstruction

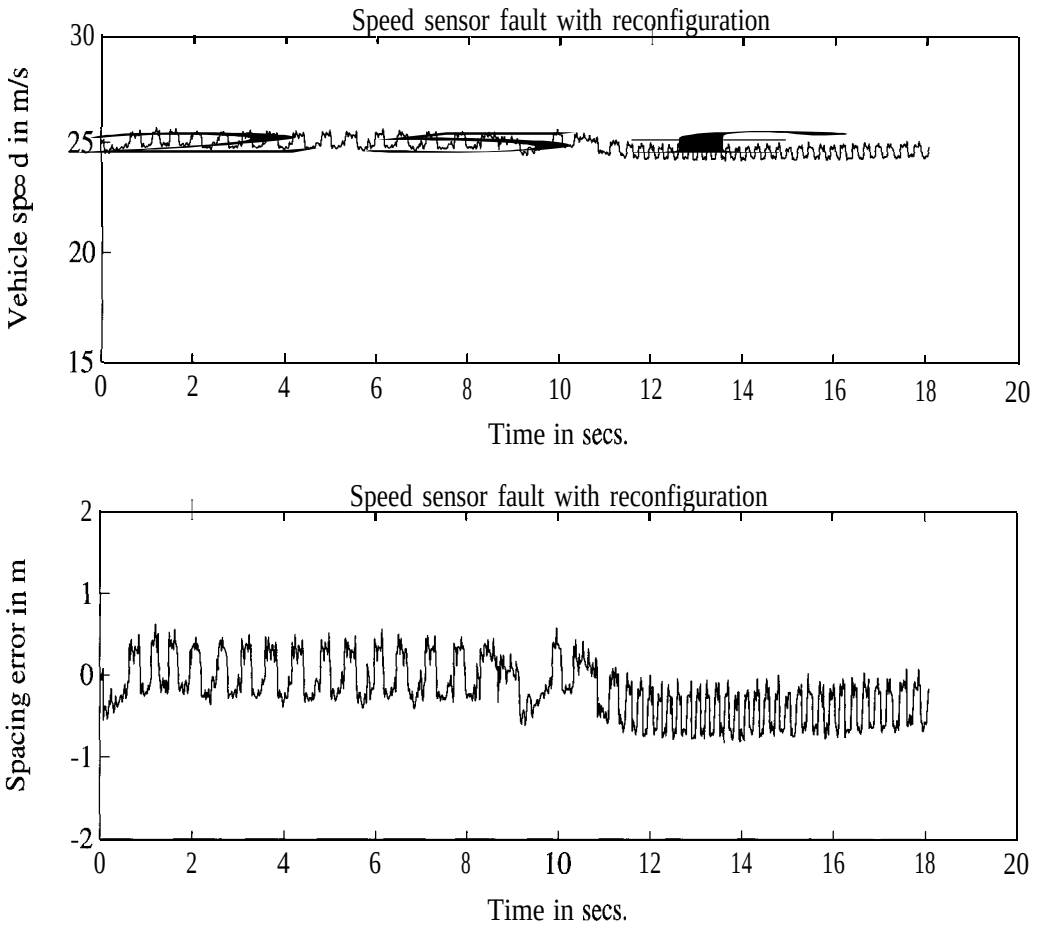

Figure 6.2: Speed Profile and Spacing Error w/ reconstruction

Chapter 7

Experimental Platoon Development

7.1 Introduction

This chapter evaluates the performance of several spacing control laws developed for the longitudinal control of a platoon of vehicles. Of principal concern is to determine how controller model fidelity/complexity affects the stability of individual vehicle in a platoon. To meet this objective a two part analysis was adopted. Firstly, the performance of each controller is evaluated on an individual basis. Implementation on an actual system can be markedly different than as predicted by a simulation model. Secondly, the comparative performance of the controllers were studied. Since the controllers are all model-based, ideal performance occurs when the controller is implemented on the exact system from which it was designed. The criticality of the mismatches between controller model and vehicle system will be examined through comparative performance studies.

A brief overview of the simplified model from which all controllers are based is presented in section 7 . 1 Since the vehicle model is nonlinear we employ the techniques of sliding control for control design. The structure of three longitudinal controllers of interest are given along with their corresponding modeling assumptions. An outline of the structure of the Experimental Platoon Control System (EPCS) is

given in section 7.2. The major hardware components of the EPCS are discussed. Details of the operating environment and software used to run/coordinate the EPCS hardware are elaborated upon in section 7.3. Experimental test results for a two car platoon are given in section 7.4. Tracking profiles and performance criteria for evaluating controller performance are specified. The chapter concludes with a summary of performance of the three control designs.

7.2 Longitudinal Control Designs

7.2.1 Baseline Control Model

The simplified model on which the control laws summarized in this chapter are based was presented in chapter 4. The model consisted of four states:

1. m_a , mass air in the intake manifold
2. ω_e, engine speed
3. ω_t, turbine speed
4. T_b, brake torque applied to wheels.

Under certain assumptions about the state of the vehicle the above model can be further simplified for control design purposes. Since throttle control algorithms were only being evaluated, the state associated with the brake dynamics will be dropped from further discussion. For a more complete control design incorporating this state see Hedrick et. al., [18] and [19].

7.2.2 Control Design

This section briefly outlines the structure for the sliding controllers that were evaluated experimentally. We present the control designs in order of increasing

complexity.

Controller A

Controller A is based upon a single state reduced order model. In this development we make the following assumptions about the dynamics of the model presented in section 2.1:

1. manifold dynamics are negligible

2. the torque converter is locked.

The remaining state equation is therefore:

$$J_e^* \dot{\omega}_e = T_{net}(\omega_e, m_a(\alpha)) - T_{load} \tag{7.1}$$

where J_e^* is the effective engine inertia and T_{load} is the effective load on the engine under assumptions 1 & 2. T_{net}, the net engine torque is a direct function of the throttle angle α. For exact expressions for these quantities see Hedrick et. al., [19].

Following the sliding control formulation adopted by Hedrick et. al., [18] we define a scalar error surface:

$$\dot{S}_{1i} = \dot{\epsilon}_i + q_1 \epsilon_i + q_2(v_i - v_{lead}) \tag{7.2}$$

Differentiating the above equation and utilizing the state equation for engine dynamics we define the desired net engine torque,

$$T_{net,des} = J_e^* \dot{\omega}_{e,des} + R_g^* h F_{f,total} + C_a R_g^{*3} h^3 \omega_e^3 \tag{7.3}$$

where

$$\dot{\omega}_{e,des} = \frac{a_{i-1} - q_1 \dot{\epsilon}_i - \lambda S_{1i} + a_{lead}}{(1+q_2) R_g^* h} \tag{7.4}$$

The throttle angle can be simply determined by inverting the closed form expression for net engine torque or via a table look up procedure

$$\alpha_{des} = f cn^{-}1(T_{net,des}, \omega_e) \tag{7.5}$$

Controller B

We relax assumption (1) of the previous design allowing for the inclusion of intake manifold dynamics. The resulting reduced order dynamics are therefore:

$$\dot{m}_a = MAX\ PRI(\frac{P_m}{P_{atm}})TC(\alpha) - c_1\eta_{vol}(m_a,\omega_e)m_a\omega_e \tag{7.6}$$

$$J_e^*\dot{\omega}_e = T_{net}(\omega_e, m_a) - T_{load} \tag{7.7}$$

where J_e^* and T_{load} are identical to those given for Controller A.

Given the increased complexity of the system we use the multiple sliding surface technique (see Hedrick et. al., [18], Green and Hedrick [16]). The first surface is identical to that of Controller A. However, from the desired net torque we calculate a desired mass of air in the intake manifold. A unique value is guaranteed for a particular value of net engine torque and engine speed. This value can be determined either from a functional inversion or a table search procedure. Given a desired mass air we define:

$$S_{2i} = m_a - m_{a,des} \tag{7.8}$$

Following the sliding surface approach we ultimately define a desired throttle characteristic as:

$$TC_{i,des}(\alpha_{des}) = (\dot{m}_{ao} + \dot{m}_{a,des} - \lambda_2 S_{2i})/(MAX\ PRI(\frac{P_m}{P_{atm}}) \tag{7.9}$$

The desired throttle angle is readily determined from a inversion of the desired throttle characteristic.

Controller C

Utilizing the full state model again adds an additional level of complexity to the control structure. The first surface is identical to that of the previous two designs. However, from the desired net torque we define a desired transmission turbine torque, $T_{turb,des}$ as:

$$T_{turb,des} = J_t^*\dot{\omega}_{t,des} + R_g^* h F_{f,total} + C_a R_g^{*3} h^3 \omega_t^3 \tag{7.10}$$

where

$$\dot{\omega}_{t,des} = \frac{a_{i-1} - q_1\dot{\epsilon}_i - \lambda S_i + a_{lead}}{(1 + q_2)R_g^* h} \tag{7.11}$$

and J_t^* is the effective turbine inertia. Using the dynamic relationships for the torque converter or a table search procedure a desired engine speed is determined. We now define an error surface as:

$$S_{3i} = \omega_e - \omega_{e,des} \tag{7.12}$$

Differentiating this equation and following the sliding formulation we can define desired net engine torque as:[1]

$$T_{net,des} = T_{pump}(\omega_e, \omega_t) + J_e^*(\dot{\omega}_{e,des} - \lambda_3 S_{3i}) \tag{7.13}$$

The rest of the control design is identical to that of the previous case from this point on. A final surface is defined as:

$$S_{2i} = m_a - m_{a,des} \tag{7.14}$$

and ultimately,

$$\alpha_{des} = TC^{-}1(TC_{des}) \tag{7.15}$$

7.3 Experimental Platoon Control System (EPCS)

A schematic diagram of the Experimental Platoon Control System (EPCS) is shown in figure 7.1. The EPCS is composed of the following hardware components:

- Test Vehicle(s)
- 486 based personal computers
- Vehicle Sensors

[1]Note that the effective engine inertia J_e^* used in equation 7-13 is NOT the same as in equations 7-1,7.

- Throttle actuator
- Brake Actuator
- Differential vehicle position sensors (Sonar)
- Digital radio transceivers and communication interface boards
- Data acquisition boards
- Data storage systems.

The test vehicles are 1990 Ford Lincoln Town Cars equipped with 5.0 liter V-8 electronically fuel injected (EFI) engines. Exact vehicle parameters are given in Hedrick et. al., [19].

The standard vehicle sensors have been supplemented with additional sensors for control purposes. Engine variables such as the manifold pressure, manifold temperature, mass air flow (through throttle body), the engine speed, and the throttle angle are available as sensor inputs to the Electronic Control Module (ECM). The manifold pressure is a product sensor mounted in the intake manifold. The temperature sensor consists of a resistor whose resistance varies as a function of temperature. A nominal value however is used for longitudinal control purposes. Mass air flow rates out of the intake manifold are determined via a hot wire anemometer mounted in the intake manifold. Engine speed is calculated using a Hall Effect sensor (Magnetic Pickup) mounted on the engine flywheel. The magnetic pickup generates 4 pulses/revolution of the flywheel. There is no post-processing the signal from the engine speed sensor. The throttle plate position is determined using a potentiometer.

Powertrain measurements downstream from the engine consists of the transmission gear state, pump speed, transmission speed, wheel speed, vehicle speed, vehicle acceleration, and the brake line and actuator supply pressures. The transmission gear state is determined automatically from engine speed and the throttle position. The technique cannot however differentiate between first and second gear states. The pump and turbine speeds are determined directly from the engine and wheel speeds

respectively. Hall effect sensors mounted on the rear wheels provide wheel speed measurements. The magnetic pickup generates 50 pulses/revolution and passes a divide by 10 counter to get the appropriate frequency range. The number of pulses per rotation does not permit accurate wheel speed measurements below 1.8 m/s. The vehicle velocity is calculated from the wheel speed sensor on some cars and a Hall effect sensor on the transmission for other models. Therefore the velocity measurement is not a true velocity measurement. Vehicle acceleration is measured via a single axis accelerometer mounted on the floor of the passenger compartment. The sensor is capable of measuring accelerations between $+/-1$ g. However, since the accelerometer is single axis vertical motion of the vehicle can degrade the accuracy of the measurement. Standard Pressure sensors have been installed in the actuator pressure lines and the brake lines to provide those measurements. The brake actuator and line sensors have limits of 500 psi and 3000 psi respectively.

The throttle plate is controlled by a stepper motor with a maximum speed of 900 steps/sec and a step size of 0.9 degrees/step. A feedback control unit has been added to the stepper motor configuration to ensure desired positioning.

The brake line pressure is controlled via a undirectional (push only) hydraulic actuator which acts directly on the brake pedal via a linkage system , see Gerdes et. al., [14]. Springs ensure pedal return during periods of decreased desired braking pressures.

Differential vehicle information was available using a sonar system mounted at the center of the front grills of the vehicles. The sonar system was capable of determining range (i.e. inter-vehicle spacing) measurements. Closing rate measurements were not available using this technology. Soon to be available are a radar system and an optical triangulation system. The radar system will provide range, closing rate, and absolute vehicle speed. The optical system produced by the Qualimatrix Corp. is expected to provide range and lateral position.

Communication between vehicles is performed using a radio link through spread-spectrum digital transceivers. Each of the transceivers is controlled by a communication interface board installed in the on board computer. Radio communication is accomplished via two cellular phone type coaxial antennas. The preceding vehicle

transmits its time clock, vehicle speed and acceleration to the following vehicle.

All measurements are input to a National Instruments AT-MIO-16 data acquisition board. The signals are first conditioned by a PATH interface board before passing to the AT-MIO-16. Signal outputs form the data acquisition board are then processed by the platoon control software. Data storage is controlled by the platoon control software.

The EPCS uses the sliding control algorithms described in section 7.1. In the two car platoon, the controller in the following car uses a maximum of eleven measurements in addition to the measurements transmitted from the preceding vehicle. The actuation signals calculated by the algorithm command the throttle and brake actuators via the data acquisition board. During these tests only throttle control was used.

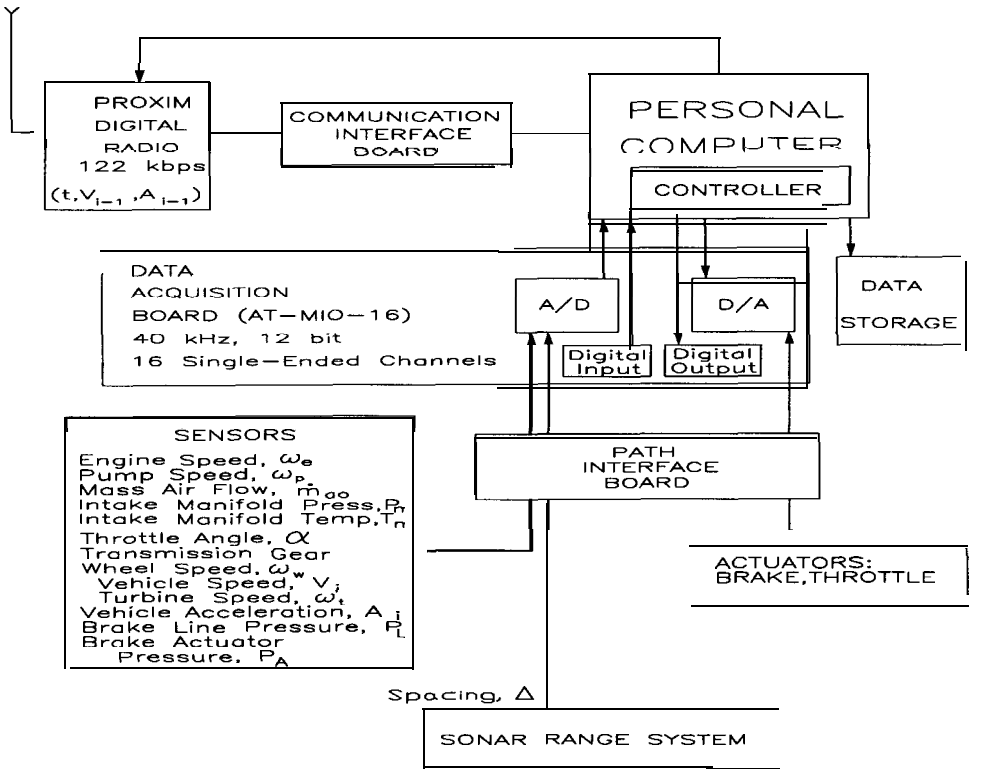

Figure 7.1: Overall System Configuration

7.4 EPCS Software and Operating Environment

The Experimental Platoon Control System (EPCS) software is a modified version of the Computerized Engine Control (CEC) software package developed by Seibum Choi for the Vehicle Dynamics Laboratory at Berkeley, see Choi and Hedrick, [7]. The EPCS software utilizes the XIGNAL real time control software for time management. The software consists of C-programs with some standard C-graphics functions running on an MS-DOS platform. Currently the EPCS software is running a 20 msec sampling interval with all control calculations being completed in 1 msec and 19 msec idle time. The XIGNAL software is actually capable of sampling intervals of lmsec. Therefore EPSC sampling intervals may be pushed as low as 2-5 msec.

The EPCS software is a menu-driven package composed of three screens. The first screen allows for specification of system inputs and outputs as well as display options via simple cursor movements and alphanumeric inputs. The results of the selected display items are displayed on the second screen. Up to eight sets of data can be displayed on a total of four windows. The display output can also be displayed in real time on the third screen, both numerically and graphically.

The system inputs specified on the first screen consist of control gains, control time step, program run time, data acquisition time step, tracking profile inputs (single car tests only), defining single/multiple car variable and file names, outputs to be display on screens 2 and 3, and outputs to be stored on the hard drive. All data storage to the hard drive is executed only after program completion.

The EPCS software is a sequential program executing the following tasks:

- Data Acquisition
- Control Calculation
- Control Signal Output
- Graphic display
- Data Storage.

Data storage and graphic display are turned off during program execution to increase program speed. Since the sonar device used for range measurements is a stand alone system its output is input directly to the data acquisition board (via the PATH interface board). No post-processing of the sonar signal in software is required thus also permitting increased program speed. Although not explicitly equipped with error checking tasks/routines the ECPS permits diagnostic analysis via real time monitoring of displayed outputs.

7.5 EPCS Experimental Results

Since the principal objective of this study was to evaluate the level of complexity of model based controllers necessary for **acceptable** performance we chose to use a single vehicle. The preceding vehicle information was generated from a mathematical profile implemented in software. This allows for removal of additional variables that could affect controller performance.

For this study we adopted qualitative as well as quantitative performance criterion. Acceleration and velocity of the trailing vehicle were required to track smoothly and with zero steady state error. This smoothness requirement is motivated by the fact that the vehicle may track the desired profile accurately but violate acceleration and jerk limits. This requirement can therefore be quantified in terms of maximum acceleration and jerk. The position tracking criteria is to minimize position tracking error. This is motivated primarily from a platoon safety perspective.

The experimental testing was conducted at the California Highway Patrol Academy in Sacramento, CA. The straight portions of the test track were used for testing in order to remove potential coupling effects between lateral and longitudinal dynamics. The tests were partitioned into low speed and high speed maneuvers. The marked difference between the maneuvers was designed to expose regions of critical differences in controller performance.

7.5.1 Low Speed Tests

At the beginning of each test sequence the vehicle was accelerated under manual control to the desired initial velocity. At this point the vehicle was switched to automatic longitudinal control while the lateral dynamics remained under driver control. The first 5 seconds of the desired profile maintained the constant initial velocity. This design attempts to remove the effects of different initial conditions on the evaluation of controller performance. After this initial phase the "lead" vehicle executed a 0.1Hz sinusoidal velocity profile.

The control gains for the primary surface for all three controllers were identical during all tests ($q_1 = 5.65$, $q_2 = 1.0$, $\lambda_1 = 0.4$). Similarly, Controller B and C had identical control gains for the manifold dynamics error surface ($\lambda_2 = 40$). Figures 7.2 to 7.16 show the tracking for the 0.1Hz sinusoidal maneuver. Velocity and acceleration tracking performance was improved by the inclusion of manifold dynamics into the control design. Figures 7.3, 7.4, 7.7 and 7.8 illustrate the effect of increasing the gain of the manifold dynamics surface on velocity and acceleration following. The improvement in velocity and acceleration tracking was accompanied by a small increase in the jerk levels. The effect of an increase in λ_2 is also evident in the improved tracking of the second surface variables (see Figures 7.10 and 7.11). Inaccurate tracking during low values of mass air (small manifold pressures) was due to lower physical saturation limits of the mass air. The inclusion of torque converter dynamics into the control design (Controller C) offered no appreciable improvement in performance.

7.5.2 High Speed Tests

The tests at high speed were subdivided into two types: (1) constant velocity and (2) acceleration maneuvers. Several different desired trajectories were designed for the acceleration maneuvers. The functional form of the desired velocity and

Case	Δ V(m/s)	f(Hz)	w = $2\pi f$	$a_{max}(m/s^2)$
1	0.4	0.2	1.26	0.5
2	1.6	0.1	0.62	1.0
3	0.8	0.2	1.26	1.0

Table 7.1: Velocity and Acceleration desired profile parameters

acceleration profiles, respectively, were:

$$V = \begin{cases} V_o & 0 \leq \text{t} \leq 5 \\ V_o + \Delta V(1 - cos(\omega(t-5)) & 5 < \text{t} < 5\text{+}.5\text{f} \\ V_o + 2\Delta V & \text{t} \geq 5\text{+}.5\text{f} \end{cases}$$

$$A = \begin{cases} 0 & 5\text{+}0.5\text{f} \leq \text{t}; \text{t} \leq 5 \\ \omega\Delta V sin(\omega(t-5)) & 5 < \text{t} < 5\text{+}0.5\text{f} \end{cases}$$

where the various values for f, ω, and ΔV are given in the table below: Note, as was the case for the low speed tests, a constant cruising initial time interval of 5 seconds was adopted. Only Controllers A & B were evaluated during these tests. The torque converter is physically locked at these velocities and consequently Controller C reduces to Controller B in these cases.

The control gains for the primary surface for the controller were identical during all tests ($q_1 = 5.65$, $q_2 = 1.0$, $\lambda_1 = 0.4$). Tracking results for a desired constant cruising velocityof 24 m/s are shown in figure 7.17 to figure 7.24. Excluding the manifold dynamics from the controller design (Controller A) resulted in small oscillations about the desired velocity (figure 7.17) and the desired acceleration (figure 7.19). Controller B eliminated such oscillations (figures 7.18 & 7.20). The spacing errors for both controllers were excellent with steady state errors of less than 6 cm.

Controller B demonstrated superior performance over Controller A for the first acceleration maneuver ($a,,, = 0.5\,m/s, f = 0.2\,Hz$). The oscillations about the steady state values indicative of controller A were again eliminated by Controller B. The vehicle acceleration was notably more smoothe and accurate for latter control design. (compare figures 7.27 & 7.28).

Results of subjecting the vehicle to a more harsh maneuver (Case 2: a_{max} = 1.0 $m/s, f$ = $0.1\,Hz$) are shown in figures 7.33 to 7.38. Figures 7.33 and 7.35

reveal that velocity and acceleration tracking was slightly smoother for the simpler control structure, Controller A. Controller B exhibited a significant lag in tracking the desired mass air (figure 7.30, t = 7 sec) resulting in a corresponding overshoot in velocity tracking. This overshoot phenomenon is more apparent during the third acceleration maneuver (Case 3: $a_{max} = 1.0\ m/s, f = 0.2\ Hz$, figures 7.40 to 7.47). The closed loop pole for the mass air error surface was not chosen sufficiently fast ($\lambda_2 = 30$). The performance improvements resulting from increasing this gain was demonstrated during the low speed tests. This pole should also be at least as fast as the corresponding open loop pole(s). Controller B again demonstrated quicker, less oscillatory of steady state values. Excluding initial condition effects, transitional and steady state position errors of 20 cm and 5 cm, respectively, were achieved during Case 2 (figure 7.30). Although Controller B performance for case 3 was not as good as that of Controller A, a peak velocity overshoot of 0.5 mph is still tolerable.

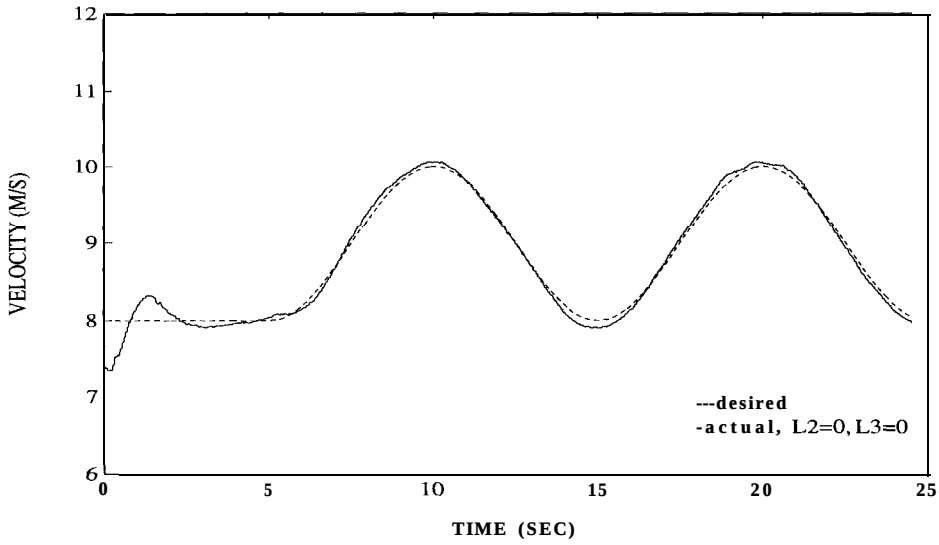

Figure 7.2: Vehicle velocity tracking - Controller A ($\lambda_1 = 0.4$)

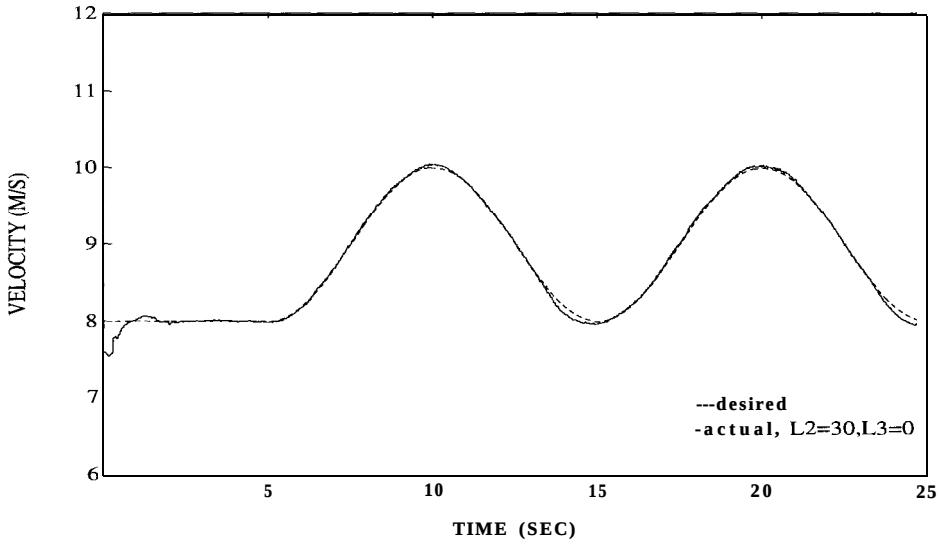

Figure 7.3: Vehicle velocity tracking - Controller B ($\lambda_1 = 0.4$, $\lambda_2 = 30$)

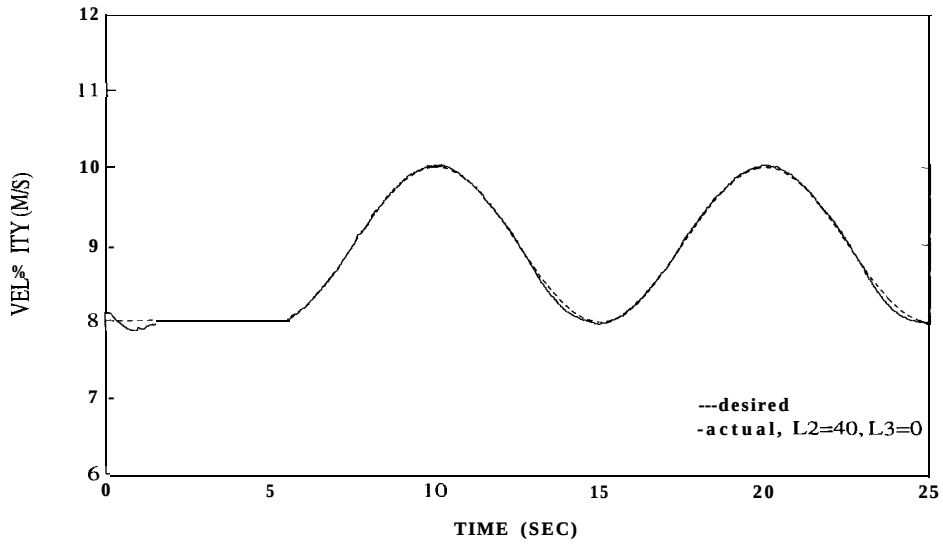

Figure 7.4: Vehicle velocity tracking - Controller B ($\lambda_1 = 0.4$, $\lambda_2 = 40$)

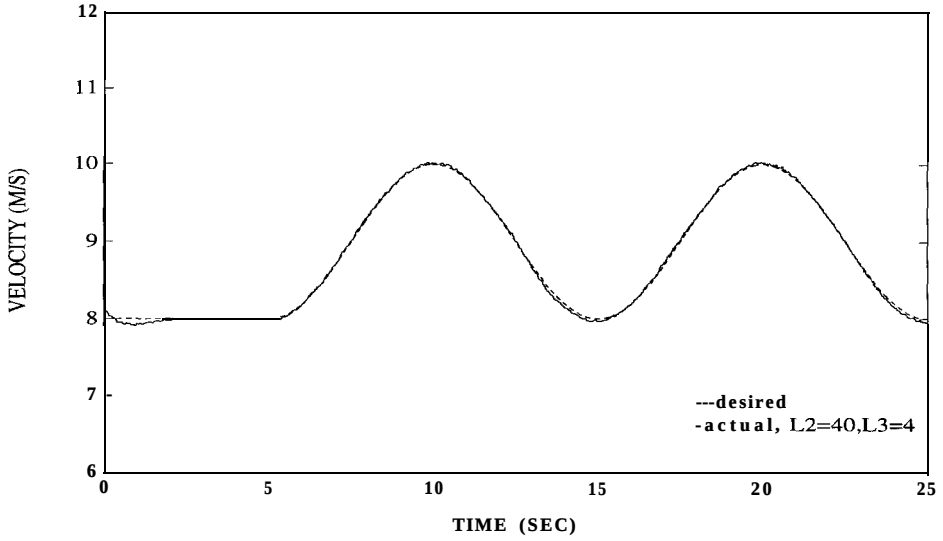

Figure 7.5: Vehicle velocity tracking - Controller C ($\lambda_1 = 0.4$, $\lambda_2 = 40$, $\lambda_3 = 4$)

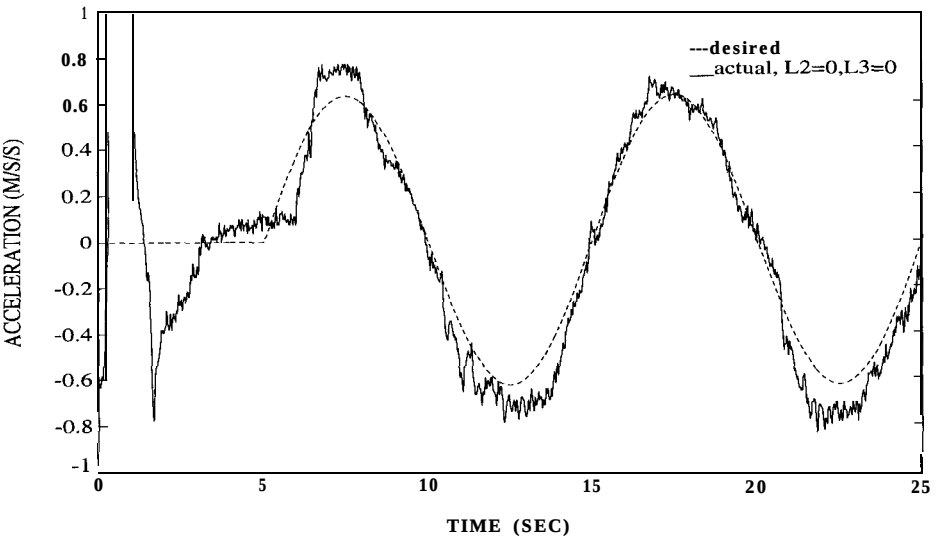

Figure 7.6: Vehicle acceleration tracking - Controller A ($\lambda_1 = 0.4$)

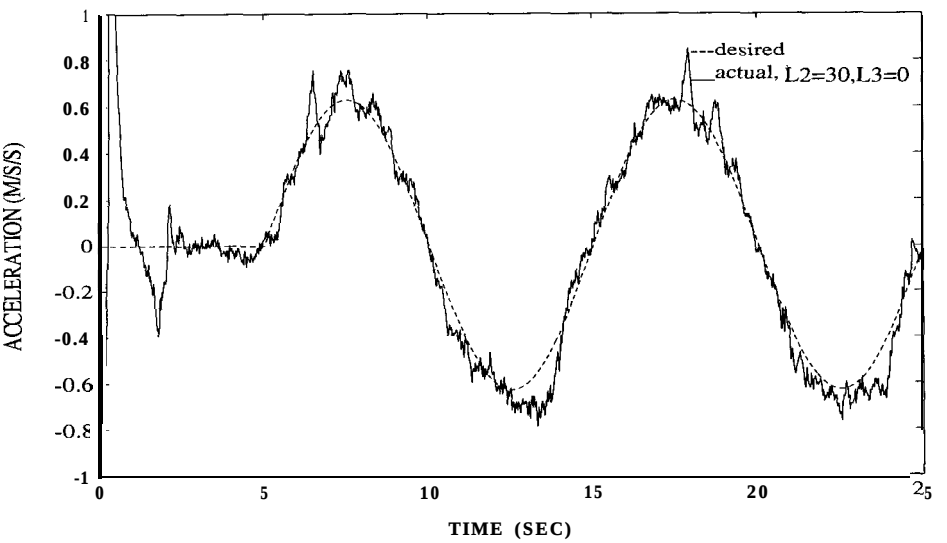

Figure 7.7: Vehicle acceleration tracking - Controller B ($\lambda_1 = 0.4$, $\lambda_2 = 30$)

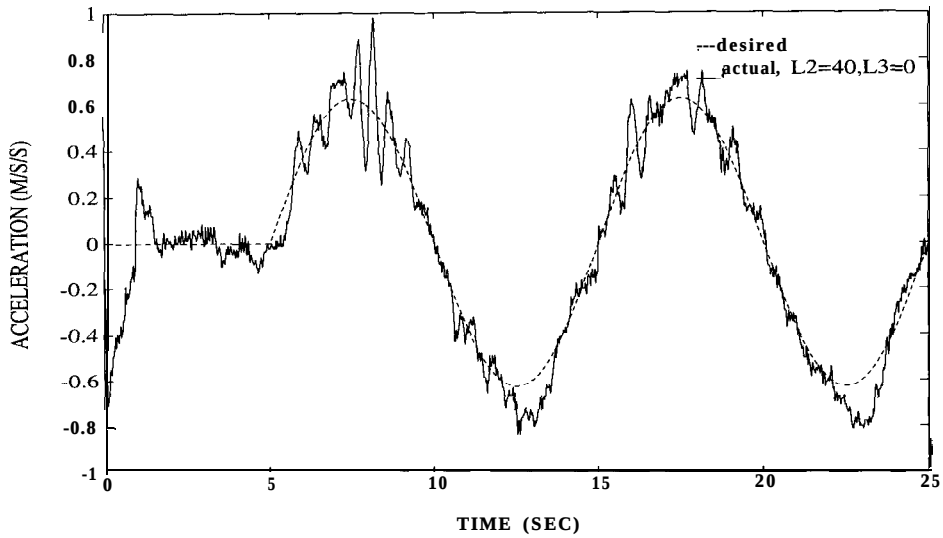

Figure 7.8: Vehicle acceleration tracking - Controller B ($\lambda_1 = 0.4, \lambda_2 = 40$)

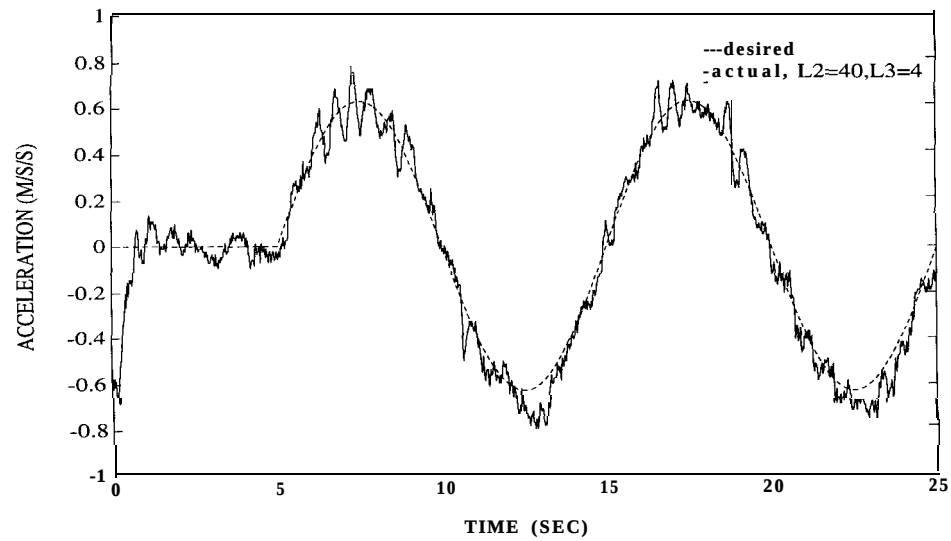

Figure 7.9: Vehicle acceleration trackine - Controller C ($\lambda_1 = 0.4, \lambda_2 = 0.4, \lambda_3 = 4$)

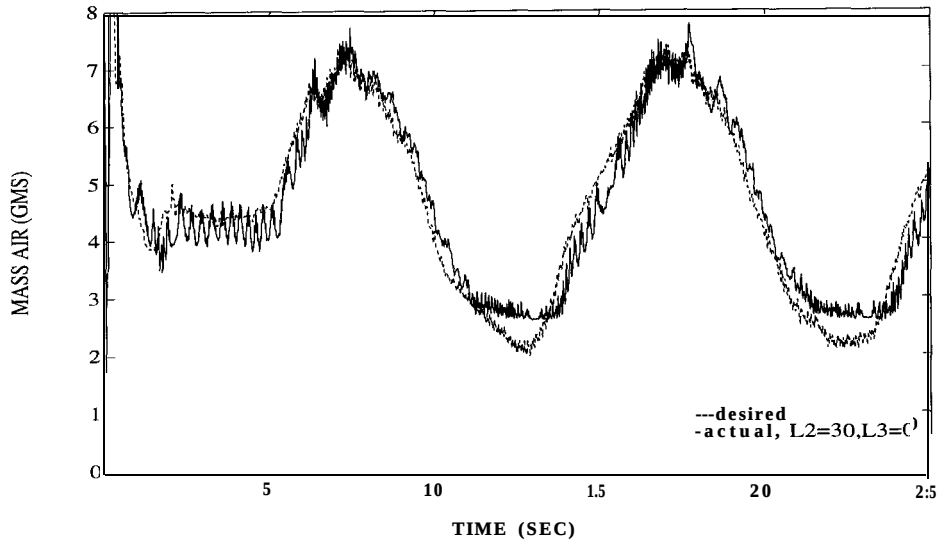

Figure 7.10: Mass air tracking - Controller B ($\lambda_1 = 0.4$, $\lambda_2 = 30$)

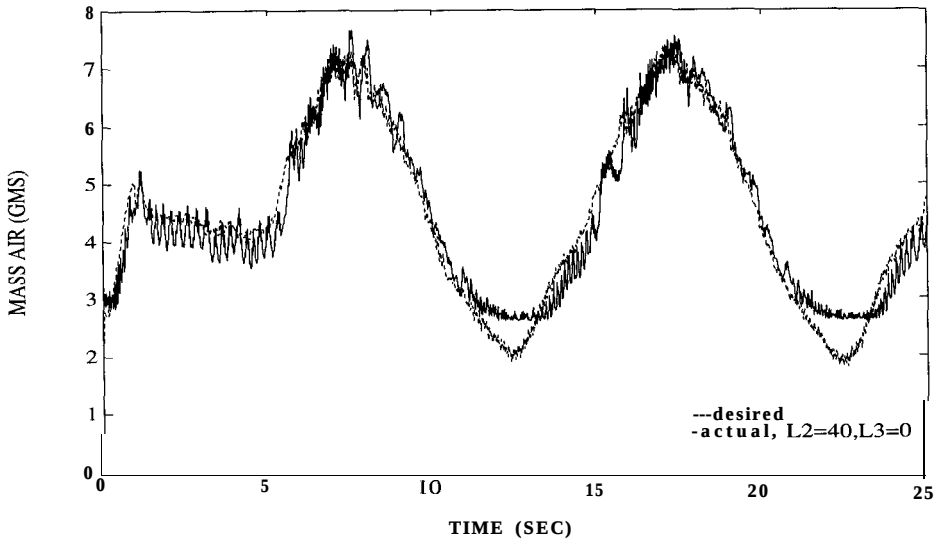

Figure 7.11: Mass air tracking - Controller B ($\lambda_1 = 0.4$, $\lambda_2 = 40$)

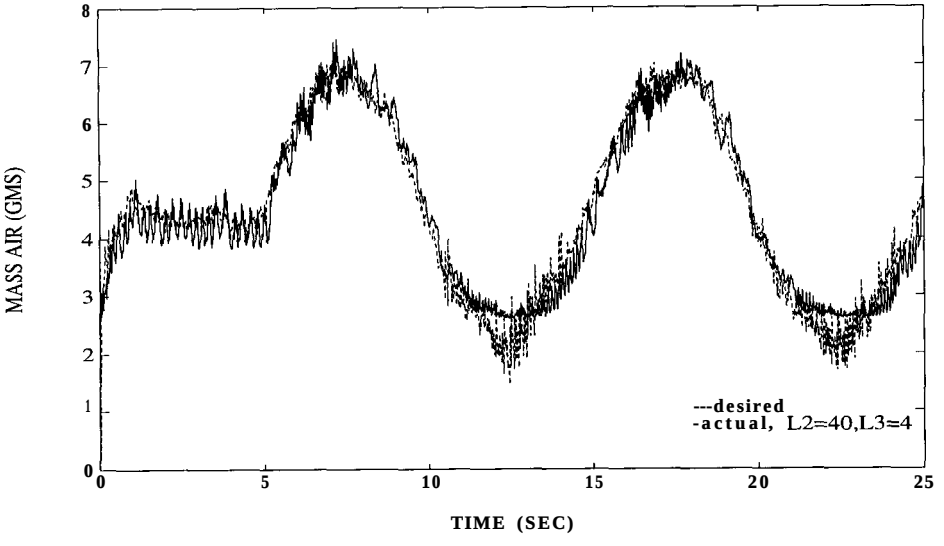

Figure 7.12: Mass air tracking - Controller C ($\lambda_1 = 0.4$, $\lambda_2 = 40$, $\lambda_3 = 4$)

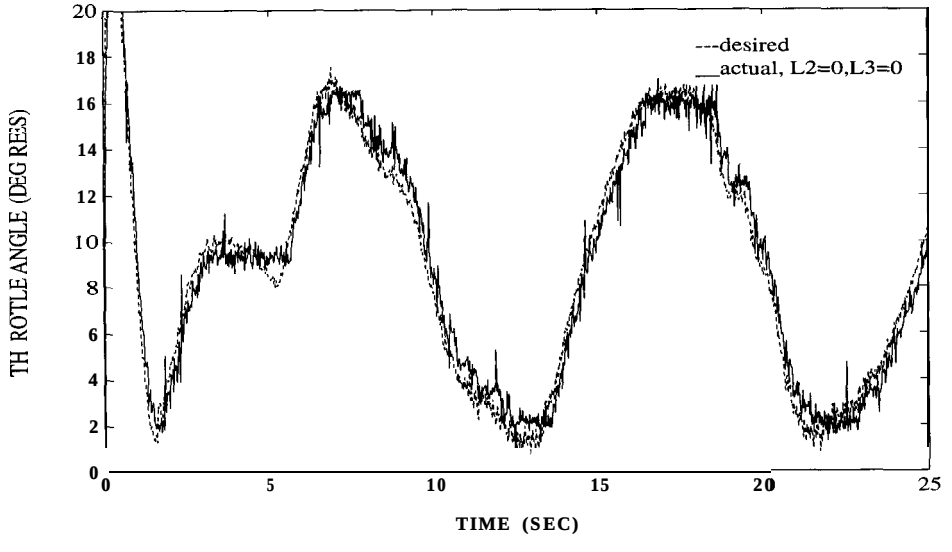

Figure 7.13: Throttle control signal tracking - Controller A ($\lambda_1 = 0.4$)

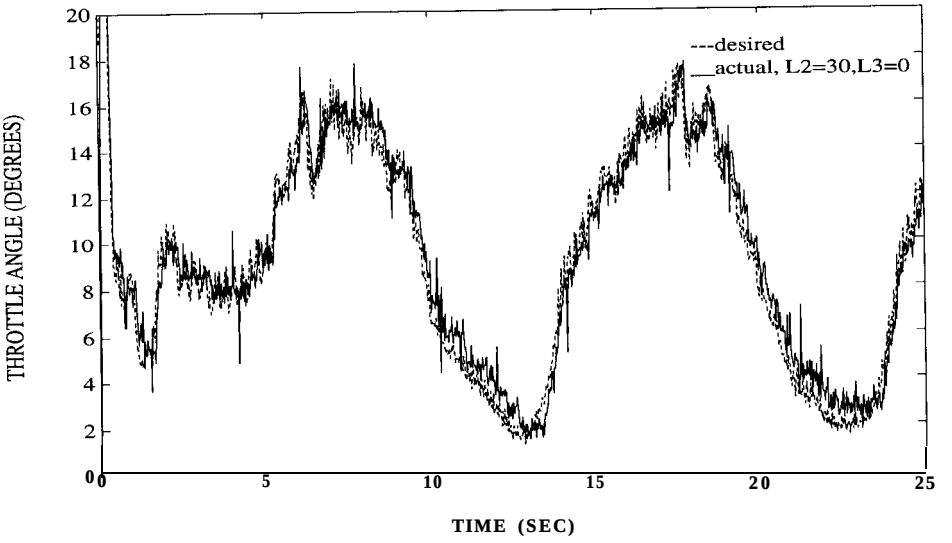

Figure 7.14: Throttle control signal tracking - Controller B ($\lambda_1 = 0.4$, $\lambda_2 = 30$)

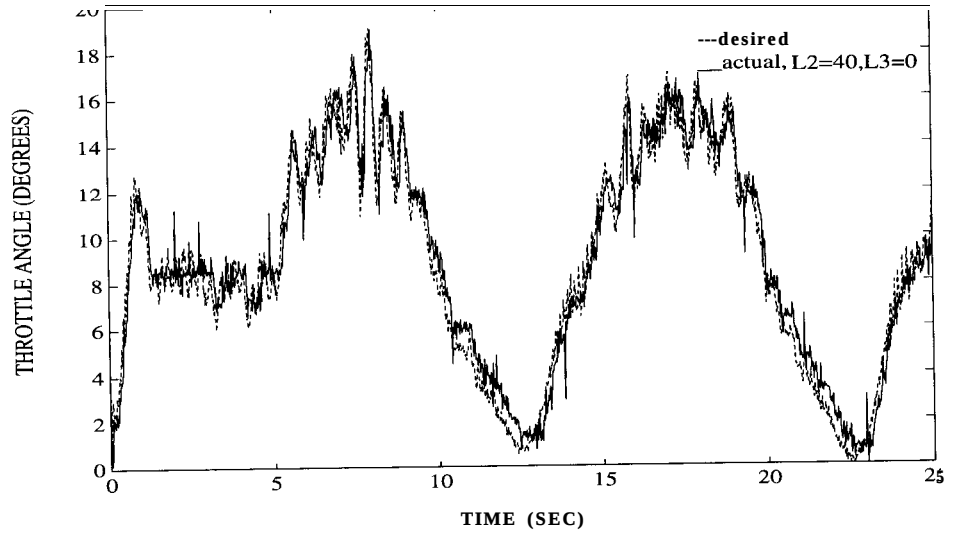

Figure 7.15: Throttle control signal tracking - Controller B ($\lambda_1 = 0.4$, $\lambda_2 = 40$)

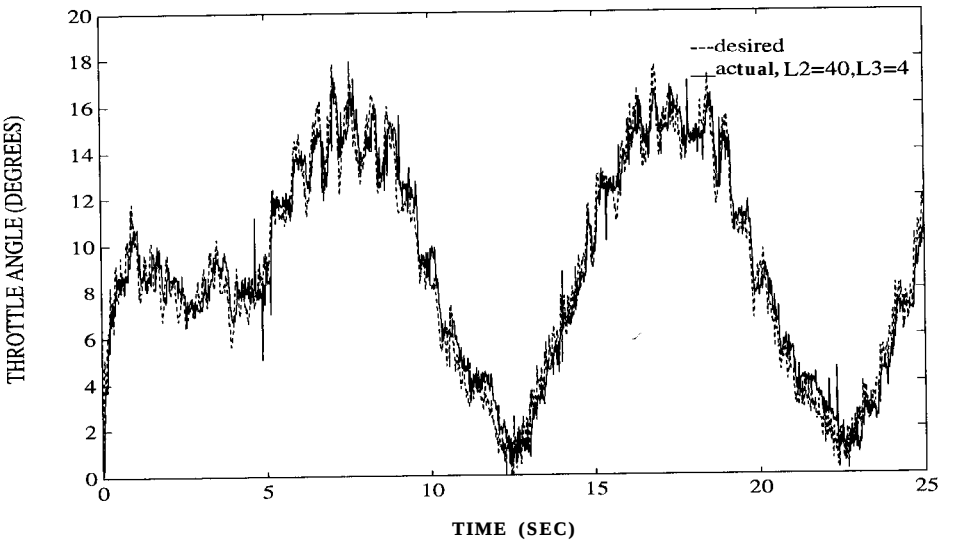

Figure 7.16: Throttle control signal tracking - Controller C ($\lambda_1 = 0.4$, $\lambda_2 = 40$,$\lambda_3 = 4$)

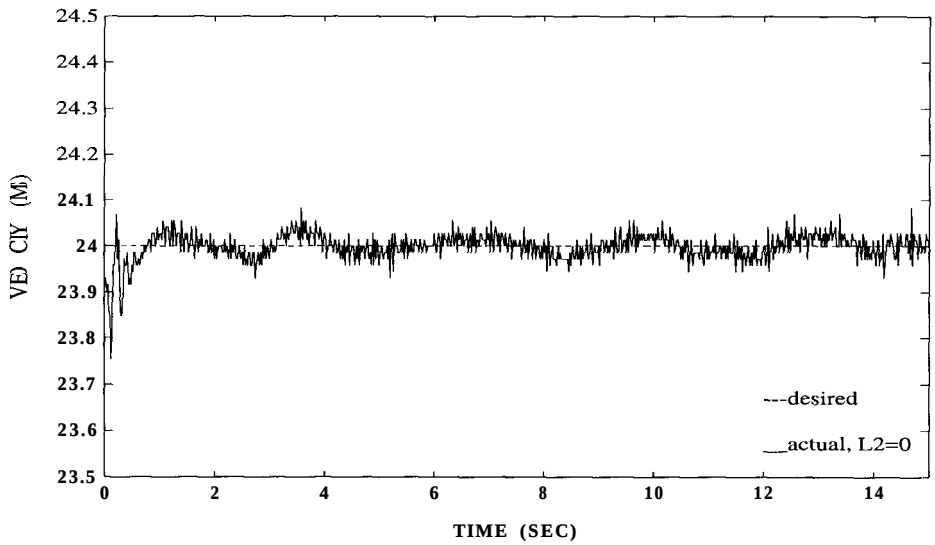

Figure 7.17: Constant velocity maneuver: Vehicle velocity tracking - Controller A ($\lambda_1 = 0.4$)

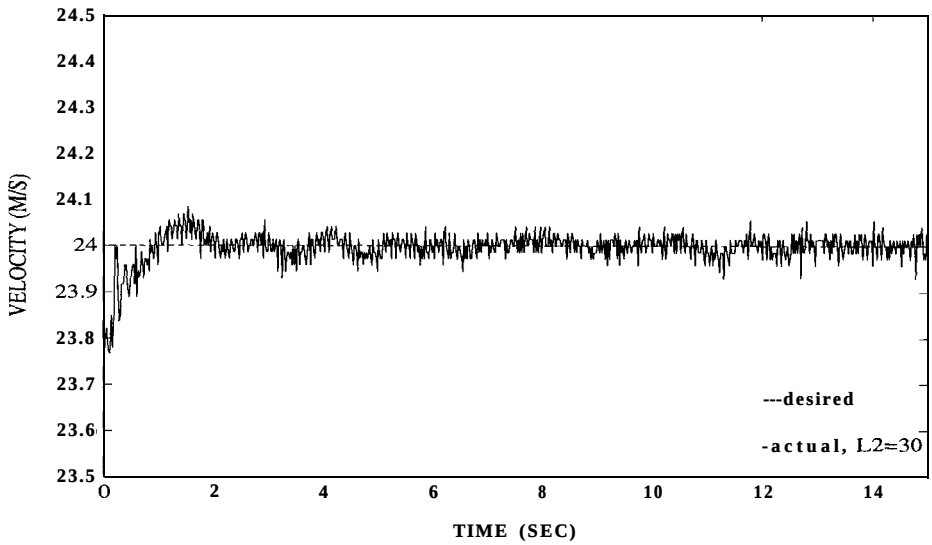

Figure 7.18: Constant velocity maneuver: Vehicle velocity tracking - Controller B ($\lambda_1 = 0.4, \lambda_2 = 30$)

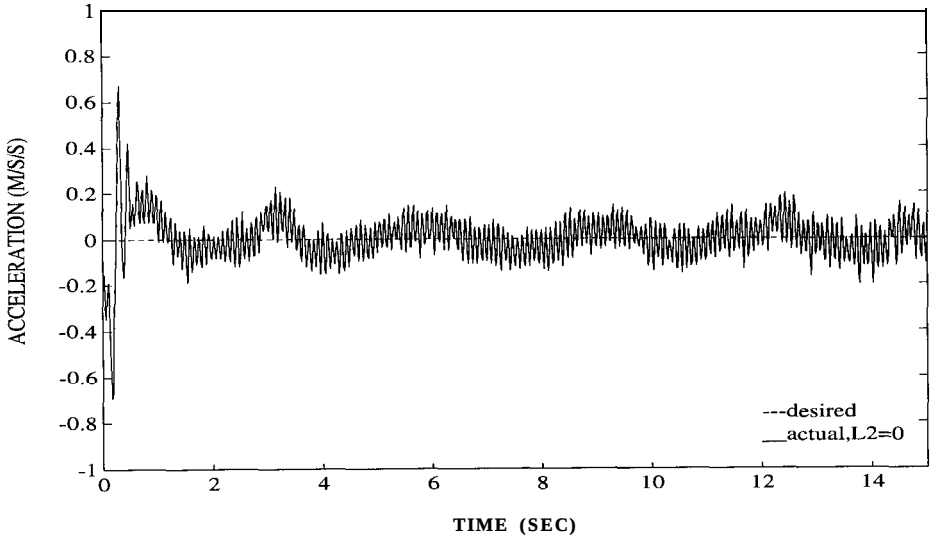

Figure 7.19: Constant velocity maneuver: Vehicle acceleration tracking - Controller A ($\lambda_1 = 0.4$)

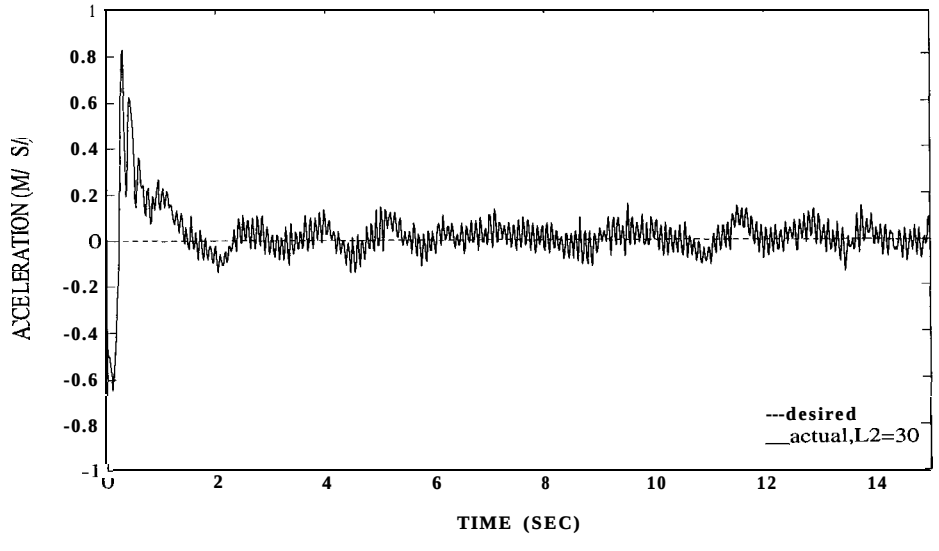

Figure 7.20: Constant velocity maneuver: Vehicle acceleration tracking - Controller B ($\lambda_1 = 0.4$, $\lambda_2 = 30$)

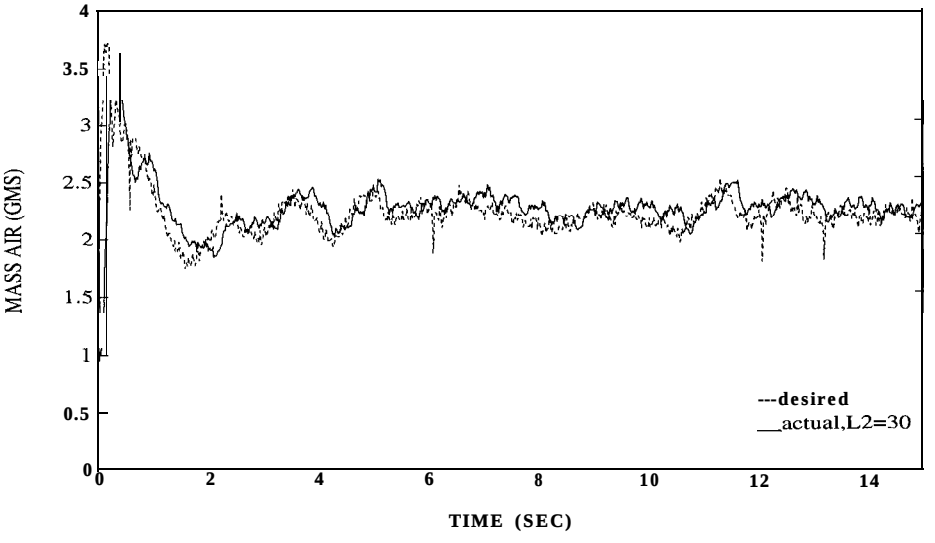

Figure 7.21: Constant velocity maneuver: Mass air tracking - Controller B ($\lambda_1 = 0.4, \lambda_2 = 30$)

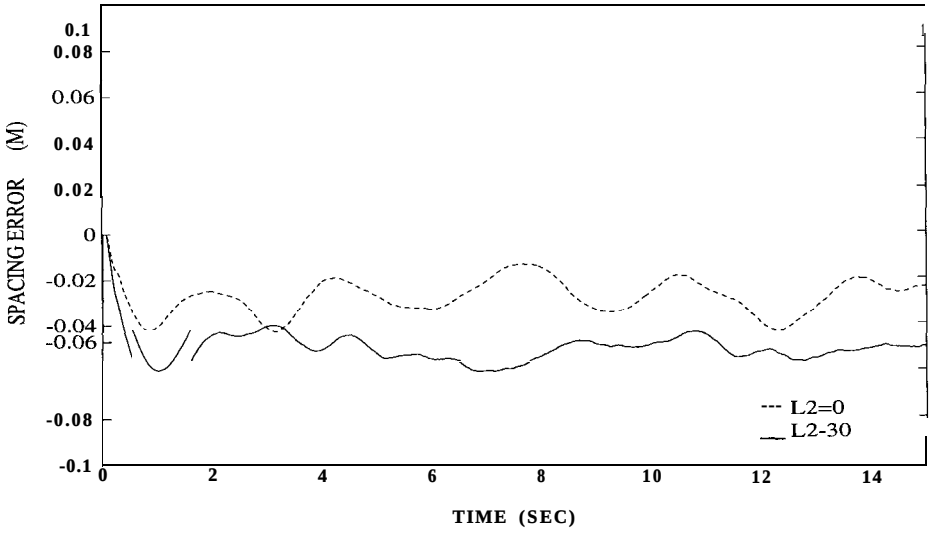

Figure 7.22: Constant velocity maneuver: Mass air tracking - Controllers A & B ($\lambda_1 = 0.4, \lambda_2 = 30$)

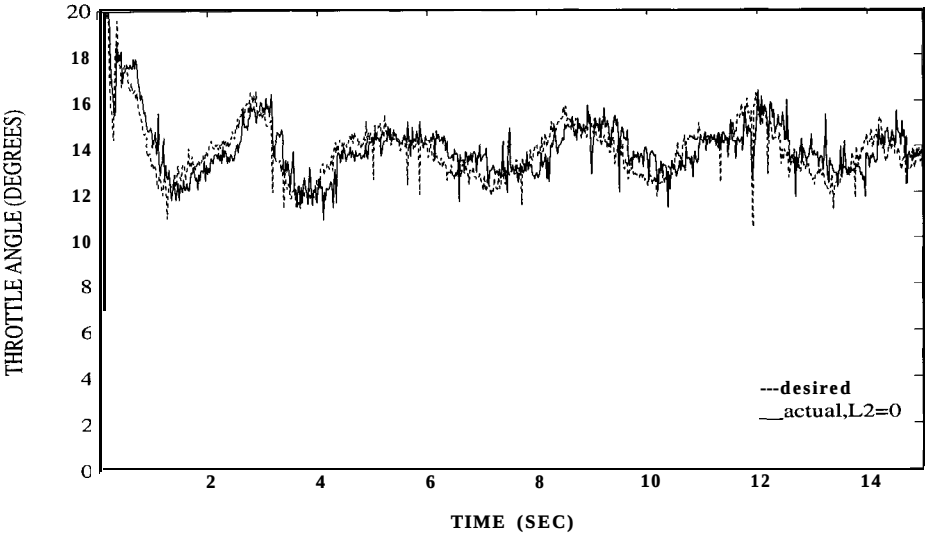

Figure 7.23: Constant velocity maneuver: Throttle control signal tracking - Controller A ($\lambda_1 = 0.4$)

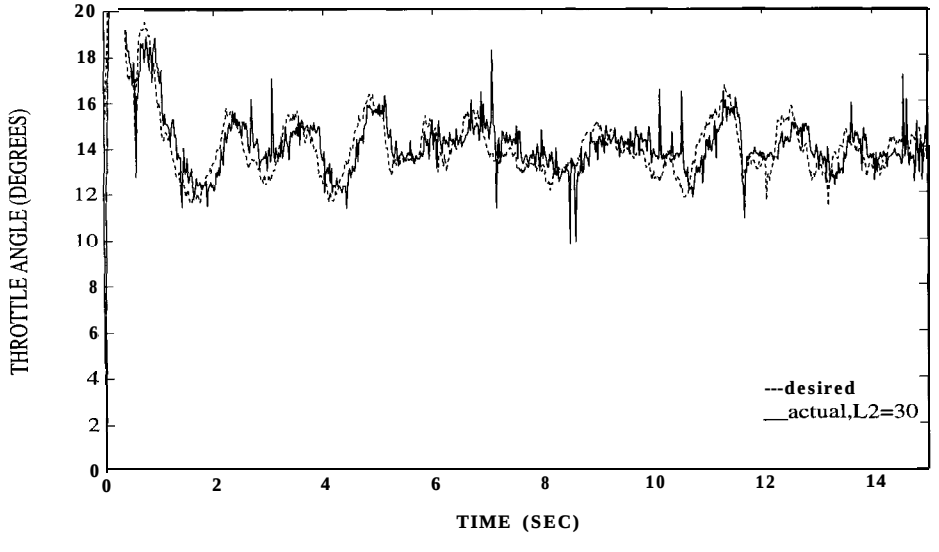

Figure 7.24: Constant velocity maneuver: Throttle control signal tracking - Controller B ($\lambda_1 = 0.4, \lambda_2 = 30$)

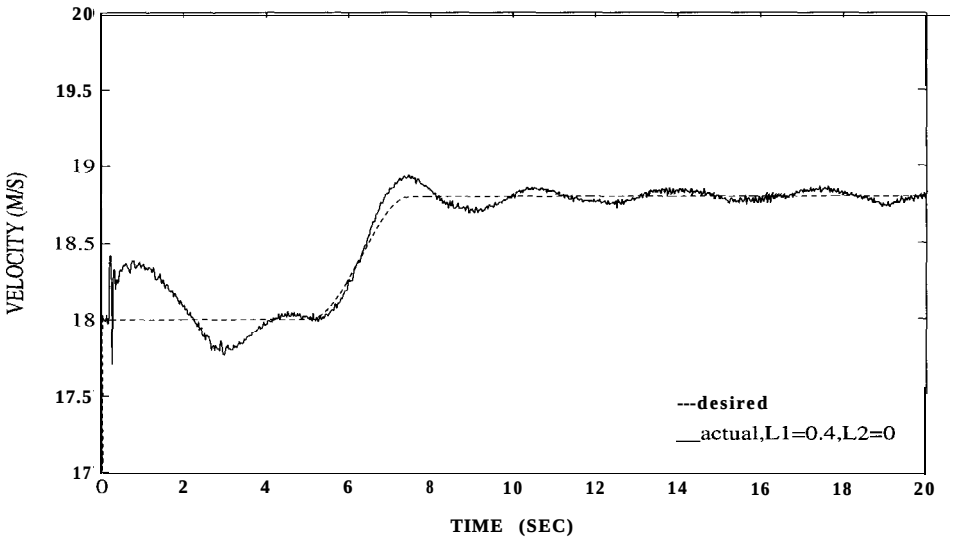

Figure 7.25: Acceleration maneuver: Vehicle velocity tracking - Controller A ($\lambda_1 = 0.4$, $a_{max} = 0.5m/s$, $f = 0.2Hz$)

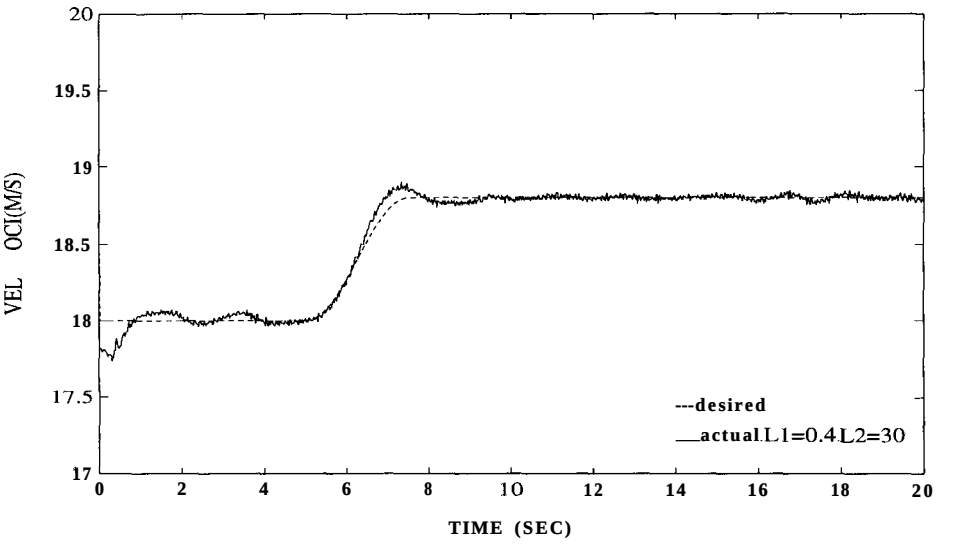

Figure 7.26: Constant velocity maneuver: Vehicle velocity tracking - Controller B ($\lambda_1 = 0.4, \lambda_2 = 30$, $a_{max} = 0.5m/s$, $f = 0.2Hz$)

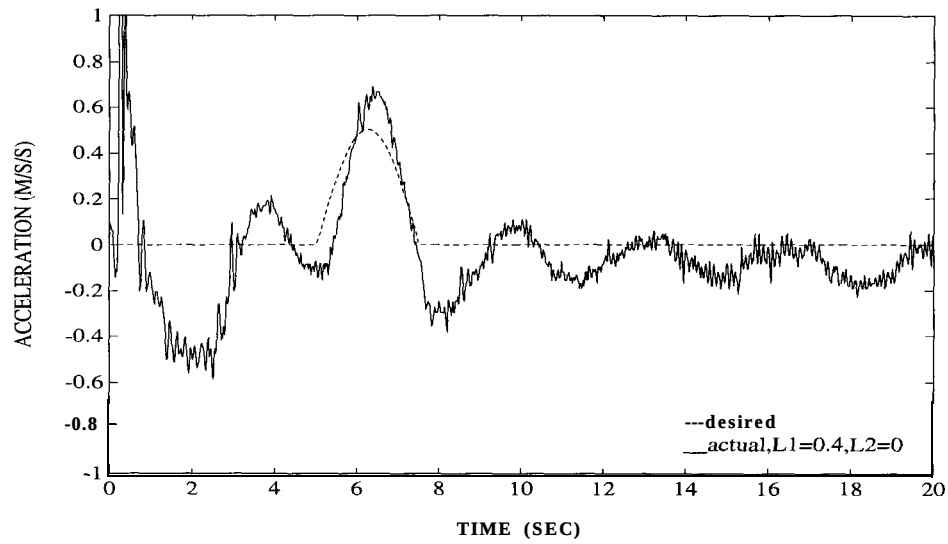

Figure 7.27: Acceleration maneuver: Vehicle acceleration tracking - Controller A (λ_1=0.4, a_{max} = $0.5m/s, f = 0.2Hz$)

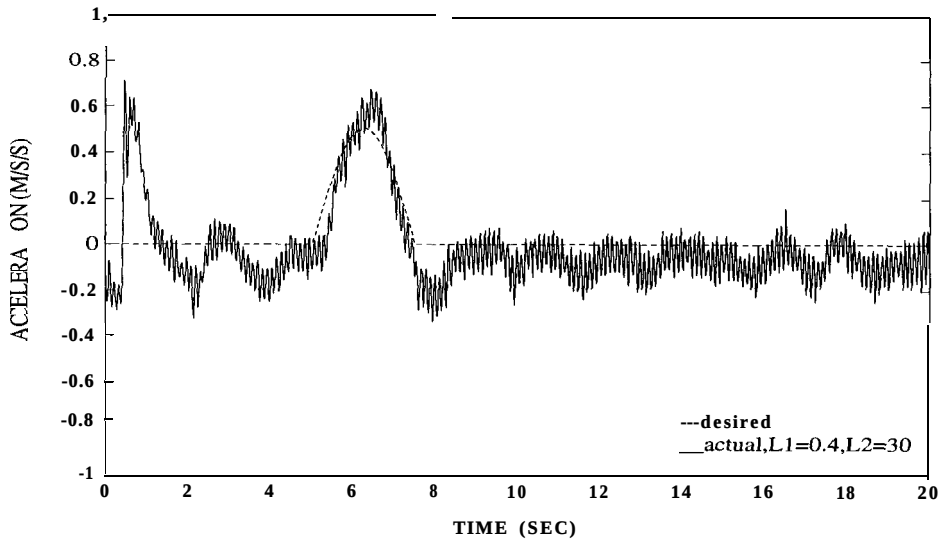

Figure 7.28: Acceleration maneuver: Vehicle acceleration tracking - Controller B ($\lambda_1 = 0.4, \lambda_2 = 30, a_{max} = 0.5m/s, f = 0.2Hz$)

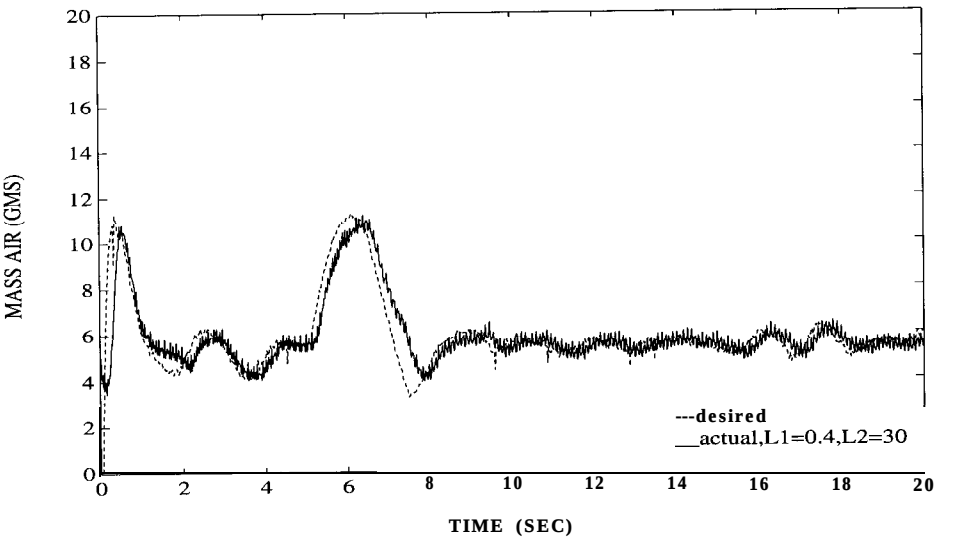

Figure 7.29: Acceleration maneuver: Mass air tracking - Controller B ($\lambda_1 = 0.4$, $\lambda_2 = 30$, $a_{max} = 0.5m/s$, $f = 0.2Hz$)

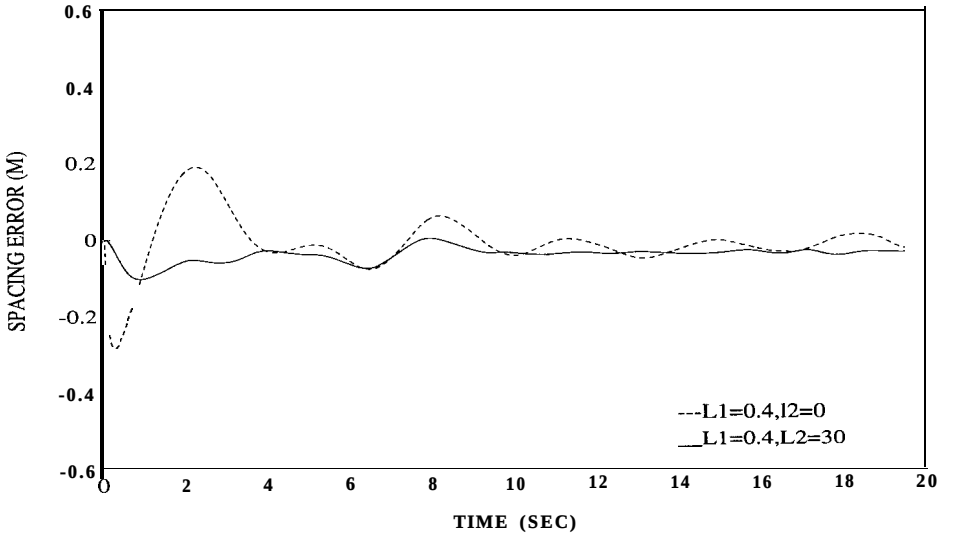

Figure 7.30: Acceleration maneuver: Spacing error - Controllers A & B ($\lambda_1 = 0.4, \lambda_2 = 30, a_{max} = 0.5m/s, f = 0.2Hz$)

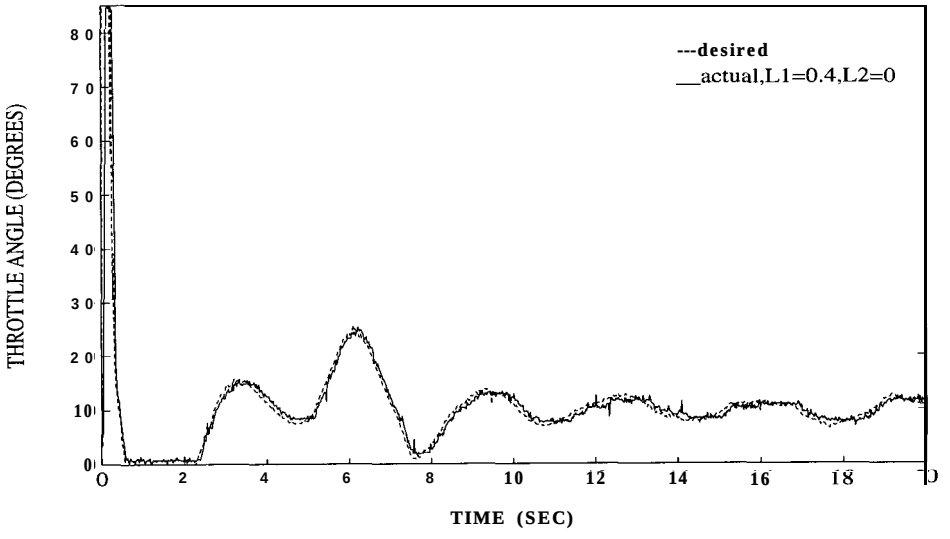

Figure 7.31: Acceleration maneuver: Throttle control signal tracking - Controller B ($\lambda_1 = 0.4$, $a_{max} = 0.5m/s, f = 0.2Hz$)

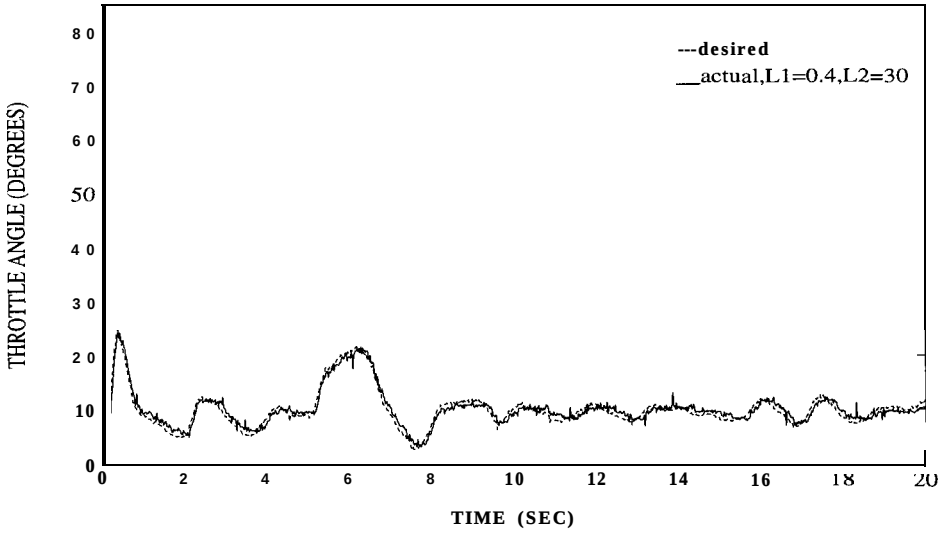

Figure 7.32: Acceleration maneuver: Throttle control signal tracking - Controller B ($\lambda_1 = 0.4$, $\lambda_2 = 30$, $a_{max} = 0.5m/s, f = 0.2Hz$)

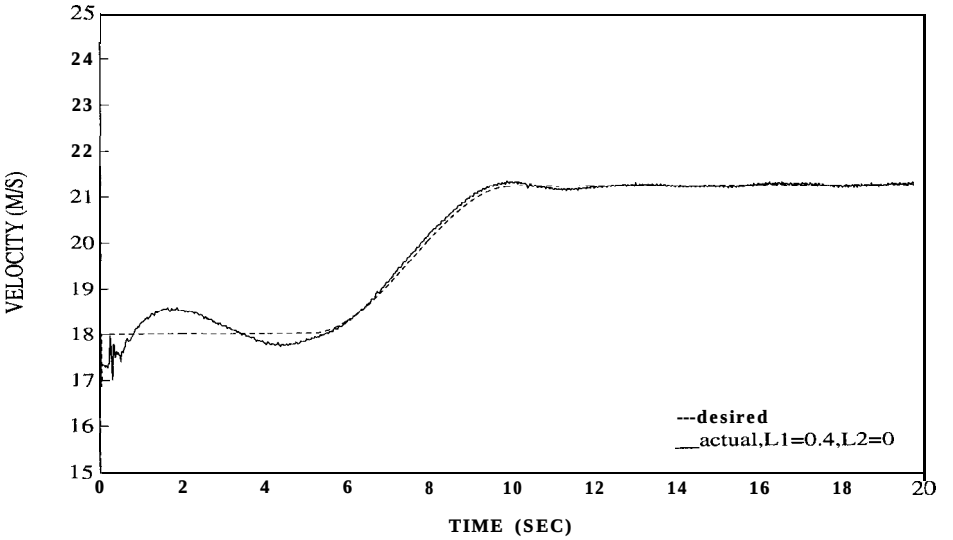

Figure 7.33: Acceleration maneuver: Vehicle velocity tracking - Controller A ($\lambda_1 = 0.4$, $a_{max} = 1m/s$, $f = 0.1Hz$)

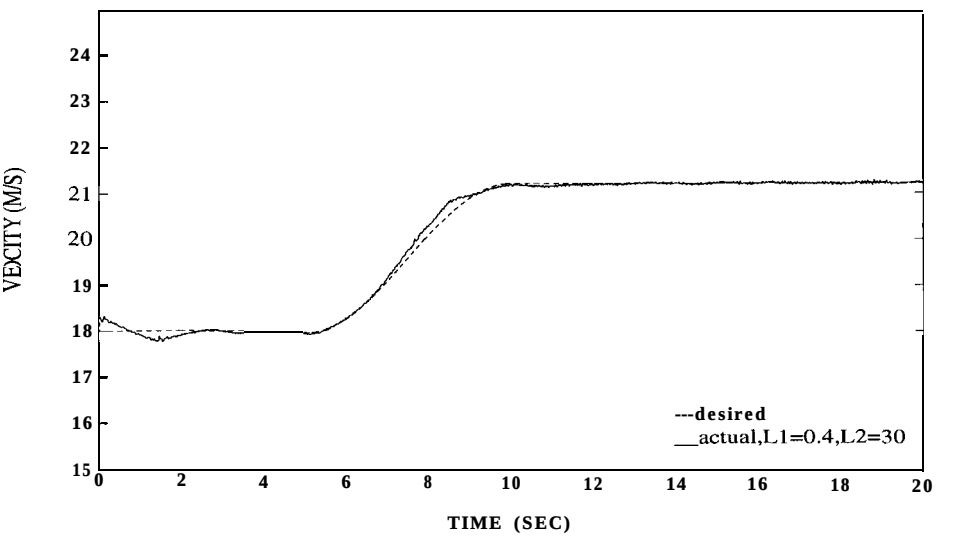

Figure 7.34: Acceleration maneuver: Vehicle velocity tracking - Controller B ($\lambda_1 = 0.4$, $\lambda_2 = 30$, $a_{max} = 1m/s$, $f = 0.1Hz$)

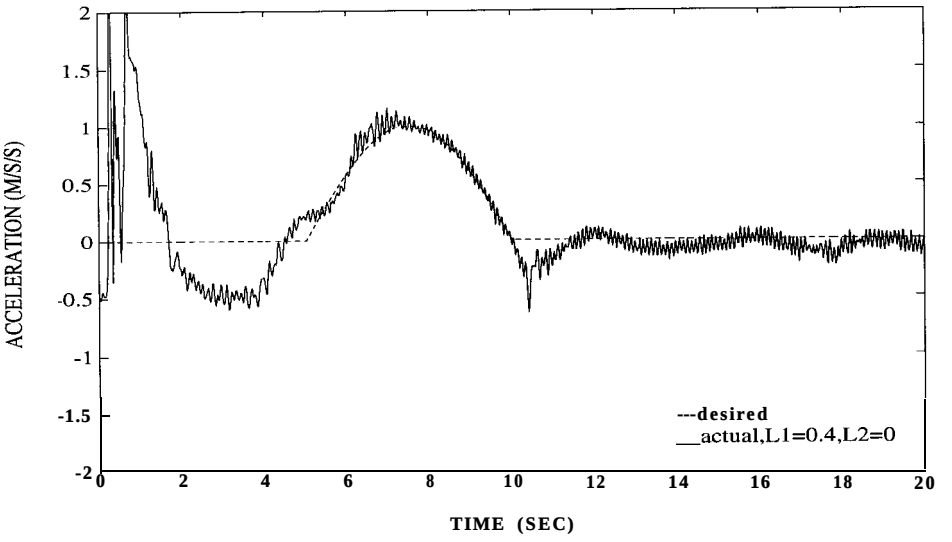

Figure 7.35: Acceleration maneuver: Vehicle acceleration tracking - Controller A ($\lambda_1 = 0.4, a_{max} = 1m/s, f = 0.1Hz$)

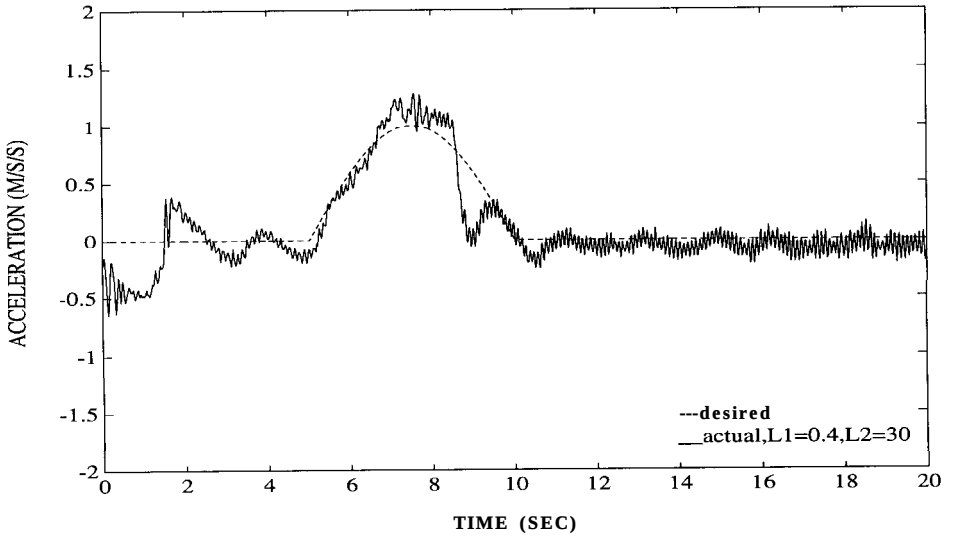

Figure 7.36: Acceleration maneuver: Vehicle acceleration tracking - Controller B ($\lambda_1 = 0.4, \lambda_2 = 30, a_{max} = 1m/s, f = 0.1Hz$)

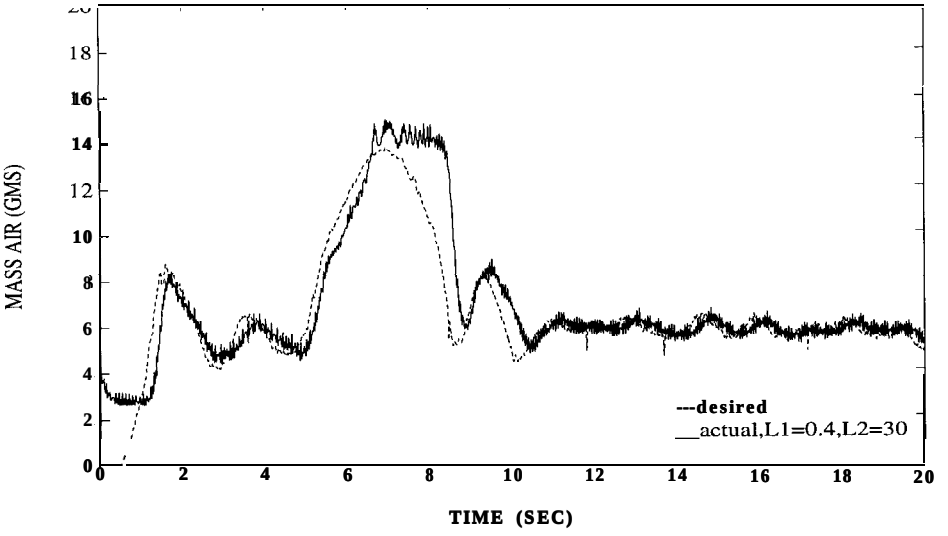

Figure 7.37: Acceleration maneuver: Mass air tracking - Controller B ($\lambda_1 = 0.4$, $\lambda_2 = 30, a_{max} = 1m/s, f = 0.1Hz$)

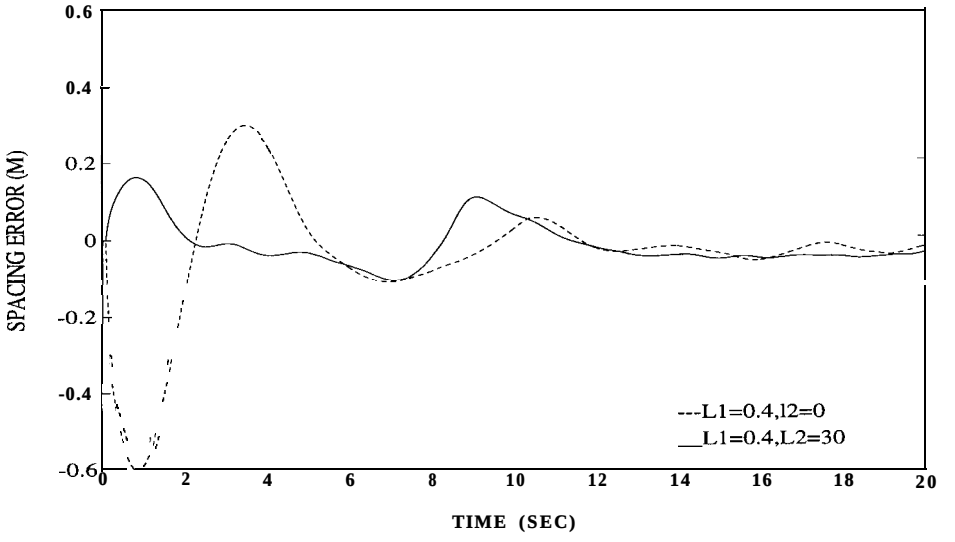

Figure 7.38: Acceleration maneuver: Spacing error - Controllers A & B ($\lambda_1 = 0.4, \lambda_2 = 30, a_{max} 1m/s, f = 0.1Hz$)

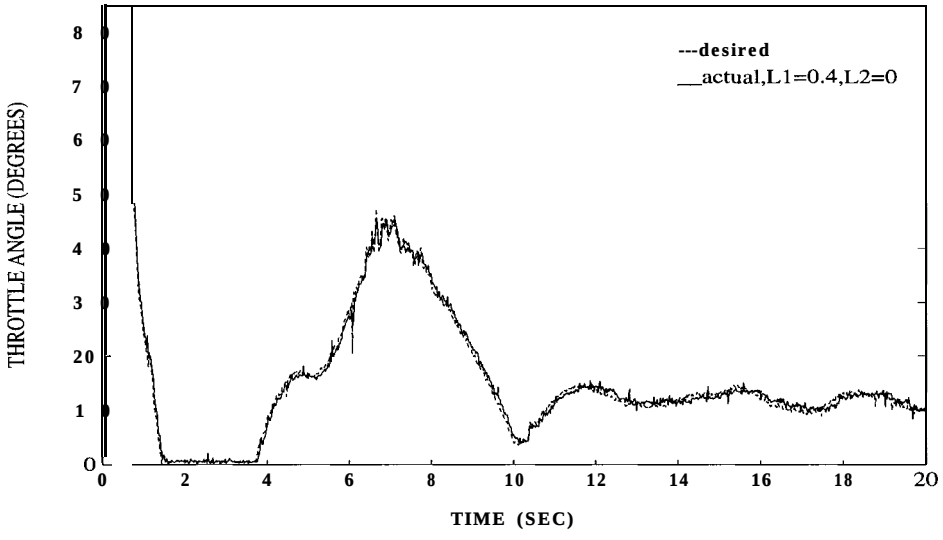

Figure 7.39: Acceleration maneuver: Throttle control signal tracking - Controller A (λ_1 = 0.4, a_{max} = $1m/s, f = 0.1Hz$)

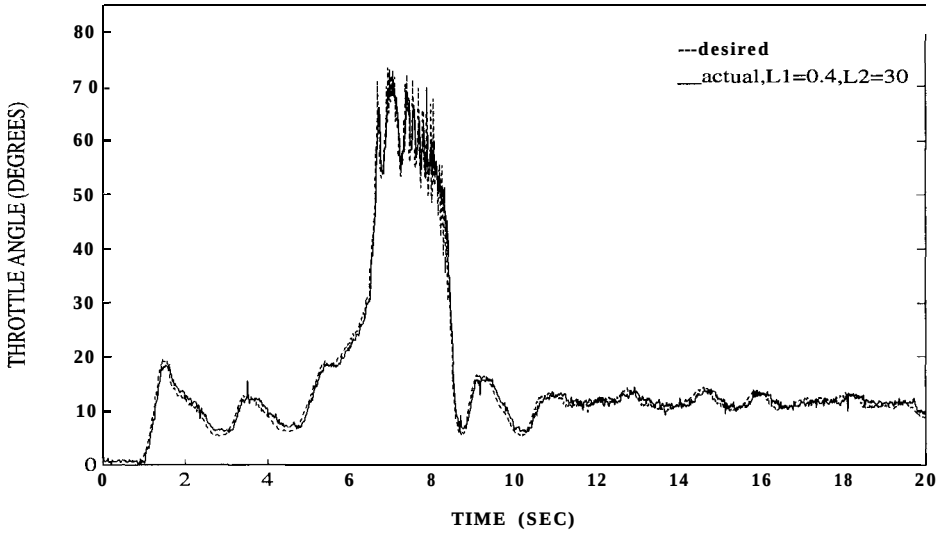

Figure 7.40: Acceleration maneuver: Throttle control signal tracking - Controller B (λ_1 = 0.4, λ_2 = 30, a $-max$ = $1m/s, f$ = $0.1Hz$)

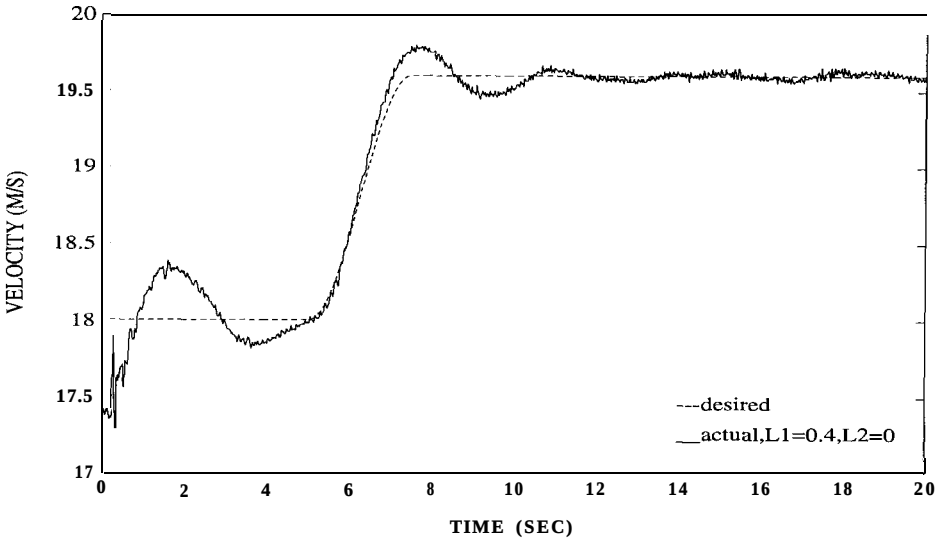

Figure 7.41: Acceleration maneuver: Vehicle velocity tracking - Controller A ($\lambda_1 = 0.4$), $a_{max} = 1m/s, f = 0.2Hz$

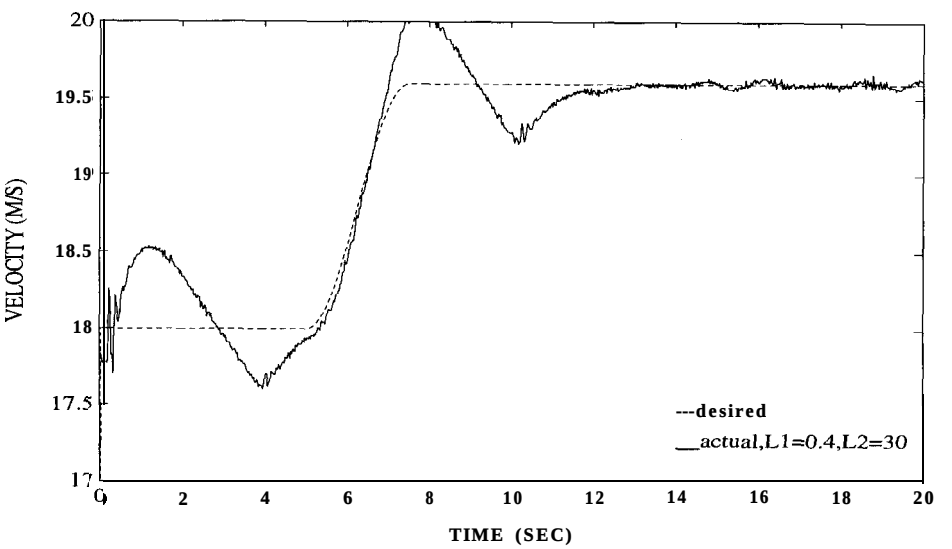

Figure 7.42: Acceleration maneuver: Vehicle velocity tracking - Controller B ($\lambda_1 = 0.4$, $\lambda_2 = 30$), $a_{max} = 1m/s, f = 0.2Hz$

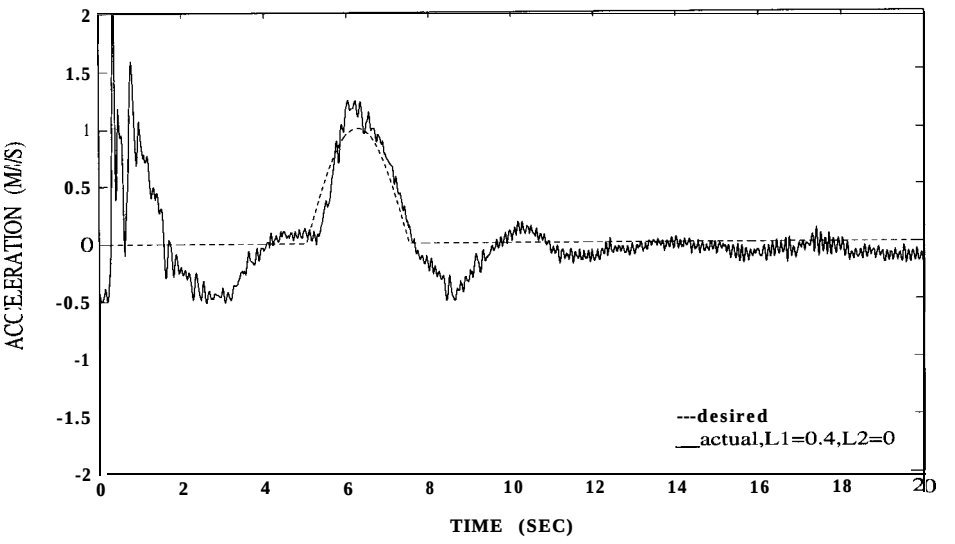

Figure 7.43: Acceleration maneuver: Vehicle acceleration tracking - Controller A ($\lambda_1 = 30$), $a_{max} = 1m/s, f = 0.2Hz$

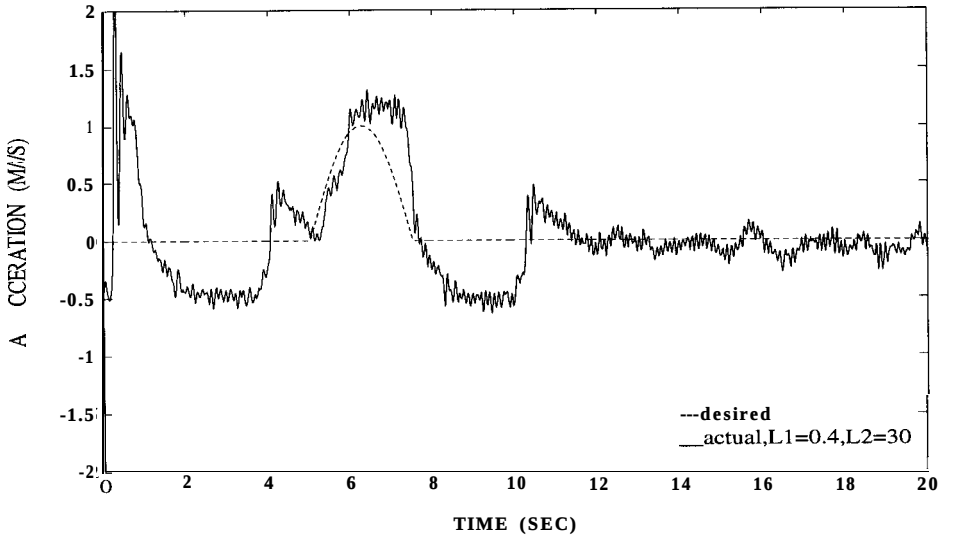

Figure 7.44: Acceleration maneuver: Vehicle acceleration tracking - Controller B ($\lambda_1 = 0.4$, $\lambda_2 = 30$), $a_{max} = 1m/s, f = 0.2Hz$

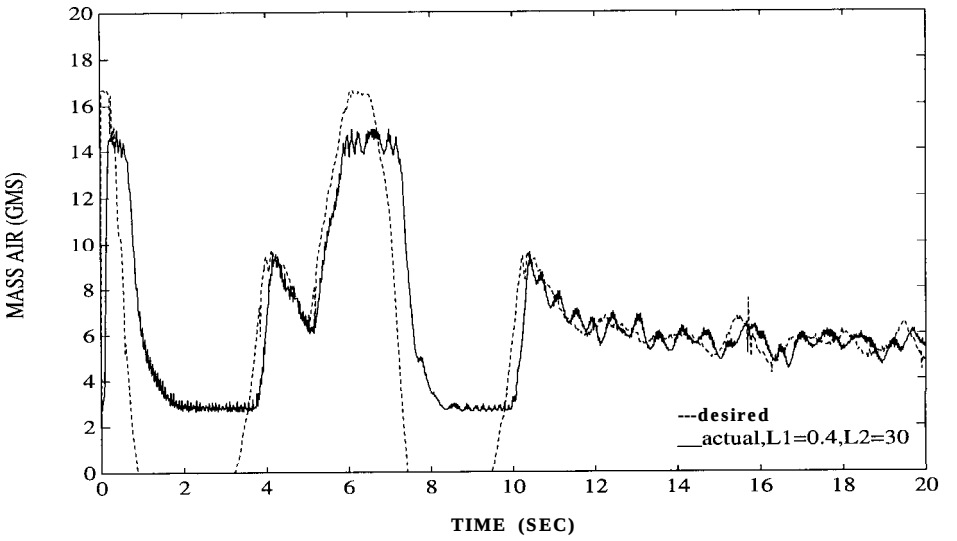

Figure 7.45: Acceleration maneuver: Mass air tracking - Controller B ($\lambda_1 = 0.4$, $\lambda_2 = 30$), $a_{max} = 1m/s$, $f = 0.2Hz$

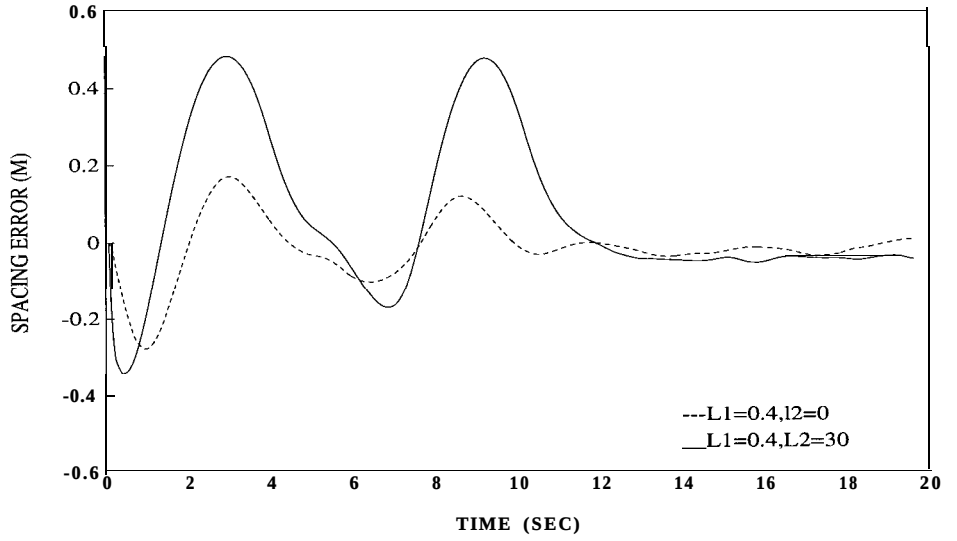

Figure 7.46: Acceleration maneuver: Spacing error - Controllers A & B ($\lambda_1 = 0.4, \lambda_2 = 30$), $a_{max} = 1m/s$, $f = 0.2Hz$

7.6 Conclusions

The experimental results show good performance for all control designs. The inclusion of manifold dynamics into controller design however generally offered improved tracking. This was especially true at low speeds where linearization reveals that open loop engine and manifold dynamics are closer in speed. As long as the closed loop manifold dynamics are sufficiently fast, as well as faster than the open loop dynamics, the additional complexity is warranted. Controllers B & C, which included the manifold dynamics, also have the added advantage of robustness to modeling errors and disturbances over Controller A. It should also be noted that the use of Controller A is only possible since the open loop manifold dynamics are asymptotically stable. If this were not the case the feedback structures compensating for the dynamics are absolutely required.

The inclusion of torque converter dynamics to the controller design added no appreciable improvement to system performance. From intuitive arguments, the usefulness of this design is during high accelerations in first and second gears. Given that passenger comfort specifications shun these type of maneuvers, the increased controller complexity is not justified.

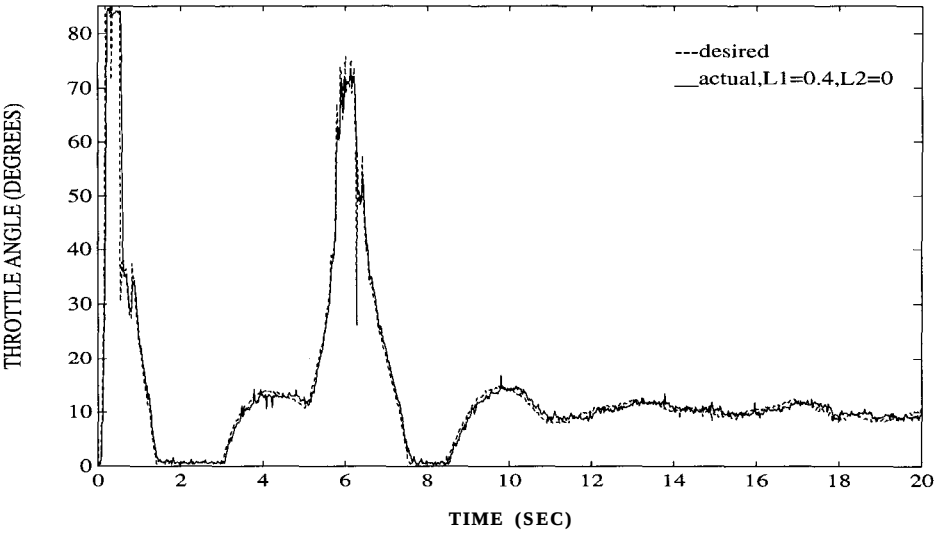

Figure 7.47: Acceleration maneuver: Throttle control signal tracking - Controller A $(\lambda_1 = 0.4), a_{max} = 1m/s,\ f = 0.2Hz$

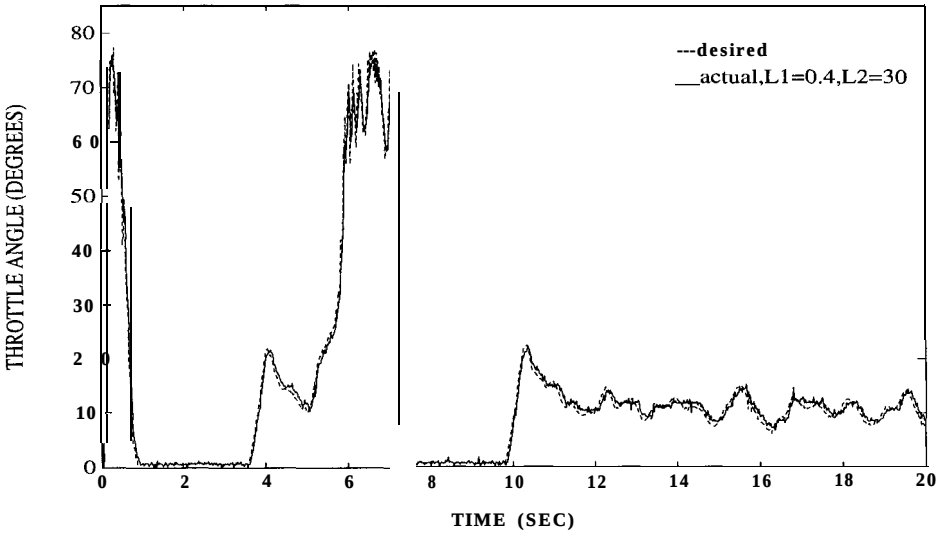

Figure 7.48: Acceleration maneuver: Throttle control signal tracking - Controller B $(\lambda_1 = 0.4,\ \lambda_2 = 30), a_{max} = 1m/s, f = 0.2Hz$

Chapter 8

Conclusions

We have developed a user-friendly and modular simulation package for a 20 vehicle platoon, which incorporates a realistic vehicle model and a simplified controller model. Any new control algorithms can easily be verified by changing the "controller" routine of the package. Anonymous ftp site and/or an account has been set up for other researchers to transfer this package to their respective computers.

Due to the highly nonlinear behavior of the brake system, a model is critical for the development of an automatic brake controller. The model emphasises the behavior of the vacuum booster which is an essential component of the brake system. The model is also ideally suited for control because all the states are measurable.

String Stability is an important concern for platooning. Various platooning strategies have been investigated for string stability. It has been established that lead vehicle information is required for string stability. Other performance tradeoffs, like complexity of implementation, have also been addressed.

Smaller intervehicular spacing requires high performance controllers, which satisfy platooning specifications in the presence of parametric uncertainities. A decentralised adaptive control algorithm has been developed to this end. Performance improvement has been demonstrated in simulation.

The problem of failure detection and signal reconstruction for various sensors used in the longitudinal control system of the vehicle has been addressed. Experimental verification for the vehicle speed sensor failure and information reconstruction was

done. Throttle and brake actuator faults are being studied too with an aim to develop some backup plan for emergency situation. Experiments have been conducted at the California Highway Patrol Academy, Sacramento to test various control algorithms developed eariler.

Bibliography

[1] R. W. Allen, H. T. Szostak, T. J. Rosenthal, D. H. Klyde, " Field Testing and Computer Simulation Analysis of Ground Vehicle Dynamic Stability," *SAE Paper No. 900127, March 1990.*

[2] R. W. Allen, T. J. Rosenthal, D. H. Klyde, K. J. Owens, H. T. Szostak, "Validation of Ground Vehicle Computer Simulations Developed for Dynamic Stability Analysis," *SAE Paper NO. 920054, December 1991.*

[3] J. G. Bender, " An Overview of System Studies of Automated Highway Systems," *IEEE Trans. on Vehicular Technology, Vol. VT-40, Noo.1, Feb. 1991.*

[4] K. S. Chang., et al., "Experimentation with a Vehicle Platoon Control System," *In Proceedings of the 1991 Vehicle Navigation and Information Systems Conference, Dearborn, MI.*

[5] D. Cho and J. K. Hedrick, "Automotive Powertrain modeling for Control," *ASME Transactions on Dynamic Systems, Measurements and Control, 111(4):-, December 1989.*

[6] S. B. Choi, "Design of Robust Controller for Automotive Engines : Theory and Experiment ," *Ph. D thesis, Vehicle Dynamics Laboratory, U. C. Berkeley, August 1993.*

[7] S. B. Choi and J. K. Hedrick, "Sliding Control of Automotive Engines: Theory and Experiment, " ASME WAM, Advanced Automotive Technologies, 1992.

[8] E. Y. Chow, A. S. Willsky, " Analytic Redundancy and the design of robust failure detection systems, *"IEEE Transactions on Automatic Control, Vol. AC-9, No.3, 1990*

[9] C. A. Desoer and M. Vidyasagar, "Feedback Systems : Input-Output Properties," Academic Press, 1975.

[10] Faris, William R. Tresselt, Carl P. and Yee, Henry C., "Collision Avoidance Radar Braking Systems Investigation - Phase III Study," *The Bendix Corporation, Prepared for the U.S. Department of Transportation, 1979.*

[11] Fisher, D. K. ,"Brake System Component Dynamic Performance, Measurement and Analysis," *SAE Paper 700373, 1970.*

[12] Frank, A. A. , Liu, S. J. , and Liang, S. C. , "Longitudinal Control Concepts for Automated Automobiles and Trucks Operating on a Cooperative Highway," *SAE Paper 891708, 1989.*

[13] V. Garg, J. K. Hedrick, " Fault Detection and Control of Automated Highway Systems," *ASME WAM, December 1993.*

[14] J. C. Gerdes, D. B. Maciuca, P. E. Devlin, J. K. Hedrick, " Brake System Modelling for IVHS longitudinal Control," *ASME WAM, Dynamic Systems and Control, DSC- Vol. 53, 1993.*

[15] Gillespie, Thomas D. , "Fundamentals of Vehicle Dynamics ", *Society of Automotive Engineers, Warrendale, PA, 1992.*

[16] J. Green, J. K, Hedrick, "Nonlinear torque Control for Gasoline Engines," *I n Proceedings of American Control Conference, San Diego, CA , 1990.*

[17] J. K. Hedrick, V. Garg, "Failure Detection and Fault Tolerant Controller Design for Vehicle Control," *PATH Research Report Draft No. 93-09, 1993.*

[18] J. K. Hedrick, D. H. McMahon, V. K. Narendran, and D. Swaroop, "Longitudinal Vehicle Controller Design for IVHS systems," *In Proceedings of American Control Conference, pp 3107-3112,* 1991.

[19] J. K. Hedrick, D. H. McMahon, D. Swaroop, "Vehicle Modelling and Control for Automated Highway Systems," *ITS Publication UCB-ITS-PRR-93-24, November 1993.*

[20] J. K. Hedrick, B. Rao, S. Sheikholeslam, D. Swaroop, and P. Varaiya, "On Autonomous Intelligent Cruise Control," *PATH REPORT 1992.*

[21] J. K. Hedrick and D. Swaroop, "Dynamic Coupling in Vehicles Under Automatic Control," *In Proceedings of IAVSD Symposium, China, August 1993.*

[22] P. Ioannou, C. C. Chien, and J. Hauser, "Autonomous Intelligent Cruise Control," *IVHS America, May 1992.*

[23] A. Isidori, "Nonlinear Control Systems," *Springer- Verlag, 1985.*

[24] H. L. Jones, "Failure Detection in Linear Systems," *Ph. D thesis, MIT, 1973*

[25] Khan, Y. , Kulkarni, P. , and Youcef-Toumi, K. , "Modelling, Experimentation and Simulation of a Brake Apply System," *Proceedings of the 1992 American Control Conference, Chicago, IL.*

[26] P. V. Kokotovic, H. K. Khalil, J. O'Reilly, "Singular Perturbation Methods in Control: Analysis and Design," *Academic Press, 1986.*

[27] W. S. Levine and M. Athans, "On the Optimal Regulation of a String of Moving Vehicles," *IEEE Transactions on Automatic Controls, Vol. AC-11, N03, July 1966.*

[28] McMahon, D. H. , Hedrick, J. K. , and Shladover, S. E. ,"Vehicle Modelling and Control for Automated Highway Systems," *Proceedings of the 1990 American Control Conference, San Diego, CA.*

[29] D. H. McMahon, V. K. Narendran, D. Swaroop, J. K. Hedrick, K. S. Chang, P. E. Devlin, "Longitudinal Vehicle Controllers for IVHS: Theory and Experiment," *In Proceedings of American Control Conference, Chicago, IL, 1992.*

[30] J. J. Moskwa, J. K. Hedrick, " Modelling and Validation of Automotive Engines for Control Algorithm Development," *ASME WAM, Advanced Automotive Technologies, DSC- Vol.* 13, 1989.

[31] H. Peng, M. Tomizuka, "Preview Control for Vehicle Lateral Guidance in Highway Automation," in *Proceedings of 1991 American Control Conference, Boston, MA, June 1991.*

[32] Puhn, Fred, "Brake Handbook", *HP Books, Los Angeles, CA, 1985.*

[33] S. Sheikholeslam, "Control of a class of interconnected nonlinear dynamical systems," *Ph. D dissertation, U. C. Berkeley, December 1991.*

[34] Shladover, S. E. ,"Roadway Automation Technology - Research Needs," *Transportation Research Record No. 1283, Transportation Systems Planning and Applications, Transportation Research Board, National Research Council, Washington, D. C., 1990.*

[35] S. Shladover, "Potential Freeway capacity effects of automtatic vehicle control systems," *Presented at the Second International Conference on Applications of Advanced Technologies in Transportation Engineering, Minneapolis, Minnesota, August* 18-21, 1991.

[36] Shladover, S. E. ,"Longitudinal Control of Automotive Vehicles in Close-Formation Platoons," ASME *Journal of Dynamic Systems, Measurement and Control, Vol. 113, pp. 231-241, 1991.*

[37] J. J. E. Slotine and W. Li, "Applied Nonlinear Control," *Prentice Hall, 1991.*

[38] S. S. Sastry and M. Bodson, "Adaptive Control: Stability, Convergence and Robustness," *John Wiley & Sons, 1990.*

[39] D. Swaroop, J. K. Hedrick, "String Stability for IVHS systems," *UC Berkeley Report, Department of Mechanical Engineering, VDL-90-08-04, July 1993.*

[40] D. Swaroop, J. K. Hedrick, C. C. Chien, P. A. Ioannou, "A Comparision of Spacing and Headway Control Laws for Automatically Controlled Vehicles," submitted to *Vehicle System Dynamics Journal.*

[41] Vadim I. Utkin, "Variable Structure Systems with Sliding Modes," *IEEE Transactions on Automatic Control, April 1977.*

[42] J. Y. Wong, "Theory of Ground Vehicles," *John Wiley & Sons, 1978.*

Appendix A

VDANL

VDANL (Vehicle Dynamics Analysis, Non Linear) is a vehicle dynamics simulation program which runs on IBM-PC compatible computers and was developed by Systems Technology, Inc. (STI) in Hawthorne, California. VDANL supports analysis of passenger cars, light trucks and sport utility vehicles with the user providing the necessary vehicle parameters through input files. Input parameters for 42 different vehicles were provided with the simulation program. VDANL can be run in either open loop simulation mode with time profiles of steering, braking, throttle and aerodynamic inputs provided by the user, or in driver model closed loop simulation mode with road curvature, lane position and speed commands as input. Initial research with the VDANL simulation program was concentrated in the analysis of the VDANL vehicle model and determination of VDANL's applicability to the PATH program. Current research efforts are being made to adapt the simulation program to test and verify algorithms for combined longitudinal/lateral control of a platoon of vehicles.

Figure A is the block diagram for the VDANL simulation program. The vehicle model for VDANL covers an extensive range of longitudinal and lateral/directional modes (23 degrees of freedom) up through the limit performance conditions. Original development of VDANL was targeted for analysis of vehicle stability and rollover [1], [2], thus requiring a highly accurate vehicle model to properly account for induced load transfer across the wheelbase due to extreme driving maneuvers. The VDANL

simulation package provided to PATH included manuals with descriptions of the vehicle model and results of experimental validation testing, as well as methods for determining the large number of vehicle parameters needed to run the simulation.

The vehicle model uses 3 mass components including a vehicle sprung mass and front and rear unsprung masses. The tire model is derived from a composite longitudinal slip and side slip angle description and uses shaping coefficients based on Calspan tire test data to fit the tire model to various types of tires. The suspension model allows for independent or solid axle suspension and specifies all suspension forces as equivalent forces acting at the tire contact patch. This is to give the suspension model broad applicability over a wide range of vehicle suspensions and allows the necessary input parameters for the simulation to be determined from vehicle geometry and static force measurements of the particular vehicle. The steering model includes Ackerman steer effects and steering compliance. The power train model includes an engine, transmission, differentials and torque splitting between the front and rear axles. However, the VDANL power train model is fairly generic and does not include an accurate model of the engine dynamics for each vehicle, since development of the VDANL simulation was targeted for the analysis of vehicle stability and rollover. The brake model simulates vacuum boost runout, a non-linear proportioning valve between the front and rear axles, and also a generic ABS model.

From the analysis of the VDANL, the following recommendations are made concerning its potential applicability to the PATH program. The extensively detailed vehicle model of VDANL is unnecessarily excessive for the development of control algorithms for the PATH program. The vehicle models of McMahon et al [28] Peng et al [31] are well suited for such control algorithm development. In addition these models are currently running on DEC workstations with considerably higher computing power than PC compatible machines on which VDANL runs. However, because the VDANL simulation program was provided with input parameter sets for 42 different vehicles, it has a potential application in testing the robustness of the longitudinal/lateral control algorithms to changes in vehicle parameters. Simulations can be run to test the effectiveness of the control algorithm across vehicle types ranging from a 2-door Ford Escort to a Chevy S10 Blazer sport utility. Also, because the VDANL

vehicle model was developed for analysis of extreme vehicle maneuvers, VDANL could also possibly be used for simulation analysis and estimation of the vehicle dynamics encountered in emergency procedures and how these effect the control algorithms.

Current research efforts are directed in adapting the VDANL simulation for use in the PATH program. Through arrangements with STI, we have been provided a means for modifying the VDANL program through user defined modules which will interface with the VDANL code. Thus, the VDANL simulation is being modified to run in closed loop mode with the VDANL driver model replaced by the PATH vehicle control algorithms. Also, user defined modules can be written to bypass certain aspects of the VDANL code. For example, the VDANL engine model can be bypassed and instead the throttle to engine torque production can be calculated through the use of engine maps as in McMahon et al [28]. Since the VDANL program simulates the dynamics of a single vehicle, a method is also being implemented to use the VDANL code for a platooning a series of vehicles. This method involves first running the VDANL simulation for the lead vehicle and storing the position, velocity and acceleration information Then run the VDANL code for each i-th vehicle in the platoon using the position, velocity and acceleration of the lead car and the i-1th car for computing input commands (throttle, braking, steering) with the combined longitudinal/lateral control algorithms developed for the PATH program.

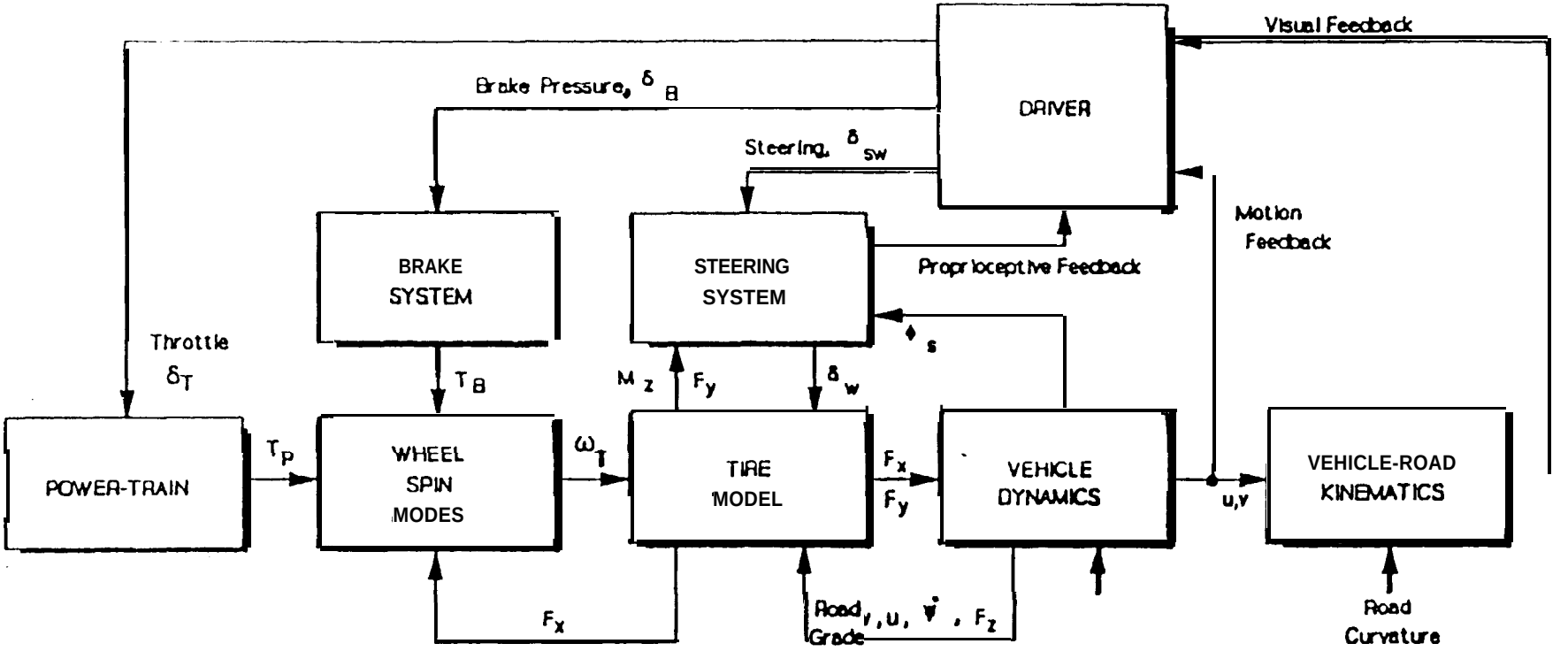

F_x, F_y, F_z = x, y, z forces from or on tire

M_z = Aligning mcfnent from tire

ω_T = Wheel spin velocity

v, u = Vehkb side and forward velocities

δ_{sw}, δ_w = Steering and road wheel angles

ϕ_s, γ = Body roll and wheel camber angles

$\dot{\psi}$ = Vshkb yaw rate

note that tire side slip = $\alpha = f(v, u, \dot{\psi}, \delta_{sw})$

tie longitudinal slip = $S = f(\omega_T, u)$

VDANL Flow Diagram